2018-09-20

The Stability of Visbroken Heavy Oil Against Asphaltene Precipitation

Rodríguez León, Sandra Liliana

UNIVERSITY OF CALGARY

The Stability of Visbroken Heavy Oil Against Asphaltene Precipitation

by

Sandra Liliana Rodríguez León

A THESIS

SUBMITTED TO THE FACULTY OF GRADUATE STUDIES
IN PARTIAL FULFILMENT OF THE REQUIREMENTS FOR THE
DEGREE OF MASTER OF SCIENCE

GRADUATE PROGRAM IN CHEMICAL AND PETROLEUM ENGINEERING

CALGARY, ALBERTA

SEPTEMBER, 2018

Abstract

Visbreaking is used in refinery and oilfield upgrading to reduce the viscosity of heavy oil (including bitumen) and residue feedstocks. However, if carried too far, this process can cause asphaltene precipitation and coke formation. A model that is able to predict the conditions at which the asphaltenes start to precipitate is required to design and optimize these thermal cracking processes. The Modified Regular Solution (MRS) approach has been widely used to model asphaltene precipitation from native and live oils (Tharanivasan, 2012, Akbarzadeh *et al*., 2005, and Akbarzadeh *et al*., 2005) and preliminary property correlations have been developed for solubility fractions from reacted oils (Yarranton *et al*., 2018, Powers *et al*., 2016). The goal of this thesis is to complete these correlations and apply the MRS model to asphaltene precipitation from visbroken heavy oils.

An Athabasca bitumen was thermally cracked in a visbreaker pilot plant at five different temperatures and residence times. The thermal conversion for each visbroken product was calculated based on SimDist data. The feed and each product were characterized into 5 pseudo-components (distillates, saturates, aromatics, resins, and asphaltenes) using distillation and SARA assays. Properties required for the model input (molecular weight, density, and solubility parameters) were measured or estimated for each pseudo-component. New correlations were proposed for the distillate fractions as a function of conversion and the existing correlations for the SARA fractions were updated. The model inputs are then the feedstock composition, the feedstock pseudo-component properties, and conversion. The RSM model was able to match the measured asphaltene precipitation yields from visbroken heavy residues and visbroken whole oils with average absolute deviations of 1.2 wt% and 0.4 wt%, respectively. At this point, the model is valid for Western Canadian heavy oils derived from the same source oil as the sample used for this thesis.

Acknowledgements

First and foremost, I am so grateful to God for allowing me to live such an amazing experience surrounded by wonderful people, your glory is beyond any limit. I would like to make a special acknowledge to my supervisor, Dr. Harvey Yarranton who gave me the opportunity to be part of his research group, you have all my admiration and respect. Thanks for having the dedication and patience to teach me many things, you have been so much more than a teacher.

I would like to extent my deep gratitude to Glen Hay for dedicating time and providing valuable feedback to my project. His professional advice and continuous support helped to line up my work in the best direction.

I also want to make a special recognition to Elaine and Florian; their continuous support and teaching methodology were fundamental to carry out my experiments successfully.

I am very fortunate for being part of such a great research group; all my colleagues made this experience more enjoyable. Thanks for the special and funny moments I shared with Adel, Andres, Franklin and, Catalina.

Thank you also to the NSERC Industrial Research Chair in Heavy Oil Properties and Processing, VMG, Inc, Schlumberger, Shell Canada, Suncor, Petrobras, and Nexen for the funding of this project.

Finally, my gratitude to the most important people in my life: my husband, my mom, my dad, and my sisters.

Dedication

A Dios

Por concederme la oportunidad de vivir esta linda experiencia acompañada de seres amados y guardar para el final una de las lecciones más maravillosas que he podido aprender.

A mi Esposo

Este logro es de los dos, una experiencia llena de muchas emociones la cual me mostró una vez más al gran hombre que tengo a mi lado.

A mis Padres

A mi mami quien tras años de sacrificio ha dedicado su vida para hacer de mi la mujer que ahora soy. A mi papa, por su incondicional compañía la cual ha marcado gran parte de mi desarrollo personal y profesional. A mi suegra, quien me ha acogido como una hija más y de quien he recibido solo amor y apoyo.

A mis hermanas

Quienes son una parte de mí y a quienes quiero profundamente. Porque las dos han hecho de mí una mejor persona y han estado siempre a mi lado en momentos difíciles.

A Patricio y Gustavo

Quienes fueron una pieza fundamental en la culminación de este proyecto y quienes con sus palabras lograron tocar profundas fibras.

Table of Contents

List of Tables

List of Figures

Nomenclature

Symbols

A	Coefficient in VPO calibration equation
Asph	Asphaltenes
δ	Solubility Parameter
m	mass
C5-Asph	Extracted asphaltenes
bit. asph	Bitumen asphaltenes
I_N	Insolubility number
SB_N	Solubility blend number
n	Shape factor of the solubility distribution
k	Equilibrium constant
X	Percent conversion
ρ	Density
τ	Shape factor of the density distribution
n	Total number of components
v	Molar Volume
w	Mass Fraction
x	Molar Fraction
l_{jk}	Interaction parameter
s	Standard Deviation
T	Temperature
V	Voltage

Greek Letter

α	Shape Factor of the Gamma Distribution
δ	Solubility Parameter
X	Percent conversion
γ	Activity Coefficient
ρ	Density
Δ	Delta
$\emptyset$	Volume Fraction

Subscripts

sat	Saturates
aro	Aromatics
b	Boiling Point
res	Resins
A	Asphaltenes
s	Solvent
f	Feed
i	component
avg	Average
mono	Monomer
mix	Mixture
min	Minimum value
max	Maximum value

Abbreviations

AAD	Average absolute deviation
AET	Atmospheric Equivalent Temperature
ASTM	American Society for Testing Materials
B	Bitumen
CCR	Condradson carbon residue
CI	Confidence Interval
DB	Diluted Bitumen
EOS	Equation of State
MRS	Modified Regular Solution
SAFT	Statistical associating fluid theory
SANS	Small angle neutron scattering
SAR	Saturates, aromatics, and resins
SARA	Saturates, aromatics, resins, and asphaltenes
SBD	Spinning band distillation
SG	Specific Gravity
SimDist	Simulated Distillation
TBP	True Boiling Point
TI	Toluene Insolubles
VB	Vacuum bottoms
VPO	Vapour pressure osmometer
WC	Western Canada

Chapter 1: Introduction

Asphaltene precipitation may occur upon changes in temperature, pressure or composition. Some oilfield applications where asphaltene precipitation can occur include: solvent injection into a reservoir, dilution of heavy oil with a solvent for transport purposes, upgrading of heavy oil feedstocks, and blending of different refinery streams. Asphaltene precipitation can lead to deposition which cause severe operational issues such as plugging in reservoirs and well bores, and fouling in surface facilities and refinery units. Deposition and fouling lead to lost production and add to operating expenses. Hence, it is so important to predict the conditions at which asphaltene precipitation occurs in order to avoid or mitigate potential deposition and fouling in both upstream and downstream processes.

One application of increasing interest in Alberta is visbreaking heavy oils prior to pipeline transport. Visbreaking is a mild thermal cracking process that has been mainly used to decrease residue viscosity and to reduce the diluent required for residue dilution. In this process, the feeds are heated for a short residence time to breakdown the heavy hydrocarbon molecules and to convert them into smaller species. As recent reports demonstrate (Fellows, 2018; Aliakbari and Stedman, 2018), limited pipeline capacity is a serious issue for Alberta. Heavy oil must be diluted with a solvent to reduce its viscosity for pipeline transport and the diluent occupies a significant fraction of the pipeline volume, reducing the pipeline capacity for the oil. Visbreaking is one option to reduce the viscosity of the oil so that the required volume of diluent can be reduced and more oil shipped through the same pipeline. The stability of mixtures of visbroken and diluent versus asphaltene precipitation must be understood to determine how much diluent can be added to the visbroken oil. This thesis focuses modeling asphaltene precipitation from visbroken fluids.

The Modified Regular Solution (MRS) Model is one approach used to model asphaltene precipitation (Hirschberg, 1984; Akbarzadeh *et al*., 2005). It is an activity coefficient model best suited for liquid-liquid equilibria. One advantage of this model is its ability to predict the effect of different solvents on asphaltene precipitation. The required inputs for the model are the molecular

weight, density, and solubility parameters of the components or pseudo-components making up the crude oil.

The MRS model has been used to predict the asphaltene precipitation from native crude oils, blends, and live oils over a range of temperatures and pressures (Alboudwarej *et al*., 2003; Akbarzadeh *et al*., 2004; Akbarzadeh *et al*., 2005; Tharanivasan, 2012). In these applications, the crude oils contained few light components and were characterized into pseudo-components based on a SARA (saturates, aromatics, resins, and asphaltenes) fractionation. Correlations were developed for the molecular weight, density, and solubility parameters of each of pseudo-component.

Powers (2014) extended the model to thermocracked and hydrocracked fluids. Two new factors were considered: 1) the presence of a significant fraction of light components; 2) the change in the pseudo-component properties after upgrading. The light components were separated from the crude oil by distillation and characterized separately. The distillation residue was characterized based on a SARA assay as before. New correlations were developed by Powers *et al*. (2016) and Yarranton *et al*. (2018) to estimate the properties of the reacted SARA fractions (*i.e.*, saturates, aromatics, resins and asphaltenes). However, these correlations were built using a limited dataset. There are no correlations available in the literature for the properties of the reacted distillates. Finally, the correlations were only tested on model solutions consisting of individual fractions, asphaltenes, and solvents. The model has not yet been extended to predict asphaltene stability in heavy residues or whole oil samples that have been subjected to a thermal cracking process. The aim of this thesis is to fill the gaps in the characterization of visbroken fluids and to extend the model to residues and whole oils.

1.1 Objectives

The goal of this study is extend the Modified Regular Solution model, using the characterization methodology previously proposed by Powers (2014), to model the asphaltene stability in visbroken oils. Specific objectives of the project are as follows:

1. Visbreak a Western Canadian bitumen in an in-house pilot plant to obtain a series of samples with different severities of visbreaking. Severity is a function of the reaction temperature and residence time.
2. Obtain SimDist assays for each sample and determine conversion which measures the material amount of residue (524°C+) that is converted to distillates.
3. Fractionate each sample into distillates and SARA fractions using Spinning Band distillation and an established SARA fractionation method.
4. Measure the density of the distillates from each fraction and determine their molecular weights from distillation data and existing correlations. Determine their average solubility parameters from solubility measurements of mixtures of asphaltenes, distillates, and *n*-heptane or whole oil and *n*-heptane.
5. Measure the molecular weight and density of the SARA fractions and determine their solubility parameter from solubility measurements of mixtures of asphaltenes, the fraction, and either *n*-heptane or toluene.
6. Identify the main variations on solubility parameters, density, and molecular weight of the visbroken fractions and whole oils as a function of conversion.
7. Test, adapt, and develop correlations to predict the pseudo-component properties of visbroken light and heavy oil fractions as a function of conversion.
8. Measure asphaltene yields from the series of visbroken heavy oils and their distillation residues diluted with *n*-heptane.
9. Model the stability of visbroken heavy oils using the Modified Regular Solution model and the correlations developed for each fraction. Modify the model as required.

1.2 Thesis Structure

This thesis is organized in six chapter as follows:

- Chapter 1 introduces the main problem, relevance and contribution of this research. The overall and specific objectives are specified.
- Chapter 2 presents the main topics directly related to this project such as petroleum chemistry, standard characterization methods based on distillation and SARA assays, and asphaltene characterization. Approaches commonly used for modeling asphaltene

precipitation or measuring asphaltene stability are discussed. Upgrading processes are reviewed with an emphasis on visbreaking processes.

- Chapter 3 outlines the experimental methods applied in this thesis. The in-house pilot plant apparatus and procedure for thermally cracking bitumen are described. The spinning band distillation, SARA fractionation, and property measurement methods are presented. Experimental procedures for performing solubility measurements on samples including crude oil fractions, vacuum residues, and whole reacted products are provided.
- Chapter 4 describes the Modified Regular Solution Model and the required input data for modeling asphaltene precipitation. The fluid characterization methodology is described including the assignment of pseudo-components and the determination of pseudo-component properties through experimental measurements or empirical correlations. Finally, the procedure to apply the model to different systems (asphaltene-solvent systems; asphaltene-solvent systems with a saturate, aromatic or distillate fraction; heavy residues with solvents, and whole oils with solvents) is specified.
- Chapter 5 presents the experimental data and modeling results. The change in the distillate and SARA fraction content and the change in the properties of each fraction with conversion is discussed. The data measured in this thesis is compared against the existing literature data (Power *et al.*, 2016 and Yarranton *et al.*, 2018). Updated and new correlations for the distillate and SARA fraction properties in reacted crude oils are proposed. The performance of the Modified Regular Solution model in predicting asphaltene yields from visbroken oils is assessed.
- Chapter 6 summarizes the major outcomes of the project and provides guidance for future work.

Chapter 2: Literature Review

In this chapter, the background material required for understanding and modeling the stability of reacted crude oils in terms of asphaltene precipitation is reviewed. First, the chemistry of crude oil is reviewed with a focus on asphaltenes. Crude oil phase behavior, characterization methods, and stability models are presented. Finally, oil upgrading processes and their impact on characterization and stability modeling are discussed.

2.1 Crude Oil Definition

Petroleum is generated by the sequential maturation of buried organic matter exposed to high temperature and pressure over a long period of time (Speight, 1998). Crude oil is a petroleum liquid and is a complex mixture of hydrocarbons. Typical ranges for the carbon, hydrogen, nitrogen, oxygen, sulfur content of crude oils are shown in Table 2.1 (Speight, 2007). Depending on the source organic material and maturation conditions, crude oil can be rich in light or heavy compounds. Crude oil is classified into conventional oil, heavy oil, and bitumen based on the oil's API gravity and viscosity, as shown in Table 2.2 (Gray, 1994).

Table 2.1 Elemental composition of petroleum (Speight, 2007).

Element	Composition (%)
Carbon	83-87
Hydrogen	10-14
Nitrogen	0.1-2
Oxygen	0.05-1.5
Sulfur	0.05-6
Metals (Ni, V)	<1000ppm

Table 2.2 UNITAR classification of crude oil (Gray, 1994).

Classification	Viscosity MPa·s	Density kg/m^3	API Gravity
Conventional Oil	$<10^2$	<900	>20°
Heavy Oil	10^2-10^5	900-1000	10°-19°
Bitumen	$>10^5$	>1000	<10°

2.2 Crude Oil Chemistry

Crude oil contains hundreds of thousands of molecules which makes it difficult to identify each individual compound (Rodgers and McKenna, 2011). Nonetheless, the hydrocarbon components of petroleum fall into the following three main chemical classes (Speight, 2002):

- Paraffins: saturated hydrocarbons including straight or branched chain alkanes (isoparaffins).
- Naphthenes (Cycloparaffins): saturated hydrocarbons with one or more rings and which may have paraffinic side chains.
- Aromatics: unsaturated hydrocarbons with one or more aromatic rings and which may have naphthenic rings and/or aliphatic side chains attached to them.

Most of those species, particularly the aromatics, may include heteroatoms (S, O, N) and metals such as nickel, vanadium, copper, and iron. Generally, as the molecular weight or boiling point of the petroleum fraction increases, the paraffin content decreases while the naphthenes, aromatics, heteroatom, and metal contents increase. Figure 2.1 illustrates how the complexity of the petroleum molecules increases with the molecular weight and boiling point (Altgelt and Boduszynsky, 1994).

Heavy oils and residues are often characterized based on chemical groupings; in particular, the saturates, aromatics, resins, and asphaltenes. Saturates are saturated hydrocarbons and include the paraffinic and naphthenic species. This fraction has the highest hydrogen to carbon ratio and the density varies between 800 to 900 kg/m^3 (León and Parra 2010). The molecular weight has been reported between 300 to 600 g/mol (Powers, 2014). Aromatics, resins, and asphaltenes are all aromatic species but with increasing size, density, aromaticity, polarity, heteroatom and metal content from aromatics to resins to asphaltenes. The densities and molecular weight of aromatics can range from 900 to 1050 kg/m^3 and from 300 to 900 g/mol, respectively (Powers, 2014; Ronningsen *et al.*, 1989). The density of resins is approximately 1000 kg/m^3 and their molecular weight varies between 500 to 1500 g/mol (León and Parra 2010). Asphaltenes are the most complex of the fractions and are discussed in more detail below.

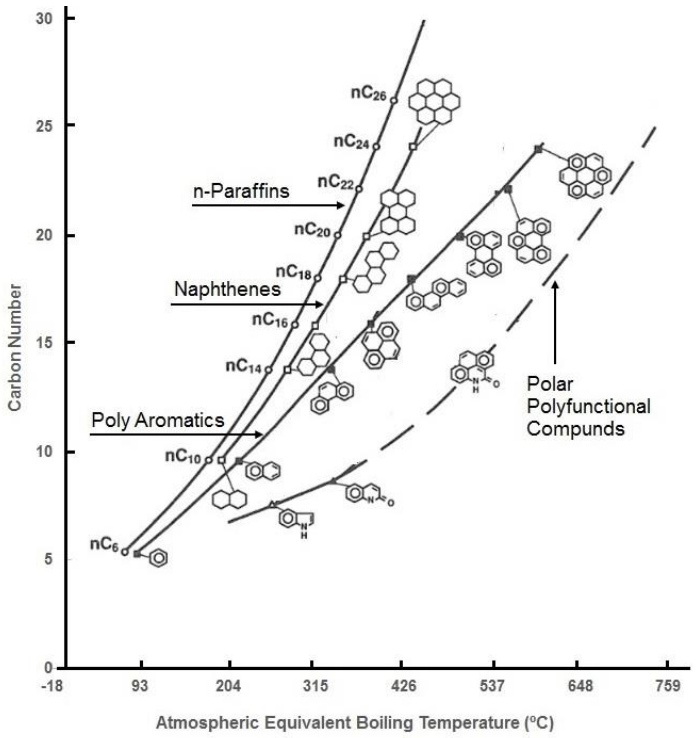

Figure 2.1 Relationship between carbon number, boiling point, and structure of chemical compounds in crude oil. Adapted from Altgelt and Boduszynsky, 1994.

2.2.1 Asphaltenes

By definition, asphaltenes are a solubility class that is insoluble in paraffinic solvents (usually *n*-pentane or *n*-heptane) but soluble in an aromatic solvent (usually toluene). Asphaltenes are in many ways the most troublesome part of the crude oil. They contribute significantly to oil viscosity, fouling, coke formation, and emulsion stabilization. They can precipitate from the oil leading to deposition and associated production losses. They are also one of the more challenging materials to study because they contain tens and perhaps hundreds of thousands of molecular species (Mckenna *et al*., 2013), some of which self-associate.

Asphaltenes are composed of polycondensed aromatics rings with aliphatic side chains. They have the highest molecular weight, density, aromaticity, polarity, heteroatom content, and metal content in a crude oil (Speight, 1998). The hydrogen to carbon ratio of different asphaltenes falls within a narrow range of 1.15±0.05% (Speight, 1991). Nitrogen is found in heterocyclic species, mostly pyrroles, with total nitrogen contents in the asphaltenes from 65 to 87% (Mitra-Kirtley *et al*.,

1993). Oxygen is present in phenolic, carboxylic, and ketonic groups with total oxygen contents from 0.3 to 4.9% (Speight, 2004; Petersen *et al*., 1974; Speight and Moschopedis, 1981). Sulfur is present as thiophenes as well as in aliphatic structures and oxidized forms with total sulfur contents from 0.04% for light crude oil to 5% for heavy crude oil (Speight and Pancirov, 1984; Speight, 2007). Asphaltenes also contain compounds combined with metals such as nickel, iron, vanadium, and copper, typically with a total metal concentration below 1000 ppm (Riazi, 2005).

The structure of asphaltenes is widely debated and difficult to determine due to their polydispersity. Two main structures have been postulated: the archipelago structure (Figure 2.2a) and the continent structure (Figure 2.2b). The archipelago structure consists of small aromatic groups (up to four rings) which are connected to each other by aliphatic chains with carbon numbers up to 24 (Murgich, 2003; Zhang *et al.*, 2007; Powers, 2014). The continent structure is aromatic core (usually consisting of more than seven rings) with a periphery of aliphatic chains (Kuznicki *et al*., 2009; Mullins, 2008; Murgich, 2003; Sheremata *et al*., 2004). Several studies of asphaltenes behaviour and association suggest that both structures may co-exist within asphaltenes (Gray *et al*., 2011; Mullins *et al*., 2012).

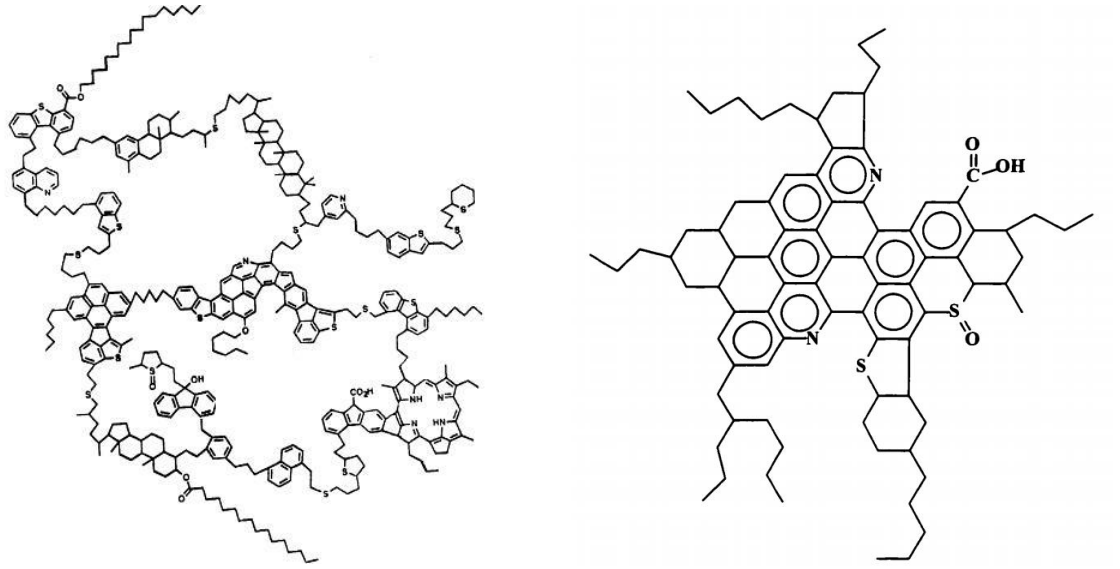

Figure 2.2 Hypothetical asphaltene structures: a) Archipelago: $C_{84}H_{100}N_2S_2O_3$ with a H/C ratio of 1.19 and a molecular weight of 1276 g/mol (Dickie and Yen 1967; Mullins 2008); b) Continent: $C_{412}H_{509}S_{17}O_9N_7$ with a H/C ratio of 1.23 and a molecular weight of 6239 g/mol (Murgich, Abanero, and Strausz 1999).

Asphaltene self-association has been observed with a number of techniques including molecular weight measurements such as vapor pressure osmometry (Yarranton *et al.*, 2000), interfacial tension (Yarranton *et al*., 2013; Yarranton *et al*., 2000), small-angle X-ray and neutron scattering measurements (Barré *et al*., 2009; Xu *et al.*, 1995; Ravey *et al*., 1988; Overfield *et al.*, 1989; Hoepfner, 2013, Eyssautier *et al*., 2011) differential scanning calorimetry (Andersen and Birdi, 1991) and dielectric spectroscopy (Maruska and Rao, 1987). The apparent molecular weight of asphaltenes increases with asphaltene concentration (Moschopedis *et al*., 1976; Sztukowski *et al.*, 2003) consistent with self- association.

Asphaltenes appear to start forming nanoaggregates at concentrations lower than 50 µg/ml (McKenna *et al*., 2013). The average nanoaggregate molecular weight in solution with toluene appears to consist of two to six monomers per aggregate (Yarranton, 2005) although they may range in size up to 30,000 g/mol (Barrera *et al.*, 2013; Yarranton *et al*., 2013; Yarranton, 2005; McKenna *et al*., 2013) or even 100,000 g/mol (Xu *et al*., 1995). The average molecular weight of asphaltene monomer is now thought to be on the order of 800 ± 500 g/mol (Mullins, 2008; Mullins, 2011; Yarranton *et al*., 2013; McKenna *et al*., 2013).

Since asphaltenes consist of many species and self-associate, an asphaltene fraction has a wide distribution of properties. The two properties of interest in this thesis, other than molecular weight, are density and solubility parameter. The density distribution of asphaltenes ranges from 1050 to 1250 kg/m³ (Powers, 2014; Barrera, 2012; Elsharkawy *et al.*, 2008). Average densities of asphaltenes from different sources vary less, typically from 1130 to 1200 kg/m³ (Akbarzadeh *et al*., 2004). Recently, Powers *et al*. (2016) reported asphaltenes densities from thermocracked, insitu-converted, and hydrocracked oils ranging from 1120 to 1250 kg/m³. Asphaltene solubility parameters are determined indirectly by modeling asphaltene precipitation data using regular solution based theory models (Akbarzadeh *et al*., 2004; Akbarzadeh *et al*., 2005). The solubility parameters have been reported in the ranges of 19 to 22 $MPa^{0.5}$ (Andersen, 1999; Laux, 1997) and 18 to 24 $MPa^{0.5}$ (Speight, 2007). Powers *et al*. (2016) determined the solubility parameters from native and reacted asphaltenes to range from 19.95 to 21.5 and 20.15 to 23.6 respectively.

2.3 Asphaltene Precipitation

In the petroleum industry, asphaltene precipitation is one of the most challenging issues encountered in both upstream and downstream processes. Asphaltenes can precipitate when the temperature, pressure or composition changes occurs leading to deposition and fouling in wellbores, reservoirs, surface facilities and refinery equipment (Powers *et al*., 2016; Leontaritis *et al*., 1989, Hammami *et al*., 2000). For example, this phenomenon can be observed during the depressurization of live oils, especially for those with a high concentration of light hydrocarbons. As the oil is depressurized, the molar volume of gases and light ends tend to increase significantly reducing the oil's ability to solubilize asphaltenes (Tharanivasan *et al*., 2011; Joshi *et al*., 2001). Another example, is asphaltene precipitation from oils diluted with a paraffinic solvent or other incompatible fluid such as carbon dioxide. In some cases, such as solvent deasphalting and paraffinic froth treatment processes, the asphaltenes are precipitated deliberately. In other cases, such as refinery blending, dilution of heavy oil for transportation, and batch pipeline operations, the precipitation is undesirable.

Figure 2.3 shows the amount of asphaltene precipitation from a heavy oil when titrated with n-pentane. In this case, precipitation is first observed at approximately 45 wt% n-pentane, defined here as the onset of precipitation. The yield of precipitate rises as the ratio of solvent to feedstock increases and then reaches a maximum. Yield is here defined as the mass of precipitated asphaltenes divided by the mass of crude oil in the feed. The yield decreases significantly as the carbon number of the n-alkane solvent increases from 3 to 7 but approaches an asymptotic value above a carbon number of 8, Figure 2.4. Since the asphaltenes are not a homogeneous material, the composition of the asphaltenes depends on the yield; the lower the asphaltene yield, the higher the aromaticity and heteroatom content of the precipitated asphaltenes (Speight, 1994; Powers, 2014).

Asphaltene solubility increases as the temperature rises to approximately 100ºC (Akbarzadeh *et al*., 2005; Hu and Guo, 2001). Based on a limited set of data, Andersen *et al*., (1998) found that asphaltenes can be less soluble at temperatures above 100ºC. On the other hand, Johnston *et al*., (2017) found that the solubility of asphaltenes in n-pentane diluted bitumen slightly decreased

above 130ºC. Johnston also found that asphaltene solubility increased slightly with increasing pressure.

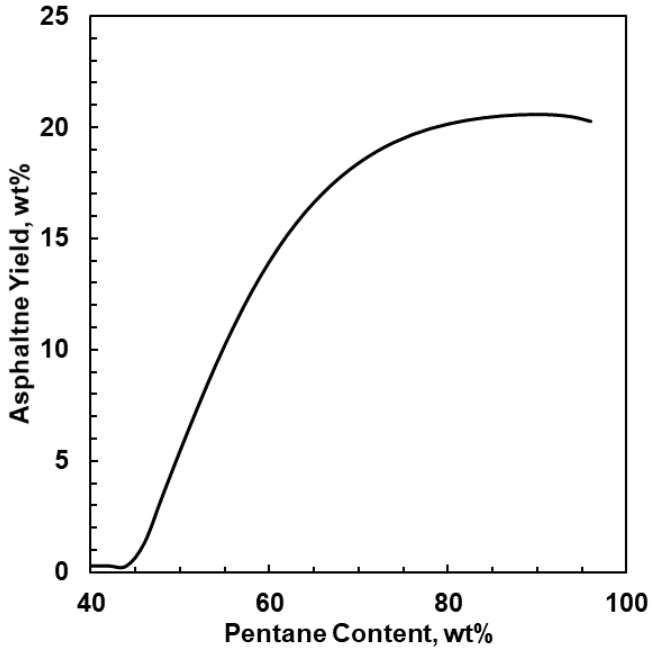

Figure 2.3 Variation of asphaltene yield with amount of *n*-pentane added for the Athabasca Bitumen Sample (WC-B-A3).

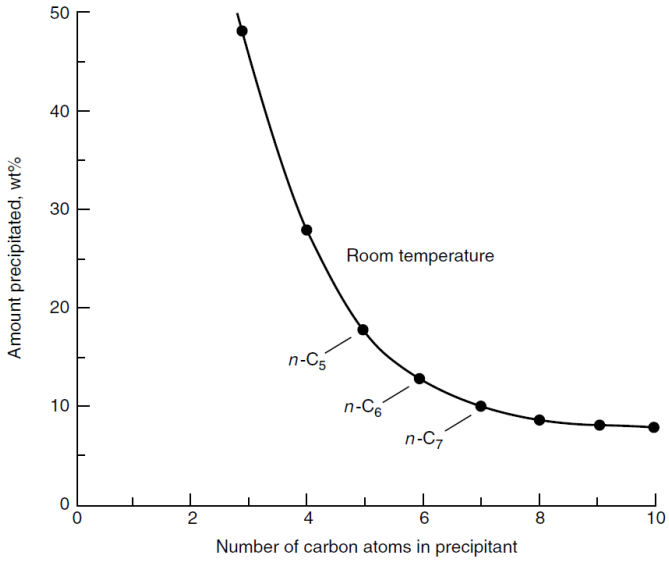

Figure 2.4 Change in asphaltene yield with carbon number of paraffin used (Adapted from Speight, 2007).

2.4 Crude Oil Characterization and Assays

In order to model the phase behavior and reactions involved in upgrading, the feedstocks and corresponding products are characterized into a set of components and pseudo-components that represent the distribution of properties and sometimes the distribution of molecules within the oils. For phase behavior modeling, the fluid is often characterized into boiling point cuts based on a distillation assay. The physical and critical properties required for the phase behavior model are determined from correlations and a limited number of property measurements such as the average density of the oil (Whitson and Brule, 2000; Riazi, 2015). For regular solution models of asphaltene precipitation, the non-distillable fraction of the oil is often divided into SARA (saturates, aromatics, resins, and asphaltenes) fractions (Akbarzadeh *et al*., 2004). For reaction modeling, the most rigorous approach is to divide the oil into representative molecule compounds each representing a reactant or product in a set of defined reaction pathways and each with its set of physical and critical properties (Wei *et al*., 2008). However, this approach requires a detailed characterization of the oil usually based on high resolution mass spectrometry data.

The approach used in this thesis is intended to be compatible with the VMG process simulator (VMG 2017). The characterization in the simulator divides the fluid into pseudo-components equivalent to boiling point cuts and then further divides each boiling cut into SARA fractions. Representative molecules are assigned to each pseudo-component and then fed into a reaction model. In this thesis, the crude oil will be divided into distillate fractions (light components), and a residue which is further divided into SARA fractions (saturates, aromatics, resins, and asphaltenes). The two assays required for this approach are distillation and SARA fractionation, and each is discussed below.

2.4.1 Distillation Assays

A distillation assay measures the mass or volume of a liquid mixture (in this case crude oil) that is distilled as the temperature is increased. A typical distillation curve is shown in Figure 2.5. The amount of the oil that can be distilled is limited by the cracking temperature of the crude oil which is approximately 300°C (Carbognani *et al.*, 2007; Speight and Özün, 2002; Gray, 1994). However, the amount that boils at a given temperature can be increased by reducing the pressure and there

are a variety of distillation assays designed at different pressures for different types of oil. For example, a heavy oil requires a vacuum distillation while a light oil may only require an atmospheric distillation. In either case, the data are reported as *atmospheric true boiling points*; that is, the boiling point at atmospheric pressure from a distillation column with 15 to 100 theoretical plates at a reflux ratio of 1 to 5 or greater (Riazi, 2005). If the boiling points were measured with a different column and/or at sub-atmospheric pressure, they are converted to equivalent atmospheric temperature (AET) using well known interconversion methods (Maxwell and Bonnell, 1957; Myers and Fenske, 1955). The most common distillation assays are described below.

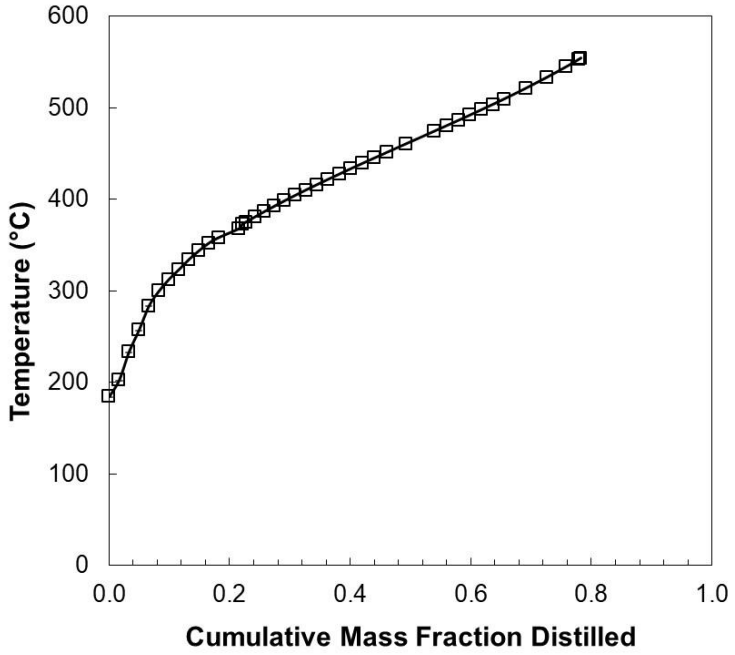

Figure 2.5 Example of a SBD distillation curve of the WC-B-A3 bitumen.

ASTM D86 is one of the oldest methods of measuring boiling points of petroleum fractions and is applicable for light products such as naphthas, kerosenes, gasoline, gas oils, and fuel oils. The assay is conducted at atmospheric pressure and the sample is distilled until 250°C. Even though the assay is performed at atmospheric pressure, the column does not meet the true boiling point

standard and the measured boiling points are interconverted to the equivalent atmospheric temperature (AET) using a correlation proposed by Riazi (2005).

ASTM D1160 was developed to extend the application of ASTM D86 to heavier petroleum compounds (heavy gas oils). The distillations are carried out at reduced pressure from 1 to 760 mmHg and the distillation data is normally reported at 1, 2, 10, or 50 mmHg. The separation is equivalent to one theoretical plate and the final boiling point is equivalent to approximately 400ºC AET. The Maxwell and Bonnell correlation (1957) is used to convert the actual distillation temperature to AET. A two-step procedure is used to convert the AET distillation curves to TBP first at 10 mmHg and then at 760 mmHg (Edmister and Okamoto, 1959; Riazi, 2005).

ASTM D2892 provides true boiling point distillation data in a fractionating column with 14 to 18 theoretical plates and a reflux ratio of 5:1. The sample is distilled to a maximum AET of 400°C. This test method is not applicable to very light naphthas and mixtures with initial boiling points above 400ºC. When vacuum is used, the vapor temperatures are converted to AET using Maxwell and Bonnell (1957) correlations.

ASTM D5236 is an extension of ASTM D2892 that is applicable for distilling heavy hydrocarbon mixtures with an initial boiling point greater than 150ºC, such as heavy crude oils, distillates, residues, and synthetic mixtures. The crude oil is distilled at absolute pressures between 0.1 to 50 mmHg reaching AET up to approximately 565ºC. If the sample has low boiling material, the lighter components are distilled using ASTM D2892 before the ASTM D5236 is run. Hence, a large volume sample (4 L) is required to run the distillation. The Maxwell and Bonnell correlation (1957) is used to convert the actual distillation temperature to AET. The drawback of this method is that it does not have the same fractionation capabilities as ASTM D2892; therefore, the TBP temperatures are higher than they would be if a more efficient fractionation was performed.

Spinning Band Distillation (SBD) includes a spiral spinning band which rotates at high speed to increase liquid-vapor contact and can reach efficiencies equivalent to 50 theoretical plates in a 100 cm length column. The reflux ratio is typically set at 5:1 to simulate ASTM D2892 and AET up to

450ºC are achievable. The vapor temperatures are converted to AET using the Maxwell and Bonnell (1957) correlations.

Short path distillation is a proposed ASTM method for molecular distillation. The separation is carried out at 0.0001 kPa to approximately 650ºC AET. The sample flows at a constant rate over a hot surface at high vacuum, where temperature and pressure are fixed. The system is equipped with rollers to assure a thin film on the wall and the collector device is closely placed so the evaporated molecules condense in the cold finger. Only one fraction and a residue are obtained in this distillation method. Simulated distillations are performed to determine the TBP temperatures of the two fractions.

Simulated distillation (SimDist) is a simulated distillation curve generated from gas chromatography measurements. The method is described in ASTM D2887 and is applicable to petroleum products having a final boiling point of 538°C. The hydrocarbon components of the sample elute through a nonpolar packed or open tubular column in order of increasing boiling point. The column temperature is increased at a linear rate and the components are detected by a flame ionization or a thermal conductivity detector. The boiling points reported by this test method are equivalent to those obtained by true boiling point distillation. Some modifications and adaptations have been made depending on the characteristics of the sample (ASTM D5307, D6352, and D7169). ASTM D7169 estimates the boiling point distribution of crude oils and residues by applying high temperature gas chromatography (up to 720°C). Although GC analysis provides fast and economical results, this technique requires calibration in order to identify the components and the equivalent boiling points. Calibration is based on the retention time of the normal paraffins and their respective boiling points. The interpretation of the results for a heavy oil or bitumen must be done with caution because these samples are known to have large amounts of aromatic compounds. The boiling point of a given paraffin may not correspond to that of the aromatic fraction that elutes at the same time.

2.4.2 SARA Fractionation

SARA fractionation (ASTM D2007 and ASTM D4124) is the most common standard method used in the petroleum industry for separation of heavy oil into compounds classes (Fan and Buckley, 2002); in particular, saturates, aromatics, resins, and asphaltenes. The fractions are separated based on solubility for the asphaltenes and adsorption for the other fractions. Initially, the asphaltenes are removed from the crude oil using a paraffinic solvent (*n*-pentane or *n*-heptane) leaving maltenes which are further fractionated using liquid chromatography. The mixture of maltenes and solvent is passed through two packed columns. The first column contains Attapulgus clay and adsorbs the resins. The second column contains silica or alumina gel and adsorbs the aromatics. The saturates pass through without adsorbing on either column. The resins and aromatics are eluted from the columns using polar solvents. The SARA fractions each consist of compounds of similar chemical family as was described previously.

2.5 Crude Oil Stability and Asphaltene Precipitation Models

Crude oil stability refers to the ability of the oil to dissolve or disperse the asphaltenes within the oil. An unstable oil precipitates asphaltenes. The stability of crude oil can be perturbed by changes in temperature, pressure, composition or chemical alteration of any of its constituents. Hence, it is important to understand and model crude oil stability to optimize refinery processes. There are two approaches to assessing crude oil stability: 1) direct assessment based on a stability test; 2) prediction using an asphaltene precipitation model. This thesis focuses on asphaltene precipitation models.

Direct measurement methods include the spot test, the p-value, the colloidal instability index (CII), the flocculation ratio, and the compatibility index (Nazar and Bayandory 2008; Guzman *et al*., 2017; Östlund *et al*., 2003). The spot test is an optical method useful for an initial identification of crude oil stability. The p-value test determines the total amount of precipitant (*n*-heptane) required to destabilize the asphaltenes. The CII method considers the crude oil to be a colloidal system composed by SARA fractions. The CII parameter is the mass fraction of asphaltene and saturates (measure of incompatibility) divided by the mass fraction of aromatics and resins (measure of stabilizing ability). The flocculation ratio method involves two parameters: the flocculation ratio

(FR) is the volume fraction of titrant solvent at the onset of asphaltene precipitation and the dilution ratio (X) is the ratio of the volume of precipitant to the volume of oil sample. A plot of FR versus 1/X is a straight line with an intercept at the maximum flocculation ratio which is related to the solubility of the asphaltenes (Andersen, 1999). Wiehe (2000) developed the compatability index method based on two parameters, the insolubility number (I_N) and the solubility blend number (S_{BN}). The first parameter represents the degree of asphaltene solubility and the second one is related to the crude oil capacity for solubilizing asphaltenes. The ratio between (S_{BN}/I_N) is used to predict the pure oil stability. Details of these and other methods can be found elsewhere (Asomaning, 2003; Rogel *et al*., 2003).

There are several approaches to modeling asphaltene precipitation which fall mainly into two categories: 1) colloidal models, and 2) thermodynamic models. The colloidal models assume that asphaltenes are colloidal particles dispersed in the oil and that each particle is stabilized by resins which are adsorbed on their surface or concentrated locally around the colloid (Leontaritis, 1989; Pan and Firoozabadi, 1998). It is believed that resins are responsible for keeping the asphaltenes in a colloidal dispersion and the precipitation of asphaltenes occur when the resins are stripped from the colloid. The chemical equilibrium criteria is established based on the chemical potential of the resins in both oil and asphaltenes phases. Asphaltene precipitation is considered to be irreversible. Precipitation models based on this approach are not predictive and have only been tested on limited data.

The second approach assumes that asphaltenes behave as macromolecules and are part of a non-ideal mixture. Their precipitation is modeled as a liquid-solid or liquid-liquid phase transition (Akbarzadeh *et al*., 2005; Chung, 1992; Ting *et al*., 2003; Gupta, 1986; Hirschberg *et al*., 1984; Gonzalez, 2008; Vargas *et al*., 2009; Arya *et al*., 2016). Asphaltene precipitation is considered to be reversible. Thermodynamics models have proven successful in fitting and predicting asphaltene precipitation over a wide range of conditions. The two main thermodynamic models applied to asphaltene precipitation are the regular solution model and equations of state.

The regular solution approach is an activity model that takes into account two contributions: 1) the enthalpy of mixing based on the Scatchard-Hildenbrand theory (Scatchard, 1949; Hildebrand, 1949), and; 2) the entropy of mixing molecules (monodisperse polymers) of different sizes based on Flory-Huggins theory (Flory, 1941; Huggins, 1941). This model assumes that excess volume of mixing is negligible and has been successfully applied to predict the onset of asphaltene precipitation. The model has successfully predicted asphaltene precipitation from bitumen and heavy oils diluted with *n*-alkanes (Alboudwarej *et al*., 2003; Akbarzadeh *et al*., 2004; Akbarzadeh *et al*., 2005). Tharanivasan (2012) adapted the model for predicting the precipitation of asphaltenes in crude oil blends undergoing depressurization. Recently, Powers (2014) used the regular solution model to predict the asphaltene phase behavior in samples that undergo thermal cracking. Note, this model is limited to liquid-liquid or liquid-solid equilibria.

Equations of state (EOS) models describe the full phase equilibria and are well suited for process simulation. The cubic EOS perform such as the Peng-Robinson and Soave-Redlich-Kwong EOS perform well in predicting phase envelopes and for vapor-liquid equilibrium calculations of petroleum fluids. However, they provide poor predictions of asphaltene yields as has been shown by Castellanos-Díaz *et al.* (2011), Johnston (2017), and Mancilla-Polanco *et al.* (2017). The cubic plus association, CPA (Li and Firoozabadi, 2010; Arya *et al*., 2016, Arya *et al*., 2017) and statistical associating fluid theory, SAFT (Chapman *et al*., 1989, Ting *et al*., 2003; Vargas *et al*., 2009, Panuganti *et al*., 2013; AlHammadi *et al*., 2015) provide better predictions of asphaltene yields but have not been widely applied due to their complexity.

2.5 Crude Oil Refining

Petroleum refining involves the physical, chemical, and thermal separation of crude oil into fractions which are further processed using different separation and reaction steps to provide commercial petroleum products with low carbon to hydrogen ratios (Speight, 2007). The primary products of a refinery fall into three categories: 1) fuels such as gasoline, diesel, liquified gas, jet fuel, and kerosene; 2) lubricating oils, wax, grease, asphalt, and coke, and; 3) chemical industry feedstocks such as ethane, naphtha, propane, butane, ethylene, propylene, butadiene, benzene, toluene, and xylene (Speight, 2007).

The conversion of bitumen to lighter components, or distillates, requires the reduction of the boiling point and molecular weight of the feedstock. Distillation is the primary method used to refine petroleum. The crude oil is fed to the lower part of a distillation tower, the lighter fractions are recovered at the top of the column, distillation cuts are drawn at different stages, and a heavy residue is recovered at the bottom of the column. Distillates are further processed by other physical methods (Speight, 2002). The residue is thermally treated with one or more of the residue upgrading processes shown in Figure 2.6. These processes can be classified into carbon rejection or hydrogen addition processes.

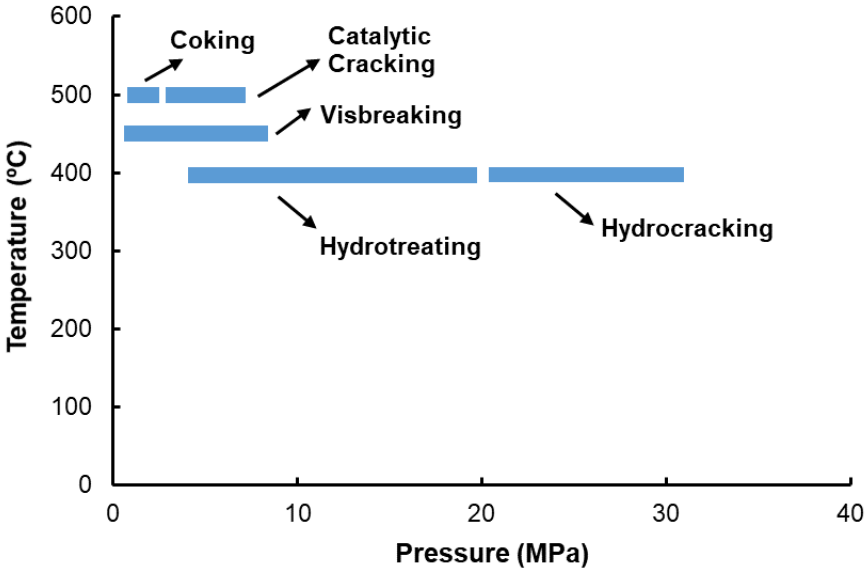

Figure 2.6 Operating ranges (temperature and pressure) for upgrading processes adapted from Speight, 1998.

2.5.1 Carbon Rejection Processes

Carbon rejection processes consist of thermally cracking heavy feedstocks at moderate pressure so that the hydrogen is redistributed among the components. Hydrogen is transferred from larger to lighter molecules and, consequently, the carbon to hydrogen ratio decreases (Gupta *et al.*, 2015). Carbon rejection includes the following technologies: visbreaking, steam cracking, fluid catalytic cracking, and coking. Since visbreaking is the focus of this thesis, it is described in more detail.

Visbreaking:

The visbreaking process is one of the oldest refinery technology and is a non-catalytic thermal cracking process where the heavy crude oil is subjected to relatively mild temperatures at low residence times. Visbreaking is mainly used to process atmospheric and vacuum residues. The main objective is to reduce the viscosity of these heavy residues in order to make them usable as heavy fuel oils. The reduction of viscosity also minimizes the amount of cutter stock required for residue dilution to meet fuel oil density and viscosity specifications (Speight, 2002). Usually, the diluent employed for this purpose is a standard fuel oil and the amount of reduced diluent is defined as the "fuel gain". The fuel gain is calculated as the difference between the initial volume of solvent required to dilute the unreacted oil and the volume needed to dilute the visbroken product (Pereira-Almao, 2017).

Visbreaking can bring significant cost savings for midstream processes by reducing the diluent requirements and the operating costs related to pumping. Lokhandwala *et al*. (2012) studied the effect of the visbreaking process along the whole heavy oil value chain based on a Cold Lake bitumen feedstock partially upgraded at 300ºC for 5 minutes. They simulated the visbreaking process using Aspen HYSYS to obtain the product properties and applied a blending model to calculate the volume of diluent required to meet the pipeline specifications. Finally, they modeled the pipeline network to evaluate the energy and cost impact of transporting a fluid with a lower density and viscosity. They found that visbreaking significantly reduced the diluent cost and allowed the transportation of larger volumes providing short payback periods for the initial capital investment. Another case study was conducted by Ventech Corporation (2005) in a Colombia oil field. A heavy oil with an API of 10.9 was subjected to a visbreaking process and it was reported that the API of the sample was increased enough to eliminate the need for diluent.

Visbreaking involves the thermal cracking of long hydrocarbon molecules such as alkanes and alkenes into smaller molecules and stripping off aliphatic side chains from highly aromatic compounds such as resins and asphaltenes. The main reactions which occur during visbreaking processes are side chain fragmentation (dealkylation), splitting of carbon-carbon bonds in the aliphatic chains, dimerization, dehydrogenation of naphthenes to form aromatics, condensation of

aromatic molecules to form polyaromatics, and condensation of aliphatics to form aromatics. These thermal cracking reactions are highly endothermic and proceed according to a free radical mechanism (Pierre, 2001; Fahim *et al*., 2010). This chemical transformation reduces the viscosity of the feedstock and produces some middle distillates (Joshi *et al*., 2008).

In the visbreaking process, the most important variables are the feedstock type, pressure, temperature, and residence time (Speight, 2012). The nature of the feedstock sets the reaction pathways and therefore impacts conversion, stability, product yield, and coking tendency. Visbreaking reactions are endothermic and require heat to proceed; the higher the temperature, the more the oil reacts. The residence time is the period at which the feedstock is exposed to the reaction temperature; the longer the residence time, the more the oil reacts. The main role of pressure on a visbreaking process is to keep the fluid in the liquid phase. At typical operating pressures for visbreakers, pressure has a minor effect on the C-C bond scission reactions but overall does not contribute significantly to the reaction of the crude oil (Joshi *et al*., 2008).

The extent or "severity" of the reaction is measured in terms of conversion and is mainly a function of temperature and residence time. The conversion is calculated as the difference between the weight percent of vacuum residue in the feedstock (+524°C) and the weight percent of the distillate products in the reacted sample (-524°C) divided by the 524°C+ content of the vacuum residue in the feedstock. The 524+ conversion is commonly known as a pitch conversion (Rahimi *et al*., 2005; Gray, 2015).

Two types of visbreaker units are used by the industry, soaker and coil visbreakers. In a soaker visbreaker, the feedstock is heated in a furnace and is then sent to a reaction vessel (soaker) for additional reaction time, Figure 2.7. Most of the conversion occurs in the soaker drum which is placed right after the furnace in order to achieve higher conversions. Finally, the reacted oil is fractionated into gas, naphtha, diesel, and the visbreaker residue. Soaker visbreaker processes use lower temperatures (430-450°C) and longer reaction times (10-30 minutes) than coil visbreakers. The advantages of this process are lower energy consumption and longer operating times before having to shut down the process to remove the coke from the furnace.

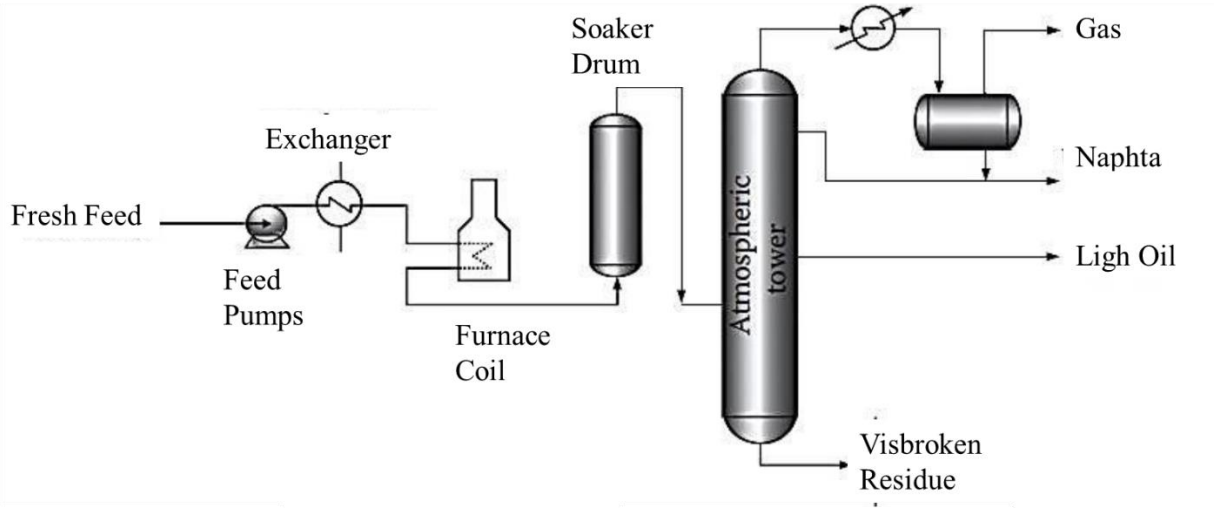

Figure 2.7 Schematic of soaker visbreaker (adapted from Wang, 2013).

The coil visbreaker operates at a relatively high temperature (470-500°C) and short residence time (from seconds to a few minutes). The process is similar to the soaker visbreaker shown in Figure 2.7; the only difference is that the coil visbreaker does not use a soaker and the conversion only takes place in the furnace. The products exiting the furnace are quenched to stop the cracking reactions and then they are separated in the fractionator. The coil cracking technology has the advantage of generating a slightly more stable visbreaker products and producing heavy cuts that boil in the vacuum gas oil range (Fahim *et al*., 2010).

Both visbreaker units (soaker and coil) are typically operated at sufficient pressure to maintain the fluid in the liquid phase. The pressure can range from 0.34 to 5 MPa and is an important operating variable which depends on the degree of vaporization of the feedstock and the residence time desired (Gray, 2015; Leprince, 2001; Rana *et al*., 2007; Speight, 2012).

The main limitation of any visbreaking process is the formation of coke that is triggered by the liquid-liquid phase separation of asphaltenes (Wiehe, 2008). As the conversion proceeds, the asphaltenes becomes more aromatic due to the removal of alkyl side chains. The reacted asphaltenes tend to be less soluble in the reacting medium and when the solubility limit is reached,

they come out from the solution. Through a sequence of polymerization and condensation reactions, the reacted asphaltenes combine with each other to form coke which forms a new phase that is rich in carbon and lean in hydrogen (Speight, 1998). Therefore, the maximum operating condition of a visbreaker unit is constrained by the stability of the bottom products and coke formation. It has been reported that at moderate severities conditions (400-430°C), conversions between 10-20% can be achieved without having considerable formation of coke (Quignard and Kressman, 2011). The tendency for coke formation can be measured through the Condrason Carbon Residue (CCR) and it has been found that feedstocks with high content of asphaltenes and with high CCR tend to produce higher coke yields (Joshi *et al*., 2008).

Coking

Coking is a severe process used to convert nondistillable fractions into lower boiling point products. Typically, the feedstock is a heavy residue and the main products are gases, fuel oil, naphtha, gas oil, and coke. It operates in semi-batch mode and uses longer reaction times compared to other upgrading technologies. The use of two or more reaction vessels makes it possible to operate in a semi-continuous mode without interrupting the process (Speight, 2007). The tendency to form coke is proportional to the Conradson carbon residue of the feed. The coke is triggered by the precipitation of asphaltenes which are highly cross-linked after undergoing polymerization reactions (Pierre, 2001). There are several coking processes including fluid coking, delayed coking, and flexicoking; details can be found elsewhere (Pierre, 2001; Speight, 1998).

Fluid Catalytic Cracking

Fluid catalytic cracking employs a catalyst to improve the process efficiency. Typical operating conditions are temperatures from 480 to 540°C and pressures between 0.07 to 0.14 MPa (Speight, 2007). Typical feedstocks are vacuum or atmospheric gas oils which are substantially converted to gasoline and lower-boiling products. The process has three main steps: a) the feedstock is reacted with the catalyst; 2) the catalyst is reactivated by burning off coke at high temperatures and then recirculated to the reactor; 3) the produced hydrocarbons are further refined into liquid petroleum gas, gasoline, light cycle oil and heavy cycle oil. The presence of the catalyst improves

the selectivity of certain cracking reactions to produce higher-octane hydrocarbon products. Some processes use high-activity hydrodesulfurization catalysts which favor the production of low-sulfur products, while others use catalysts designed to inhibit coke formation and promote demetallization (Sadeghbeigi, 2012).

2.5.2 Hydrogen Addition Processes

In hydrogen addition processes, the heavy crude oil reacts in the presence of hydrogen resulting in an overall increase in the hydrogen to carbon ratio. The reaction pathway changes significantly when hydrogen is continuously injected into the process. As usual, aliphatic side chains are thermally cracked and then form light hydrocarbons. Aromatics can be hydrogenated at lower temperatures and the presence of hydrogen radicals can terminate polymerization reactions and supress coke formation. The process is carried out at high pressure (above 6.9 MPa) and at temperatures up to 470ºC. Usually, a cobalt-molybdenum-alumina catalyst is used by industry to remove some of the nitrogen and most of the sulfur present in the feedstock (Speight, 1998).

The hydrogen addition process involves a reaction in the vapor phase or in a mixed-phase depending on the application. Some of the advantages of this process are sulfur removal, reduction in the level of corrosion, improvement in the catalytic cracking quality of the gas oil fraction, minimization of coke formation, and achieving higher conversions. Heteroatoms such as sulfur, nitrogen, and oxygen undergo reaction with hydrogen to remove hydrogen sulfide, ammonia, and water, respectively. Unstable compounds which can form gums or insoluble materials are transformed into more stable compounds (Speight, 2007). There are a variety hydroprocessing technologies which are briefly discussed below.

Hydroconversion

Hydroconversion processes applies temperatures over 410ºC to initiate the thermal rupture of the chemical bonds. The addition of hydrogen helps to inhibit the coke formation and the presence of a catalyst promotes reactions such as hydrogenation of aromatics and removal of sulfur (Gray, 2015). Generally, the feedstock is preheated and mixed with hydrogen at a specified ratio. The

reactions take place in the reactor where the residence time can vary from 1-10 hours. Then, the hydroprocessed products are passed into a series of liquid and vapor separators (Speight, 1998).

Hydrotreating

Hydrotreating processes run at temperatures below 410ºC to minimize thermocracking and instead use hydrogen and a solid catalyst to remove sulfur and nitrogen from distillate feeds and to hydrogenate aromatics and olefins. These processes operate with cleaner feeds, at lower temperature, and at higher hydrogen partial pressures than other hydroconversion processes in order to maximize the life of the catalyst (Gray, 2015). Hydrotreating catalysts are a combination of nickel, cobalt, molybdenum and tungsten on an alumina support. The operating conditions of the hydrotreating processes are temperature, pressure, catalyst loading, hydrogen partial pressure and feed flow rate (Fahim *et al.*, 2010).

Hydrocracking

Hydrocracking is a catalytic process in which high molecular weight compounds are hydrogenated and converted into lower molecular weight products. More severe conditions than hydrotreating are required to convert these feeds. A continuous high-pressure hydrogen stream is fed to the reactor and a bifunctional catalyst is used to convert gas-oil or deasphalted oil. The catalyst is composed of a metallic part which promotes hydrogenation and an acid part which favors cracking. Hydrogenation removes impurities such as nitrogen, sulphur and metals. Cracking breaks the chemical bonds and the formed unsaturated products are subsequently hydrogenated into stable compounds (Fahim *et al.*, 2010).

Usually hydrocracking units employ two stages: 1) the feedstock is hydrotreated to reduce sulfur and nitrogen levels, and; 2) the conversion is completed (Gray, 2015).

2.6 Thermal Cracking Effects on Petroleum Oil Fractions

When crude oil is subjected to temperatures above 350ºC, the petroleum fractions undergo a series of thermal cracking reactions leading to chemical changes of the *in-situ* species and the formation of new compounds. The saturate fraction is mostly converted to shorter paraffinic chains, gas, and olefins by free radical mechanisms. Olefins may continue cracking to produce smaller olefins and

diolefins which are highly reactive and can cause stability problems due to the formation of gums (Gray, 2015).

Some investigations have shown that the aromatic fraction has the potential to form smaller molecules including saturates through de-alkylation reactions. They can also polymerize to generate larger aromatic molecules and small amounts of coke (Dawson *et al*., 1989). The reaction sequence is shown in Figure 2.8.

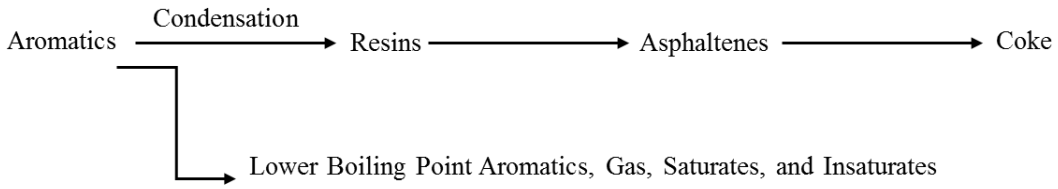

Figure 2.8 Generated products from aromatic fraction (Adapted from Speight, 1998).

It has been demonstrated that resins and asphaltenes fractions are responsible for promoting coke formation which is the main limitation of thermal cracking processes (Speight, 1998). Coke yield can vary from 25 to 60% by weight (Speight, 1999). During thermal conversion, these polynuclear aromatic molecules are stripped off alkyl moieties and become more aromatic. As the reaction proceeds, the denuded aromatics polymerize to form larger polynuclear aromatic systems of higher molecular weight. In addition, volatile species (paraffins and olefins) are produced by the thermolysis of aromatic-alkyl systems (Speight, 1987). As condensed aromatic compounds are formed, they are combined to form higher molecular weight species by a sequence of polymerization and condensation steps. This leads to a phase separation of asphaltenes which triggers the formation of coke (Magaril *et al*., 1968; Levinter, 1966). The reaction scheme is summarized in Figure 2.9.

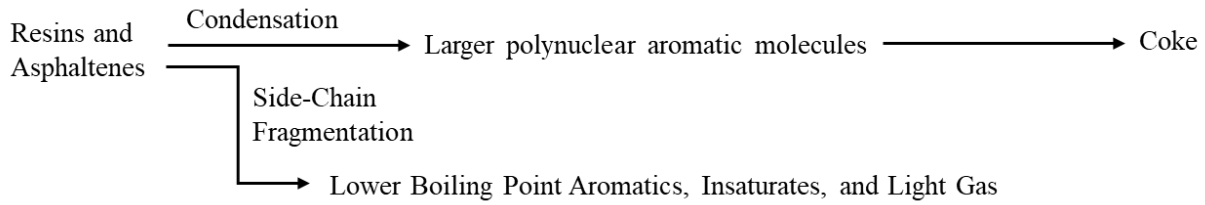

Figure 2.9 Products generated from resins and asphaltene fractions (Adapted from Speight, 1998)

Some studies have investigated the influence of visbreaking processes on the physicochemical and structural characteristics of visbroken products. Wiehe (1992) investigated the physical properties of eight different residues and their corresponding reacted petroleum fractions. He found that each solubility class (SARA fraction) could be clearly distinguished based on its molecular weight and hydrogen content. All fractions showed a reduction in molecular weight consistent with the cracking of alkyl and paraffinic fragments as was also reported by Fainberg *et al*., 1996. The heavy aromatic fractions reported a decrease in hydrogen content indicating higher aromaticity. In terms of solubility, the reacted asphaltenes were less soluble due to size growth and reduction in hydrogen content.

Rogel (1997) studied the solubility parameter distributions of asphaltenes in residues before and after visbreaking. She found that, as the severity of the process increased, higher solubility parameter molecules were created and there was a significant decrease in the amount of low solubility parameter asphaltene molecules. Similar observations were found by Casalini *et al*. (1990) for 10 visbroken residues from different origins. As has been reported elsewhere (Speight, 1999), the hydrogen to carbon ratio varied inversely with the solubility parameter indicating that cracking of aliphatic chains produces asphaltene molecules with lower solubility.

Some authors have found that asphaltenes have less tendency to associate with conversion. Wiehe (1993) investigated the change in asphaltene association behavior with thermolysis reaction time. A Cold Lake vacuum residue was subjected to thermal cracking in a closed reactor at 400ºC under different reaction times. He found that reacted asphaltenes combined with each other to start forming coke and the residual asphaltenes had less tendency to self-associate.

Powers (2014) studied the effect of thermal and hydrocracking processes on the properties of saturates, aromatics, and resins fractions. She observed significant reduction in molecular weight for all fractions except for saturates which showed slight changes. A similar tendency was observed for density: density increased for the aromatic fractions while the density of saturates did not change considerably. However, there was no a clear trend found for the solubility parameters of saturates and aromatics with the conversion. Overall, although the effects of thermal cracking

reaction on stability and physical properties of reacted visbroken products have been studied, there are still few available data and correlations that can be used to predict crude oil stability.

Chapter 3: Experimental Methods

This chapter presents the experimental methods used in this thesis to prepare and characterize the feedstock and the reacted samples. The procedure used to thermally crack the crude oil samples is described. The characterization and property measurement procedures are provided including distillation assays, SARA fractionation, asphaltene precipitation, removal of toluene insolubles, solubility experiments, and density and molecular weight measurements.

3.1 Materials

One bitumen sample was examined in this thesis and is referred to as WC-B-A3. WC-B-A3 is an Athabasca bitumen from a SAGD process supplied by Japan Canada Oil Sands Ltd. (JACOS). As will be discussed later, the WC-B-A3 sample was thermally cracked at 950 psig (6.5 MPa) in an in-house continuous visbreaker pilot plant at the University of Calgary at five different severity conditions. The in-house visbreaker is described later.

The studied feed and cracked products are listed in Table 3.1. The conversion of the visbroken samples was calculated from SimDist data, based on the change in 524°C+ content according to the following equation (Rahimi *et al*., 2005):

$$Conversion = \frac{+524℃\ (feed) - 524 + ℃\ (\text{product})}{+524℃\ (feed)} \tag{3.1}$$

where $+524℃$ is the weight percent of the +524ºC boiling cut.

Table 3.1 Crude oil samples and nomenclature used in this thesis.

Sample	Reaction Conditions	Conversion (%)
WC-B-A3	Feed	-
WC-B-A3-VIS5A	6.5 MPa, 420ºC, 10 min	5.1
WC-B-A3-VIS5B	6.5 MPa, 430ºC, 10 min	5
WC-B-A3-VIS8	6.5 MPa, 440ºC, 10 min	8.1
WC-B-A3-VIS19	6.5 MPa, 430ºC, 20 min	19.3
WC-B-A3-VIS38	6.5 MPa, 440ºC, 20 min	38.1

ACS grade *n*-pentane, *n*-heptane, and toluene were purchased from VWR International LLC and were used in the asphaltene precipitation and fractionation, toluene insolubles removal, and solubility measurements discussed later. Asphaltene molecular weight measurements were performed with OmniSolve high purity toluene (99.99%) also obtained from VWR. Sucrose octaacetate (98%) and octacosane (99%) for vapor pressure osmometer calibrations were purchased from Sigma-Aldrich Chemical Company.

3.2 In House Lab Scale Visbreaker Pilot Plant

3.2.1 Apparatus

The continuous flow visbreaking bench pilot plant is shown in Figure 3.1 and has three main sections: feed filtering, the reactor, and product recovery. If required, the apparatus can also be configured to batch filter the feed as shown in Figure 3.2. Each section is described in detail below. The whole plant is controlled by a LabVIEW program that allows the user to set the temperatures, flow rates, pressures, and the operation of the pumps. The visbreaker bench plant can process 11 liters of bitumen sample operating in a continuous mode. The operating condition limits are: flow rates from 1 mL/min to 204 mL/min, temperatures from 300 to 500°C, and pressures up to 1300 psig (9 MPag).

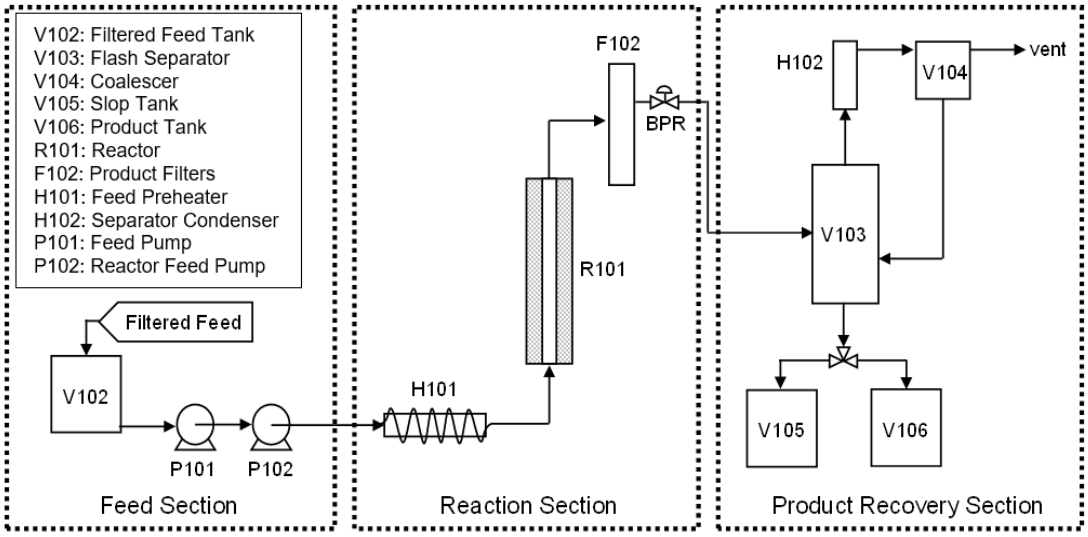

Figure 3.1 Schematic of the continuous visbreaking bench pilot plant.

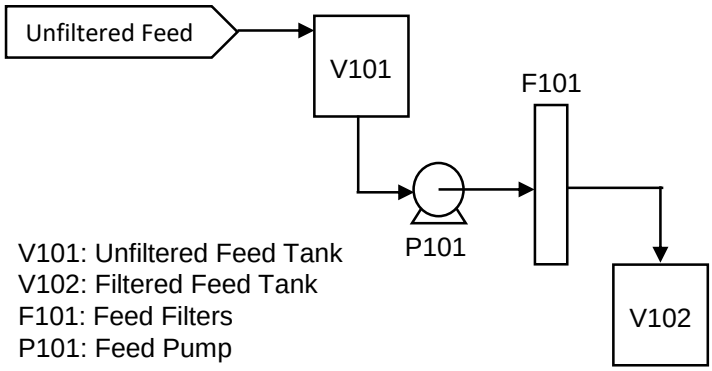

Figure 3.2 Schematic of the batch feed filtering system.

Feed Filtering System: The batch feed filtering system operates in a continuous mode and consists of two storage tanks, a feed pump, and parallel filters. Each component is described below:

- The Unfiltered Feed Tank (V101 in Figure 3.1) and Filtered Feed Tank (V102 in Figures 1 and 2) are 11 L stainless steel vessels equipped with a heating mantle (electrically heated from an external power source). The tanks are also equipped with a port through which nitrogen can be injected. An internal thermocouple is placed inside the tank to monitor the temperature of the feedstock and two wall thermocouples are used to control the heating mantle.
- The Filtered Feed Pump (P101) is a Liquiflo Model H3FL3333500000US 3-Series Magnetic Drive positive displacement pump equipped with a pressure relieve valve set at 150 psig (1 MPag).
- The filters (F101) are Porvair Filtration Group Model 6008 parallel filters each equipped with a filter cartridge and a Rosemount pressure transmitter with an operating range of 0 to 300 psig (2.1 MPag).
- The lines are all ¾ inch I.D. stainless steel pipe and are insulated and heated with Briskheat heating cables.

Feed Section:

The continuous feed section consists of a feed tank and two pumps as described below:

- The Filtered Feed Tank (V102) was described above.

- The Filtered Feed Pump (P101) is a Liquiflo Model H3FL3333500000US 3-Series Magnetic Drive positive displacement pump equipped with a pressure relieve valve set at 150 psig (1 MPag). This pump provides the required head pressure for the Reactor Feed Pump.
- The reactor feed pump (P102) is a Teledyne Isco 500HV high pressure syringe pump which can provide continuous flow in a range from < 1 µL/min to 204 mL/min with a maximum operating pressure of 3750 psig (26 MPag). The accuracy of the flow rate is ± 0.5% of the set point flow rate.
- The lines are all 1/4 inch I.D. stainless steel pipe and are insulated and heated with Briskheat heating cables.

Reactor Section: The reactor section includes: a preheater, a reactor, and product filters as described below:

- The Feed Preheater (H101) is a Watlow electric cartridge heater which is centered within a spiral shaped aluminium casing. This electric unit has a length size of 40 cm and can be subjected to a maximum voltage of 500 V. Two thermocouples are used to control the preheater: one for sensing the temperature of the unit and the other for measuring the temperature of the fluid exiting the preheater.
- The Reactor (R101) consists of a Hastelloy C276 reactor tube introduced into an electrically heated ATS furnace (Serie 3210). The reactor tube is 68.5 cm of length with an internal diameter of 1.27 cm. The furnace is electrically heated with nichrome wire embedded in a ceramic shell and can reach a maximum temperature of 550°C. It has three side ports located equidistant to each other (bottom, middle, and top) where thermocouples can be connected to measure the wall temperature of the reactor tube. Pressure transducers are located at the inlet and at the outlet of the reactor.
- The Product Filter (F102) is a Serie 4100 high pressure mini tee-type filter. The filter housing is made of 316 stainless steel and the cartridge element consists of a 304 stainless steel woven wire mesh (10 micron absolute).
- Pressure is controlled with a back pressure regulator at the exit of the Product Filter.

- The lines are all 1/4” I.D. stainless steel pipe, insulated and heat taped with the following exceptions. The first 37 inches after the reactor is uninsulated and untaped (for cooling) and there is no heat tape on the line exiting the filters.

Product Recovery Section: This section was designed to separate and recover the products obtained from reaction and consists of the following units: a flash separator, a slop tank, and a product tank as described below.

- The Flash Separator (V103) is 316 stainless steel vertical vessel with a capacity of 0.9 L (0.052 m I.D. and 0.4 m length) and is rated for 175 psig (1.2 MPag) at 100°C. The pressure inside the flash separator is controlled by a pressure control valve located on the vapor outlet line.
- The Slop Tank (V104) and Product Tank (V105) are cylindrical stainless steel vessels with capacities of 11.4 L and 1.25 L, respectively, and are rated for a maximum temperature of 100°C.
- The lines are 1/4” I.D. 316 stainless steel, all insulated but only heat taped at the liquid product outlet.

3.2.2 Procedure

For this study, the WC-B-A3 bitumen was not filtered because its solid content was less than 1%. Therefore, the Unfiltered Feed Tank and filters were not used and the feedstock was manually charged into the Unfiltered Feed Tank at ambient conditions. With the lid slightly open, the tank was purged with nitrogen for about 10 minutes to remove the air. Then, it was immediately sealed and more nitrogen was injected until the tank was pressurized and maintained at 10 psig (70 kPag). The Filtered Feed Tank was heated to 60°C in order to reduce the viscosity of the feedstock and facilitate the pumping process.

The 60°C feedstock was pumped from the Filtered Feed Tank through the Reactor Feed Pump (where the flow rate was set) to the Feed Preheater, where the temperature was increased to 250°C, and then on to the reactor where it was brought up to the reaction temperature (420 to 440°C in this study). The flow rate was set to obtain a desired residence time in the reactor and, for this

study, residence times of 10 and 20 minutes were examined with corresponding flow rates of 8.7 and 4.3 mL/min. For all experiments, the reactor pressure was set at 950 psig (6.5 MPag). The pressure was monitored using the pressure transducers placed at the inlet and at the outlet of the reactor. The temperature was monitored using three thermocouples located along the length of the reactor tube. The apparatus was considered to have reached reaction temperature when the temperature readings were within ± 0.5% of the set point.

The fluid exiting the reactor was cooled by flowing it through an uninsulated line and then passed through the product filter to remove coke and solids that may have formed during the reaction. The reacted fluid continued on through another line where the temperature was maintained at 90ºC. This temperature was monitored with a thermocouple located at the inlet of the Flash Separator.

In the Flash Separator, the pressure was reduced to 1.3 atm. The vapor was vented because the collection of a gas sample was not required for this study. The liquid product was collected in the Slop Tank until the visbreaking operation stabilized (reaction conditions achieved). Once, the visbreaking process was stabilized, the liquid product was discharged into the Liquid Product Tank at atmospheric pressure.

3.3 Characterization Methodology

The feed and visbroken bitumen liquid products were separated into a distillate fraction and a residue (300°C+) fraction using spinning band distillation (SBD) as discussed in Section 3.3.1. Simulated Distillation assays were obtained for selected samples, Section 3.3.2. The residue was further divided into saturate, aromatic, resin and asphaltene (SARA) fractions using the modified ASTM D4124 method, Section 3.3.3. The density and molecular weight of the whole oil, distillates, and SARA fractions were measured, Section 3.4. Solubility experiments were performed on the whole crude oil, heavy residue, and SARA fractions, Section 3.5.

3.3.1 Spinning Band Distillation (SBD)

A spinning band distillation apparatus was used to distill the WC-B-A3 bitumen samples. The spinning band distillation apparatus (B/R Instrument Corporation, Model # 18-100) is equipped

with a heating mantle, a round 200 mL boiling flask, a spinning band column, two thermocouples, a condenser, four 40 mL receivers, a VAC-1000 vacuum system, and an automatically controlled reflux valve, as shown in Figure 3.3. The distillation column is a Monel type 45 cm length and 8 mm diameter with a maximum column efficiency of 30 theoretical plates. Two thermocouples are placed in the apparatus; the first is introduced into an adapter that is connected to the round flask to measure the fluid temperature and the second is located at the top of the column to measure the temperature of the vapors coming out from the condenser. Operation of the spinning band is controlled through a computer using the B/R Instrument distillation software.

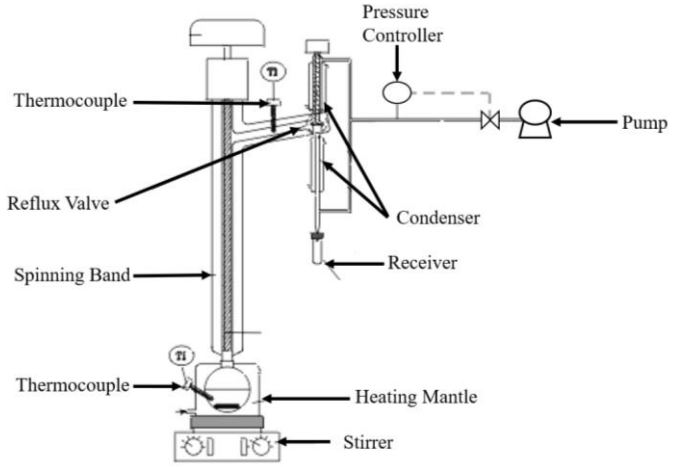

Figure 3.3 Schematic of spinning band distillation apparatus (Adapted from Powers, 2014).

To start an experiment, approximately 120 g of bitumen was placed into a round 200 mL flask set on a heating mantle. The flask was connected to the lower part of the spinning band column and the thermocouples along with the receivers were put in place. The vacuum pressure was set to 3 mm Hg. The temperature intervals at which to collect the distillates were set based on the desired boiling cut range and were adjusted as the distillation progressed. In order to avoid cracking, the maximum temperature was 300ºC. The reflux ratio of the column was set to 5:1. The equilibrium time required to equilibrate the liquid and vapor that flows through the column was fixed at approximately 10 minutes.

The heating rate was initially set at 15% to increase the temperature of the system. The sample was heated with constant stirring and when the first liquid drop was visible exiting the condenser, the spinning band was rotated, and the heating rate was increased such that a drop rate of 1 per second could be maintained. Equilibration between vapor and liquid was monitored in the software until the liquid and vapor temperatures curves reached a plateau. Once, 10 minutes of equilibrium time was complete, the reflux valve was opened, and the distillates were collected in the assigned receiver. Each cut was collected until the collection rate slowed and the color of the collected material started to change. Then, the temperature was raised, and the next cut collected. Throughout the distillation, the heating rate was manually increased such that the liquid and vapor temperature curves were parallel to each other. Once, the cracking temperature was reached, the distillation was stopped.

The vapor temperature was converted to atmospheric equivalent temperature using the Maxwell-Bonnell inter-conversion method for reduced distillations (Riazi, 2015). The normal boiling point is calculated as follows:

$$T_b = \frac{748.1 * Q * T}{1 + T * (0.3861 * Q - 0.00051606)} \tag{3.2}$$

$$Q = \frac{5.994296 - 0.972546 * \log_{10} P}{2663.129 - 95.76 * \log_{10} P} \tag{3.3}$$

where T_b stands for the normal boiling point in K, T is the vapor temperature measured at pressure P, in K, and P is the reduced pressure in mmHg. The interconverted atmospheric boiling points are considered to be true boiling points because the apparatus meets the following standards: a distillation column with 15 to 100 theoretical plates and a high reflux ratio between 1 to 5. A mass balance was performed after each distillation to estimate the losses and the amount of bitumen distilled. The average loss was approximately 2% for all distillations.

3.3.2 Simulated Distillation by Gas Chromatography

Simulated distillation (SimDist) is a gas chromatographic method where boiling points are determined from correlations to the measured retention times.

SimDist, is described in detail in ASTM D2887 or ASTM D7160 and the selection of the appropriate method depends on the characteristics of the crude oil. This analysis provides a distillation curve expressed as boiling point versus weight percent of the sample. Simulated distillations following the ASTM D7160 were performed for the WC-B-A3 feedstock and for the five reacted samples at Core Laboratories, Calgary.

3.3.3 SARA Fractionation

SARA fractionation was performed on the distillation residues using a modified ASTM D4124 procedure (Alboudwarej *et al*., 2002). SARA fractionation includes the following two main steps: a) asphaltene precipitation and maltenes separation from the oil sample, and; b) liquid chromatographic separation of the maltenes into saturate, aromatic, and resin fractions.

Asphaltene Precipitation and Toluene Insoluble Content:

To precipitate asphaltenes from an oil sample, *n*-pentane was added to 40 g of bitumen at a ratio of 40:1 volume (mL)/weight (g) and sonicated for 60 minutes or until all components were dissolved. After 24 hours of total contact, the mixture was filtered through a VWR GR413, 25 cm diameter filter paper until approximately 25% of the solution remained in the beaker. Then 10% of the original *n*-pentane volume was added to the mixture and the solution was sonicated for 90 minutes, left to settle for up to 16 hours, and filtered through the same filter paper. The filter cake was washed using 25 mL of *n*-pentane at least three times per day over five days or until the effluent from the filter was nearly colorless. Filter papers were placed in a fume hood for 4 days and then in a 60°C vacuum oven to dry until a constant weight was achieved. The dried residue was termed “C5-Asphaltenes+Solids.” The asphaltene+solids content is the mass of residue divided by the original mass of the oil sample and the repeatability of the asphaltene content was +/- 0.15 wt%.

The filtrate consists of maltenes (*i.e.*, deasphalted oil) and *n*-pentane. The maltenes were recovered by evaporating the *n*-pentane in a rotary evaporator. The maltenes were then dried first in a fumehood, then in a 60°C vacuum oven, until the weight did not change significantly. The dried maltenes were used for the chromatographic separation explained later.

To remove the solids from the asphaltenes, 200 mL of toluene was added to two grams of asphaltene (with solids) to make a 10 kg/m^3 solution. The mixture was dissolved in an ultrasonic bath for 20 minutes and put aside to settle for 60 minutes. The solution was divided into centrifuge tubes and centrifuged at 4000 RPM for 6 minutes. The supernatant (solids-free asphaltene solution) was decanted into small flasks through a Grade #42 Whatman filter paper at vacuum. The solids were collected in the bottom of the centrifuge tubes and the filter cake. The beakers and tubes were placed in a fumehood for 3 days, then a 60°C vacuum oven for at least two days to evaporate the toluene. The dried weights of each were recorded and the solids content was calculated gravimetrically. The solids were termed "Toluene Insolubles" (TI). The TI content is the mass of TI over the mass of C5-Asphalenes+Solids.

Chromatographic Separation of Maltenes into Saturates, Aromatics and Resins:

The SARA fractionation apparatus consists of three glass columns; two upper columns each packed with approximately 150 g of Attapulgus clay and a lower column packed with approximately 250 g of silica gel. By definition, the saturates are the material that elutes directly through both columns, aromatics adsorb on the silica gel, and resins on the Attapulgus clay.

To begin a separation, one of the upper columns was connected to the lower column and the upper column was wet with 25 mL of *n*-pentane. 5 grams of maltene fraction were dissolved in 25 ml of pentane and then the diluted maltene solution was charged to the columns followed by 480 mL of *n*-pentane was flowed through. The same procedure was repeated with the second upper column. The aromatics were eluted using a mixture of *n*-pentane:toluene (200 mL:200 mL). The elutions were performed with the upper and lower columns connected and a total of 800 mL of each solvent mixture was used for each upper column.

The residual aromatics in the lower column were recovered by refluxing toluene through the silica gel using a Soxhlet apparatus. To collect the resin fraction, the two upper columns were connected, and the resins were eluted twice with a mixture of acetone: toluene (200 mL: 200 mL). Solvents were recovered from each of the eluted fractions in a rotary evaporator. Each recovered SAR fraction was weighed, and the SARA composition of the sample determined.

3.4 Property Measurements

The density and molecular weight were measured for the SARA and distillate fractions, as described below.

3.4.1 Molecular Weight

The molecular weights of the SARA fractions were measured using a Jupiter Model 833 Vapor Pressure Osmometer (VPO, Figure 3.4). All the measurements were performed in toluene at 50°C. In the VPO, a droplet of pure solvent and a droplet of solvent-solute are placed on two respective thermistors. The difference in vapor pressure between the two droplets results in a difference in temperature between both thermistors. The temperature difference causes a voltage difference (or resistance change) between the thermistors.

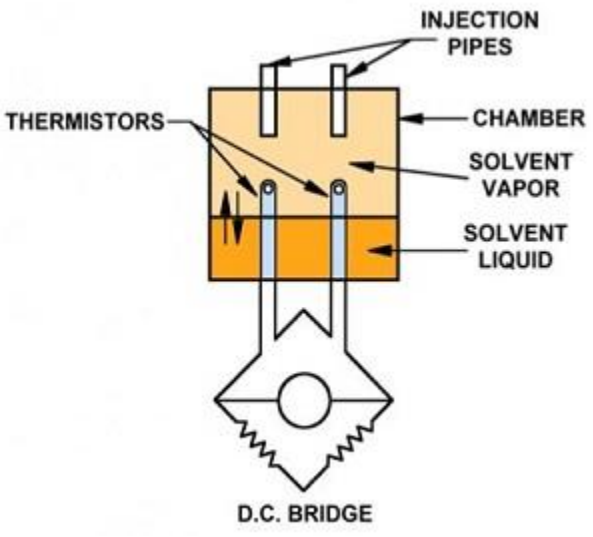

Figure 3.4 Vapor Pressure Osmometer (Figure taken from http://www.uicinc.com/model-833/).

The voltage difference, the output of the VPO, is related to the molecular weight of the solute, M_2 as follows (Powers *et al*., 2016):

$$\frac{\Delta V}{C_2} = K\left(\frac{1}{M_2} + A_1 C_2 + A_2 C_2{}^2 + \ldots\right) \tag{3.4}$$

where ΔV is the voltage difference between the thermistors, C_2 is the solute concentration, K is the proportionality constant, and A_1 and A_2 are coefficients arising from the non-ideal behavior

of the solution. In most cases, at low concentrations, most of the higher order terms become negligible, and Eq. 3.1 reduces to:

$$\frac{\Delta V}{C_2} = K\left(\frac{1}{M_2} + A_1 C_2\right) \tag{3.5}$$

For an ideal system, the second term in Eq. 3.2 is zero and $\Delta V/C_2$ is constant. In this case, the molecular weight is determined from the average $\Delta V/C_2$ as follows:

$$M_2 = \frac{K}{\left(\Delta V / C_2\right)} \tag{3.6}$$

For the calibration, the molecular weight of the solute is known, and the proportionality constant, *K*, is calculated by extrapolation of a plot of $\Delta V/C_2$ versus C_2 to zero concentration as per Eq. 3.2. For a non-ideal solution with an unknown solute, the molecular weight is calculated from the intercept of a plot of $\Delta V/C_2$ versus C_2 this time solving for M_2. For an ideal solution with an unknown solute, the molecular weight is calculated at each concentration from Eq. 3.6 and then averaged. The instrument was calibrated with sucrose octaacetate (679 g/mol) as solute and octacosane (395 g/mol) was used as standard. The measured molecular weight of octacosane was within 3% of the correct value.

The saturate and aromatic fractions exhibited slightly non-ideal behavior with positive slopes (A_1) in the plot of $\Delta V/C_2$ versus C_2. The average slopes for native saturates and aromatics were found to be 0.13 mV/(g/L)² and 0.09 mV/(g/L)² respectively (Okafor, 2013). Powers (2014) found that the slopes for reacted (thermocracked and hydrocracked) saturates and aromatics were systematically lower than those of the native fractions with average values of 0.04 mV/(g/L)^2 and 0.02 mV/(g/L)^2, respectively. The molecular weights for these fractions were determined by extrapolation using the average slopes and Eq. 3.5. The VPO response for the resin fractions did not exhibit any consistent trend. Given the relatively small slope for these fractions, A_1 was set to zero and the resin molecular weights were determined from the average VPO response, Eq. 3.6.

3.4.2 Density

Densities were measured using an Anton Paar DMA 4500M density meter at atmospheric conditions (20°C and 1 atm). The instrument precision is ±0.00001 g/cm^3 with an accuracy of ±0.00005 g/cm^3. The distillates, saturate and aromatic densities were measured directly. Resin and asphaltene densities could not be measured directly because they were too viscous to handle or were solid at ambient temperature. Instead, their densities were determined indirectly from the measured densities of solutions of resins or asphaltenes in toluene at different concentrations, from 2 to 160 g/L. Density values were determined from a mixing rule. As noted by Yarranton *et al.* (2015), a mixture of resins or asphaltenes and these solvents appear to form regular solutions and therefore the resin densities are given by:

$$\frac{w_{res}}{\rho_{res}} = \frac{1}{\rho_{mix}} - \frac{w_s}{\rho_s} \tag{3.7}$$

where w is mass fraction, ρ is density, and subscripts *mix*, *res*, and *s* indicate the mixture, resin, and solvent, respectively.

3.5 Solubility Measurements

The solubility parameters of the SARA and distillate fractions are to be determined later from the solubility measurements described below.

3.5.1 Mixtures of Asphaltenes and Solvents

Asphaltene precipitation (solubility) measurements were performed at 21°C and atmospheric pressure with mixtures of 10 g/L of asphaltenes in: a) *n*-heptane/toluene; b) saturates/toluene, and c) aromatics/*n*-heptane. The mass of precipitate was determined gravimetrically. The data are reported as an asphaltene solubility curve, a plot of the yield of precipitated asphaltenes versus the mass fraction of the poor solvent.

For asphaltenes in *n*-heptane/toluene, the asphaltenes were dissolved in a specified mass of aromatic solvent, here toluene, by sonicating for 20 minutes. The paraffinic solvent, here *n*-heptane, was added and the mixture sonicated for 45 minutes and left to settle for 24 hours. The mixture was then centrifuged at 3200 rpm for 5 minutes. The supernatant was decanted and the

recovered/precipitated asphaltenes were dried first in a fume hood, then in a vacuum oven at 60°C until the mass was constant. Asphaltene precipitation yields were calculated as the mass of precipitated asphaltenes divided by the initial mass of asphaltenes.

For the mixtures with saturates, asphaltenes were dissolved in toluene for about 20 minutes and then a specific mass of saturates was added. The solutions were sonicated at 60ºC until the mixtures were completely dissolved. For the case of aromatics, they were not easily dissolved, and the above procedure was modified (Okafor, 2013) as follows: the aromatic fraction was initially weighed into a vial followed by the addition of a fixed amount of asphaltenes and then the *n*-heptane was added. These mixtures were sonicated at 60ºC until they were totally dissolved. The vials were settled for 24 hours and then were centrifuged at 3200 rpm for 5 minutes. The supernatant was removed and the precipitated asphaltenes were washed using pure *n*-heptane for saturates and using a solution of 95 vol% *n*-heptane and 5 vol% toluene for the aromatics.

The asphaltene precipitation measurements were conducted with at least 10 cm^3 of solvent. However, it was very time-consuming to prepare enough of the saturates and aromatics required for these experiments. Therefore, the volume of solvent was scaled down to less than 2 cm^3 to minimize the consumption of the saturates and aromatics.

3.5.2 Mixtures of Bitumen and n-Heptane

For the feedstock and mildly reacted samples, a specific mass of crude oil (1.5 to 5 g) was poured into a 10 mL glass vial and diluted with *n*-heptane at a specific ratio.

The mixture was sonicated for at least 60 minutes and left to settle for 24 hours at room temperature. Then, the mixture was centrifuged at 4000 rpm for 5 minutes and the supernatant was decanted. The precipitated asphaltenes were washed with *n*-heptane until the supernatant was almost colorless. The precipitated asphaltenes were dried first in a fume hood, then in a vacuum oven at 60°C until their mass was constant.

For high viscosity samples, (highly reacted samples such as WC-B-A3-VIS19 and WC-B-A3-VIS38, as well as 300°C+ residue fractions), the above procedure was modified to reduce the

viscosity of the sample with toluene addition. A known mass of oil (0.6 - 4 g) was initially diluted in toluene at a ratio of 0.5 g toluene/g oil. The mixtures were sonicated at 60°C until the bitumen was completely dissolved. Then, a specified mass of *n*-heptane was added, and the mixtures were sonicated for another 60 minutes. The vials were left to settle for 24 hours and the centrifuging, washing, and drying procedures were performed as described above. In both procedures, the asphaltene yield was reported as the mass of precipitated asphaltenes divided by the original mass of bitumen.

Chapter 4 Asphaltene Precipitation Modeling

In this chapter, the application of the modified regular solution model for asphaltene precipitation is described. The model is presented including its inputs: the mole fraction, molar volume (ratio of molecular weight to density), and solubility parameter of each component in the mixture. The fluid characterization methodology employed to generate the model inputs is discussed. Previously determined average values or empirical correlations for the molecular weight, density, and solubility parameters of distillates, saturates, aromatics, resins, asphaltenes are presented. Gaps are identified where correlations are to be updated or new correlations developed. Finally, the workflows for modeling the stability of different fluid systems (asphaltene-solvent mixtures, heavy residues, reacted samples or heavy oils) are provided.

4.1 Modified Regular Solution (MRS) Model

Regular solution theory is an activity coefficient approach based on the internal energy of mixing for solutions where there is no volume change upon mixing. Hirschberg (1984) modified the model for application to asphaltenes (treated as a single component) by adding an entropic contribution based on Flory-Huggins polymer solution theory (Flory, 1941) to account for the significant size difference between asphaltenes and the other constituent molecules. Later, Yarranton and Masliyah (1996) adapted the model to treat the asphaltenes as a mixture of pseudo-components and successfully predicted asphaltene fractional yields in asphaltene-solvent systems. This approach has been extended to model asphaltene precipitation from blends, live oils, crude oils, and reacted fluids (Alboudwarej *et al*., 2003; Akbarzadeh *et al*., 2004; Akbarzadeh *et al*., 2005, Tharanivasan 2012 and Powers, 2014).

Asphaltene precipitation is modeled assuming a liquid-liquid equilibrium between a light liquid phase (solvent-rich phase including all components) and a heavy liquid phase (asphaltene-rich phase including only asphaltenes and resins). The equilibrium constant, *K*, that is the ratio of the mole fractions of a component *i* in each phase is given by the following expression:

$$K_i = \frac{x_i^H}{x_i^L} = \frac{\gamma_i^L}{\gamma_i^H} \qquad (\mathbf{4.1})$$

where K_i is the equilibrium ratio, i is the component, superscripts H and L denote the heavy and light phases, respectively, x is the mole fraction, and γ is the activity coefficient. Since only asphaltenes and resins are allowed to partition into the heavy phase and they are chemically similar, the activity coefficients of the components in the heavy phase are set to unity. Therefore, the resulting expression for the equilibrium constant K of component i becomes:

$$K_i = \frac{x_i^H}{x_i^L} = \gamma_i^L \tag{4.2}$$

For a component in a regular solution, the activity coefficient in a liquid phase is defined as follows (Prausnitz, 1999):

$$ln(\gamma_i) = ln\left(\frac{v_i}{v_{mix}}\right) + 1 - \frac{v_i}{v_{mix}} + \frac{v_i}{RT}\sum_j^n \sum_k^n \phi_j \phi_k \, (D_{ij} - 0.5 D_{jk}) \tag{4.3}$$

where R is the universal gas constant, T is temperature, υ is the molar volume, ϕ is the volume fraction, subscript *mix* denotes the mixture, and n is the total number of components. The term D_{jk} is defined as follows:

$$D_{jk} = (\delta_j - \delta_k)^2 + 2 l_{jk} \delta_j \delta_k \tag{4.5}$$

where δ is the solubility parameter and l_{jk} is the interaction parameter between the two components j and k.

For asphaltene precipitation modeling, the solution is defined as the mixture of self-associated nano-aggregates with the other oil components and any added solvent. While there may be specific interactions between the asphaltenes and resins to form the nanoaggregates in the first place, it is assumed that, once formed, the nano-aggregates are stable (unaffected by phase transitions of the bulk fluid) and interact with the other components in the same way as other molecules. With these assumptions, the mixture can be treated as a solution with no strong specific interactions between the components; that is, that the interaction parameter between any of the components is zero. Therefore Equation 4.3 reduces to:

$$ln(\gamma_i) = ln\left(\frac{v_i}{v_{mix}}\right) + 1 - \frac{v_i}{v_{mix}} + \frac{v_i}{RT}(\delta_i - \delta_{mix})^2 \tag{4.6}$$

where δ_m, is the solubility parameter of the mixture determined and is defined as follows:

$$\delta_{mix} = \frac{\phi_i \delta_i}{\sum \phi_i \delta_i} \quad \textbf{(4.7)}$$

Equation 4.6 is substiututed into Equation 4.2 to obtain the following expression for the equilibrium ratio:

$$K_i = \frac{x_i^H}{x_i^L} = exp\left\{ln\left(\frac{v_i^L}{v_m^L}\right) - \frac{v_i^L}{v_m^L} + \frac{v_i^L}{RT}(\delta_i^L - \delta_m^L)^2\right\} \quad \textbf{(4.8)}$$

Once the equilibrium ratios are known, multicomponent flash calculations are performed using standard techniques (Rijkers and Heidemann, 1986). The required inputs are the mole fraction, molar volume, and solubility parameter of each component in the mixture.

4.2 Fluid Characterization for the Modified Regular Solution Model

Fluid characterization involves representing the fluid as a set of pure components and pseudo-components each with an assigned mole or mass fraction and assigned properties; in this case, molecular weight, density, and solubility parameter. The molar volume is calculated as the ratio of molecular weight to density. The solvents used in this study (toluene and heptane) are pure components and their properties are known. The heavy oils (feedstocks) and reacted fluids are characterized into pseudo-components based on the methodology recommended by Powers (2014) and shown in Figure 4.1. The distillable fraction of the oil is treated as a single pseudo-component. The non-distillable residue is divided into pseudo-components corresponding to SARA fractions (saturate, aromatic, resins, and asphaltenes) plus a toluene-insoluble fraction. The mass fraction of each pseudo-component in the mixture is calculated from the weight percent of oil distilled, the SARA composition, and the toluene insoluble content. The mole fractions are determined based on the average molecular weights of the components.

The saturates, aromatics, and resins are each treated as a single uniform pseudo-component. The asphaltenes are assumed to be a continuum of aggregates with a broad range of molecular weight. They are further divided into 30 pseudo-components with a uniform increment in molecular weight. The minimum molecular weight (the monomer value) for asphaltenes in unreacted oils was set to 800 g/mol (Powers *et al.*, 2017). However, this value is expected to change with reaction. Therefore, the monomer molecular weight was scaled to the measured molecular weight of the

aromatics. The aromatic molecular weight was chosen because it is the closest measurable value (from a non-associating fraction) to the asphaltene monomer molecular weight. The maximum value for the asphaltene molecular weight is set to 30,000 g/mol. The mole fraction for each interval is determined by integrating a Gamma function representing the molecular weight distribution (described later). The determination of the molecular weight, density, and solubility parameter for the solvents and for each pseudo-component of the mixture is discussed below. Note, the toluene insoluble fraction is defined as insoluble at all conditions and therefore its properties are not used or discussed.

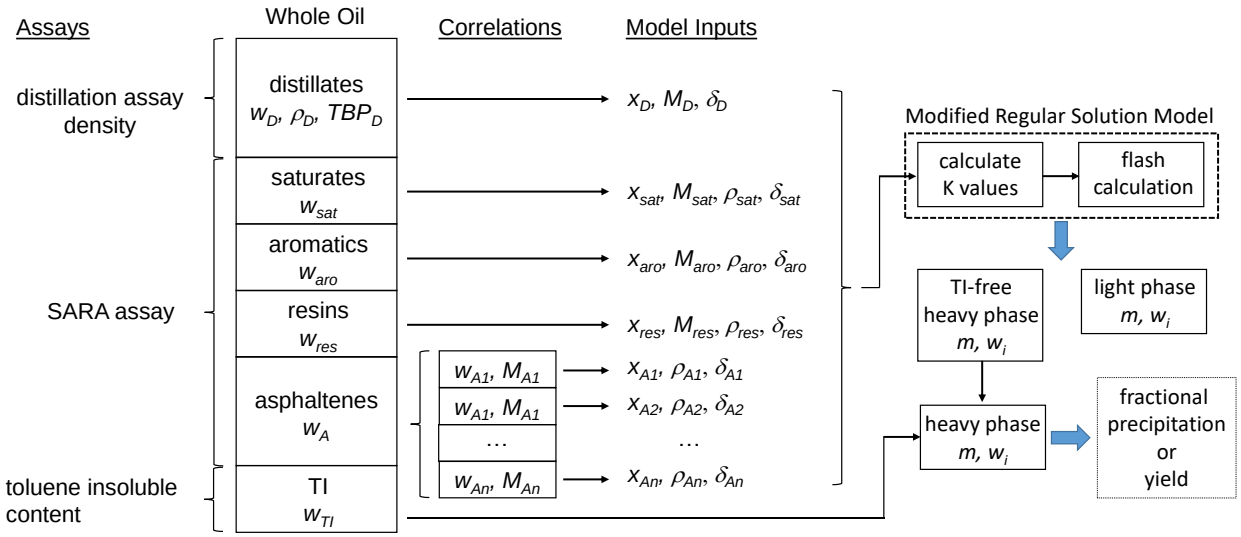

Figure 4.1 Schematic of implementation of Modified Regular Solution model for a crude oil characterized into pseudo-components; *w* is mass fraction, *x* is mole fraction, ρ is density, *M* is molecular weight, δ is solubility parameter, *m* is mass, and subscripts *D*, *sat*, *aro*, *res*, *A*, *TI*, and *i* denote distillates, saturates, aromatics, resins, asphaltenes, toluene insoluble and component *i*, respectively. The asphaltenes are divided into component 1 to *n*.

4.2.1 Solvent Properties

Table 4.1 provides the density, molecular weight, and solubility parameter of the solvents used in this thesis.

Table 4.1 Properties of *n*-heptane and toluene (Tharanivasan *et al*., 2011).

Solvent	Density kg/m^3	Molecular Weight g/mol	Molar Volume cm^3/mol	Solubility Parameter $MPa^{0.5}$
n-Heptane	681	100	147.1	15.2
Toluene	866	92	106.4	18.3

4.2.2 Distillate Properties

The distillate properties are determined from a distillation assay and the measured densities of the cuts at 21°C. The raw data from the distillation assay is the cumulative volume distilled at a series of atmospheric equivalent temperatures (AET). The molecular weight and specific gravity corresponding to each measured atmospheric equivalent temperature (AET) are estimated with an iterative procedure as follows:

- guess initial values for the molecular weight of each AET cut,
- calculate the specific gravity of each cut using the Sanchez-Lemus correlation (function of molecular weight and AET),
- calculate the AET with the Modified Soreide correlation (function of specific gravity and molecular weight)
- iterate the molecular weight of each cut until the sum of squared difference between experimental and calculated AET reaches the minimum value.
- compare the calculated and measured specific gravity of the distillates and apply a multiplier to the calculated specific gravity if required,
- repeat the procedure with the new multiplier until both AET and specific gravity are matched.

The correlations used in this procedure were taken from Sanchez-Lemus *et al*. (2016).

The cumulative mass percent distilled is calculated from the distilled volume and the calculated density for each AET cut. The average molecular weight of the distillates is the molar average of the calculated molecular weights of each cut. The solubility parameter of the distillates was determined from solubility data using the procedure provided in Section 4.3 and a correlation for the solubility parameter is proposed in Chapter 5.

4.2.3 Saturate, Aromatic, and Resin Properties

Previously, Yarranton *et al*. (2018) determined average values for the molecular weight, density, and solubility parameter of native, thermocracked, and hydrocracked oils, Table 4.2. These values are to be tested and updated. First, the molecular weights and densities will be measured directly. The solubility parameters will be determined from solubility experiments as discussed in Section 4.3. Then, if required, the correlations will be modified as discussed in Chapter 5. Note that, since resins may self-associate with the asphaltenes to an unknown extent, their solubility parameters cannot be determined from the modeling of solubility experiments. Therefore, the solubility parameter of the resins is set to the minimum asphaltene solubility parameter, as discussed in Chapter 5. The asphaltene precipitation process is modeled assuming

Table 4.2 Recommended properties for the SAR fractions for native oils, vacuum residues, thermocracked oils, and hydrocracked oils (Yarranton *et al.*, 2018); *MW* is molecular weight, ρ is density, *X* is the conversion percent, subscripts *f* and *i* indicate the feed and a component.

Fraction	Molecular Weight g/mol	Density at 21°C kg/cm^3	Solubility Parameter MPa$^{0.5}$
Native Oils			
Saturates	440	880	16.1
Aromatics	500	990	20.1
Resins	1050	1060	20.15
Vacuum Residues			
Saturates	740	880	16.4
Aromatics	790	990	20.4
Resins	1360	1060	20.15
Thermocracked			
Saturates	same as feed	same as feed	14.5
Aromatics	$MW_{fi}(1 - 0.0037X)$	$\rho_{fi}(1 + 0.049X)$	same as feed
Resins	$MW_{fi}(1 - 0.0037X)$	$\rho_{fi}(1 + 0.049X)$	20.15+0.20(1-exp(-0.037X))**
Hydrocracked			
Saturates	same as feed*	same as feed	14.5
Aromatics	$MW_{fi}(1 - 0.0059X)$	$\rho_{fi}(1 + 0.049X)$	same as feed
Resins	$MW_{fi}(1 - 0.0059X)$	$\rho_{fi}(1 + 0.049X)$	20.15+0.85(1-exp(-0.050X))**

* valid up to conversion of approximately 65%; ** minimum asphaltene solubility parameter

4.2.4 Asphaltene Properties

Molecular Weight

The Gamma probability function is used to represent the asphaltene molecular weight distribution:

$$f(MW) = \frac{(MW - MW_{mono})^{\alpha-1}}{\beta^{\alpha}\Gamma(\alpha)} exp\left(\frac{MW_{mono} - MW}{\beta}\right) \quad \textbf{(4.10)}$$

$$\beta = \frac{MW_{avg} - MW_{mono}}{\alpha} \quad \textbf{(4.11)}$$

where α is the shape factor of the Gamma distribution and MW_{mono} and MW_{avg} are the monomer and average molecular weight respectively. The monomer molecular weight is set to a value of 800 g/mol as recommended by Yarranton *et al*., 2013. Powers *et al*., 2016 observed that the molecular weight distribution for most of the asphaltene samples (native and reacted) followed an exponential distribution. Hence, the shape factor of the gamma distribution is set to unity for the feedstock and for thermally cracked material. In this thesis, the average molecular weight of asphaltenes in solvents was obtained from the VPO experimental data of extracted asphaltenes in toluene. A correlation and a tuning procedure for the molecular weight of asphaltenes in bitumen are provided in Chapter 5. Note, the average molecular weight of the asphaltene nano-aggregates in bitumen are less than those of the extracted asphaltenes in solvents because asphaltenes self-associate less when resins are present (Yarranton *et al*., 2007).

Density

The density of each asphaltene pseudo-component is determined with the following correlation (Powers *et al*., 2016):

$$\rho_A = \rho_{min} + (\rho_{max} - \rho_{min}) * (1 - exp(-w_A * \tau)) \quad \textbf{(4.12)}$$

where w_A is the cumulative mass fraction, ρ_{min}, $\rho_{max,}$ and ρ_A are the asphaltene densities in kg/m³ at w_A = 0, w_A = 1, and w_A, respectively, and τ is the shape factor of the density distribution. The minimum density is set to 1050 kg/m^3 for all samples and the shape factor is set to 9 for the feedstock and 7 for the reacted asphaltenes (Powers *et al*., 2016). The maximum density is calculated so that the average density calculated from the distribution matched the average measured value. A correlation for the asphaltene average density is proposed in Chapter 5.

Solubility Parameters

The solubility parameter for each asphaltene pseudo-component was determined from the following correlation (Powers *et al*., 2016):

$$\delta = \delta_{min} + (\delta_{max} - \delta_{min}) * (w_A)^n \quad \textbf{(4.13)}$$

where δ is the solubility parameter, w_A is the cumulative mass fraction of asphaltenes, and δ_{min} and δ_{max} parameters are the minimum and maximum solubility parameter, respectively. The exponent *n* determines the shape of the distribution. Previously, Powers *et al.* (2016) determined average values for these parameters for extracted asphaltenes from native, thermocracked, and hydrocracked oils, Table 4.3. These values are to be tested and updated. The three parameters were determined by fitting the modified regular solution model to asphaltene yield data from asphaltenes in solutions of heptane and toluene. The fitting procedure are discussed in Section 4.3. The fitted and modified correlations as well as a tuning procedure are presented in Chapter 5.

Table 4.3 Recommended asphaltene solubility parameter equation coefficients for extracted asphaltenes (Powers *et al.,* 2016); *X* is the fractional conversion.

Asphaltenes:	**Native**	**Thermocracked**	**Hydrocracked**
δ_{min}, MPa$^{0.5}$	20.15	20.15+0.20(1-exp(-0.037X))	20.15+0.85(1-exp(-0.050X))
δ_{max}, MPa$^{0.5}$	21.30	21.30+2.20(1-exp(-0.042X))	21.30+2.20(1-exp(-0.042X))

4.3 Modified Regular Solution Model Implementation

The characterization and model implementation were shown schematically in Figure 4.1. The minimum measurements required for the characterization are a vacuum distillation assay (spinning band distillation in this thesis), the density of the distillates, a SARA assay, and the toluene insoluble content. The toluene insolubles (TI) are assumed to be completely insoluble at all conditions and are assigned to the heavy phase. The properties of all of the pseudo-components are determined from the correlations provided above or developed later in this thesis. Then, the *K*-values are calculated and a conventional flash calculation is performed on an in-house program implemented in Visual Basic.

The outputs of the model are the moles and molar composition of each phase. The masses and mass composition are determined from the input molecular weights. If the feed is a mixture of asphaltenes and solvents, the *fractional precipitation* of the asphaltenes is calculated as the mass of precipitated asphaltenes divided by the mass of asphaltenes in the feed. If the feed is a mixture of crude oil and solvent, the asphaltene *yield* is calculated as the mass of asphaltenes in the heavy (asphaltene-rich) phase divided by the mass of crude oil in the feed.

In this thesis, the Modified Regular Solution model is used to model the solubility data of asphaltene-solvent systems, asphaltene-solvent systems with a saturate, aromatic or distillate fraction, heavy residues with solvents, and whole oils with solvents. A brief description of the modeling procedure applied to each system is provided below.

Mixtures of Extracted Asphaltenes and Pure Solvents

When modeling asphaltene-solvent systems, the objective is either to predict the fractional precipitation of the asphaltenes or to determine asphaltene solubility parameters by fitting the solubility data. In both cases, the fluid is characterized as described above but with only solvents and asphaltenes. In predictive mode, the fluid property inputs and correlations are not modified. In fitting mode, the measured asphaltene average density and molecular weight are inputs, and the parameters in the asphaltene solubility parameter correlation (δ_{min}, δ_{max}, and n) are adjusted to fit the solubility data.

Mixtures of Extracted Asphaltenes, Pure Solvent, and a Saturate, Aromatic, or Distillate Fraction

Here, the objective is either to determine the saturate, aromatic or distillate solubility parameter by fitting the solubility data. The mixtures are typically asphaltenes/toluene/saturates, asphaltenes/*n*-heptane/aromatics, or asphaltenes/*n*-heptane/distillates. The fluid is characterized as described above but with only solvents, asphaltenes, and the saturate, aromatic or distillate fraction. The asphaltene parameters will have been previously determined and are inputs. The measured density and molecular weight of the saturate (aromatic or distillate) fraction are input, and its solubility parameter is adjusted to fit the solubility data.

Mixtures of Heavy Residues with Pure Solvent

Recall that the heavy residue is the sample that remains after the light components are distilled off. Here, the objective is either to predict the yield of the asphaltenes or to determine asphaltene solubility parameters by fitting the solubility data. In both cases, the fluid is characterized as described above with all components except the distillates. In predictive mode, the saturate, aromatic, resin, and asphaltene parameters will have been previously determined and are inputs. In fitting mode, the saturate, aromatic, resin, and asphaltene parameters are inputs. The measured asphaltene average density is also an input but the average molecular weight and/or the asphaltene solubility parameter correlation parameters (δ_{min}, $\delta_{max,}$ and n) are adjusted to fit the solubility data.

Mixtures of Whole Oil with Pure Solvent

The objective is either to predict the yield of the asphaltenes or to determine distillate solubility parameters by fitting the solubility data. In both cases, the fluid is characterized as described above with all components. In predictive mode, all of the component parameters will have been previously determined or correlated and are inputs. In fitting mode, all of the component parameters except for the distillates are inputs. The distillate density and molecular weight are also inputs but the distillate solubility parameter is adjusted to fit the solubility data.

Chapter 5: Results and Discussion

This chapter presents the fluid characterization, property measurements, and property correlations required to apply the Modified Regular Solution model to predict asphaltene yields from visbroken samples. Figure 5.1 illustrates the methodology used to characterize the feed and visbroken products for the solubility model. Recall that the samples were fractionated into a distillate and a residue (300°C+) fraction using spinning band distillation. The residue was further subdivided into SARA (saturate, aromatic, resin, and asphaltene) fractions as described in Section 2.4.2. The density and molecular weight of the SARA fractions were measured. The distillate properties were determined mainly from SBD distillation data. Solubility parameters of saturates, aromatics and distillates were indirectly determined by modeling asphaltene yield data from asphaltene-solvent mixtures. For asphaltenes in bitumen, the solubility parameter distribution and average molecular weight were determined by modeling the solubility data in heavy residues. Then, the solubility of the whole reacted samples was modeled using the characterization data collected for both the distillates and SARA fractions. Finally, property correlations were developed based on the data collected in this thesis supplemented with data from Powers (2014), Powers *et al.* (2016) and Yarranton *et al*. (2018). The trends in composition and properties with conversion, solubility modeling, and correlations development are discussed in detail below.

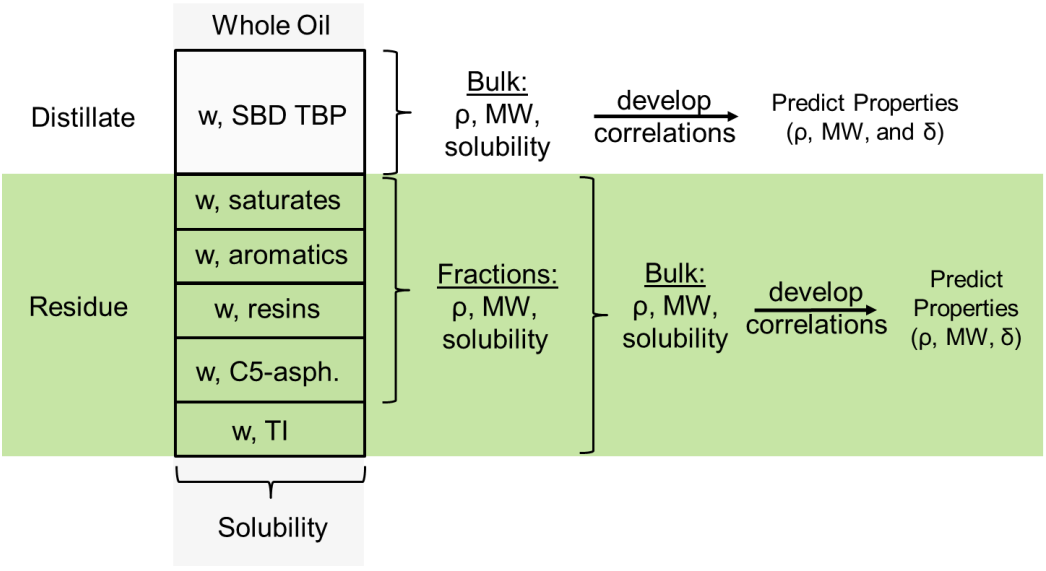

Figure 5.1 Schematic of the fluid characterization methodology.

5.1. Distillate Content and Conversion

Both spinning band (SBD) and SimDist assays were performed on all of the feed and visbroken samples. Recall that two feed samples were used in this study both from the same source: Feed 1 and Feed 2, designated as WC-B-A3(1) and WC-B-A3(2), respectively. Figure 5.2 compares the SimDist distillation curve for Feed 1 with the SBD distillation curves for Feed 1 and Feed 2. The two SBD distillation curves overlap within the error of the measurement (±0.21 wt% or ±7°C) and it was concluded that the feeds were the same for the purposes of this study. The Feed 2 assay was used for all further results since most of the visbroken samples were produced from this feed.

Figure 5.2 also shows that the SimDist and SBD data for Feed 2 overlapped within the error of the measurement. The SimDist and SBD curves also overlapped for each of the other samples (not shown here). Therefore, both assays were considered to be validated up to the maximum physically distillable atmospheric equivalent boiling temperature of approximately 370°C.

Figure 5.3 compares the distillation curves for the feed and visbroken samples. The curves shifted to the right as the conversion increased, consistent with the generation of lighter compounds. For each sample, the mass fraction of the distillates was obtained from the SBD assay and the mass fraction of the 524°C+ cut was determined from the SimDist assay, as shown in Figure 5.2. The mass fractions for each sample are provided in Table 5.1. The conversions were determined from the change in the 524°C+ cut (Equation 3.1) and are also reported in Table 5.1. In general, the conversion and the mass fraction of distillates increased with temperature and residence time. The increase in the distillates content indicates that cracked off side chains accumulated in the distillable fraction. Surprisingly, visbroken samples VIS5A and VIS5B had the same conversion despite the different reaction temperature; however, this result is consistent with their estimated physical properties as will be shown later.

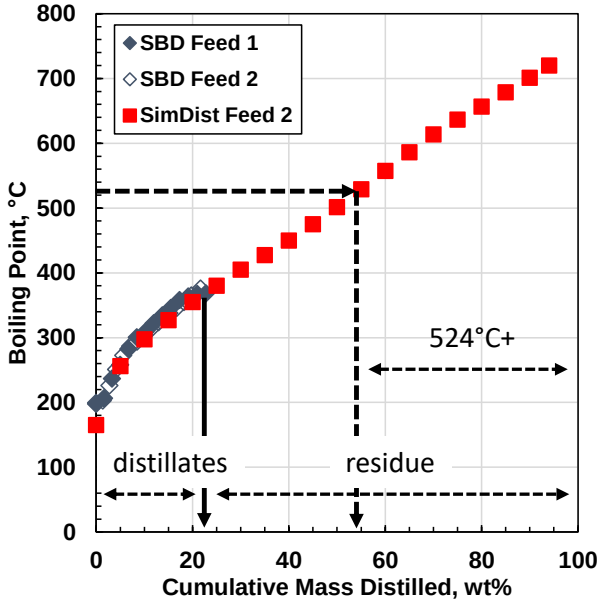

Figure 5.2 Spinning band (SBD) and SimDist distillation curves for the two feeds: Feed 1 is WC-B-A3(1) and Feed2 is WC-B-A3(2). The repeatability of the SBD and SIM-DIST measurements are ±1.7ºC and ±7ºC, respectively.

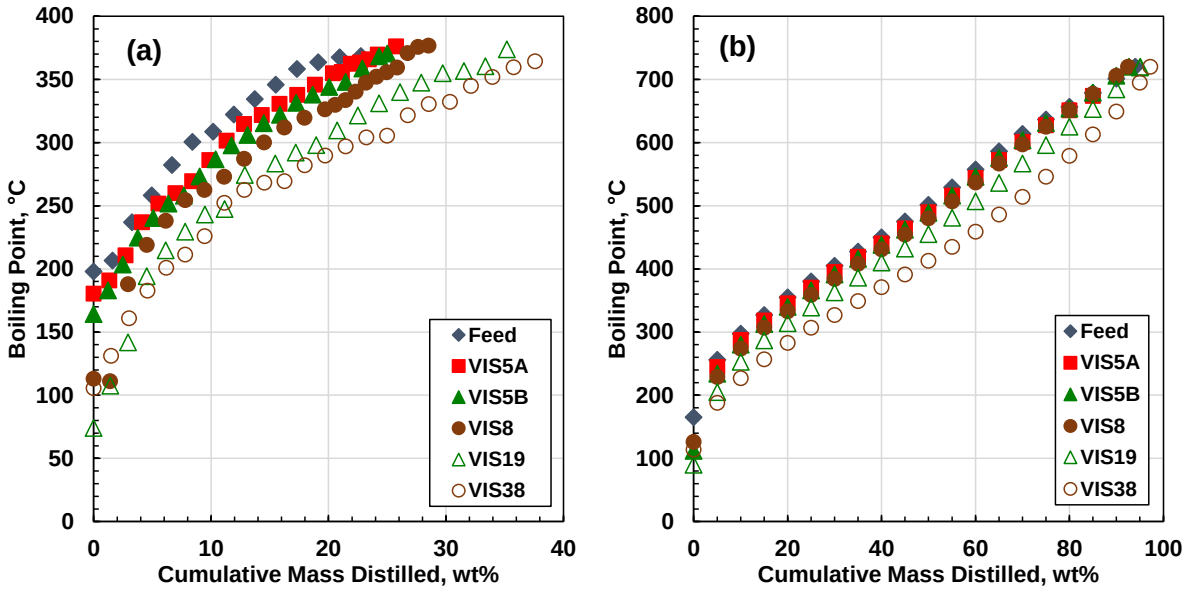

Figure 5.3 Distillation curves for WC-B-A3 feed (Feed 2) and visbroken products: a) Spinning Band distillation; b) SimDist. The repeatability of the SBD measurement is ±0.21 wt%.

Table 5.1 Mass fraction of distillates and 524°C+ cut for WC-B-A3 feed and visbroken products, and calculated conversions for products.

Sample	Conditions	Distillate wt %	524°C+ wt %	Conversion %
WC-B-A3(1)	Feed1	22.8	-	-
WC-B-A3(2)	Feed2	21.7	45.9	-
WC-B-A3-VIS5A	420C, 10min	25.7	43.6	5.1
WC-B-A3-VIS5B	430C, 10min	25	43.7	5.0
WC-B-A3-VIS8	440C, 10min	28.5	37.1	8.1
WC-B-A3-VIS19	430C, 20min	33.6	42.2	19.3
WC-B-A3-VIS38	440C, 20min	37.6	28.4	38.1

5.2. SARA and Toluene Insoluble Content of Distillation Residue

Table 5.2 provides the composition of each sample in terms of the distillates, SARA fractions, and toluene insolubles. The dominant change with conversion is the production of distillables. Figures 5.4a and 5.4b show the SARA composition and the toluene insoluble content, respectively, of the feed and visbroken distillation residues. As the conversion increased to 10%, the saturate content increased while the asphaltene and resins content decreased. The aromatic and toluene insoluble contents did not change significantly. These trends are consistent with the removal of alkyl-side chains and/or naphthenic fragments from the resins and asphaltenes. The newly formed fragments are collected in the distillate and saturate fractions increasing their content. At conversions above 10%, the saturate and aromatic contents did not change significantly, the resin content continued to decrease, and the asphaltene content reversed trend and increased. The increase in the asphaltene content can be attributed to two effects: 1) continued removal of side chains and naphthenic fragments from aromatic and resin fractions leaving highly aromatic fragments that now have solubilities in the asphaltene class; 2) the start of condensation reactions to form asphaltenes and eventually coke from aromatic, resin, and asphaltene species. The significant increase in the amount of toluene insolubles content above 10% conversion suggests that condensation reactions occurred.

Table 5.2 Composition of the WC-B-A3 feed and visbroken products. The repeatabilities of the SARA fractionation were ±0.7 wt%, ±0.5 wt%, ±0.4 wt% and ±0.9 wt% for saturates, aromatics, resins, and asphaltenes, respectively. The repeatability of TI composition measurements is ± 0.2 wt%.

Sample	Distillate wt %	Saturates wt%	Aromatics wt%	Resins wt%	Asphaltenes wt%	TI wt%
WC-B-A3	21.7	7.1	31.6	17.4	21.9	0.28
WC-B-A3-VIS5A	25.7	8.3	30.9	16.1	18.7	0.33
WC-B-A3-VIS5B	25.0	9.4	30.8	16.2	18.3	0.29
WC-B-A3-VIS8	28.5	8.6	28.8	15.1	18.6	0.38
WC-B-A3-VIS19	33.6	7.9	27.1	13.6	17.1	0.66
WC-B-A3-VIS38	37.6	7.1	26.1	10.9	17.3	1.01

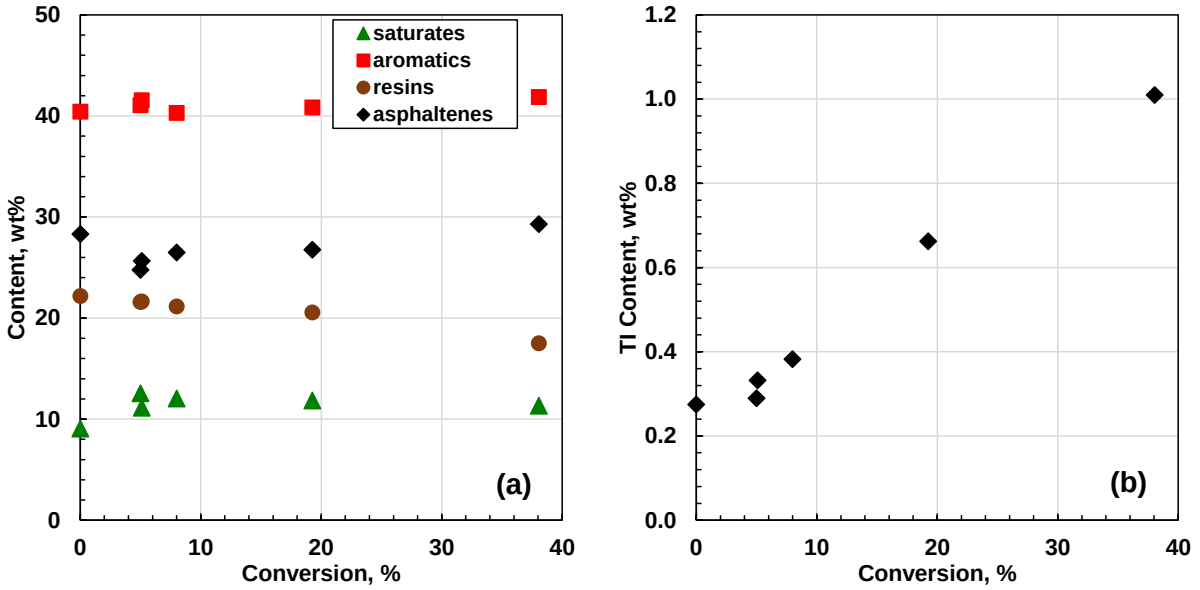

Figure 5.4 Change in WC-B-A3 distillation residue composition with conversion: a) SARA components; b) toluene insoluble (TI) content (residue-basis). The repeatabilities of the SARA and TI composition measurements were reported in Table 5.2.

5.3. Distillate and SARA Fractions Properties

The molecular weight, density, and solubility parameter of the distillates, saturates, aromatics, and resins are summarized in Tables 5.3 to 5.6, respectively. The repeatabilities of the measurements are ±15% for molecular weight, and ±0.3 $MPa^{0.5}$ for solubility parameter (Powers *et al*., 2016; Yarranton *et al*., 2018). The repeatabilities of the direct density measurements were ±0.03, ±0.9,

and ±1.1 kg/m³ for distillates, saturates, and aromatics, respectively. The repeatabilities of the densities of the viscous fractions were ±7.7 and ±8.5 kg/m³ for the resins and asphaltenes, respectively. The molar volume was calculated from the density and molecular weight and is also reported. The asphaltenes extracted from the oil are represented by property distributions and the parameters for their molecular weight, density, and solubility parameter distribution functions are provided in Tables 5.7 to 5.9, respectively. As will be discussed later, the asphaltenes self-associate differently in the oil and the distribution parameters were modified as noted in Table 5.10. The effect of visbreaking on each property is discussed below.

Table 5.3 Properties of distillates from the WC-B-A3 feed and visbroken products.

Sample	Molecular Weight g/mol	Density kg/m³	Molar Volume cm³/mol	Solubility Parameter [a] MPa$^{0.5}$	Solubility Parameter [b] MPa$^{0.5}$
WC-B-A3	217	914	237	19.3	18.7
WC-B-A3-VIS5A	206	912	226	18.3	18.2
WC-B-A3-VIS5B	199	907	219	18.1	18.3
WC-B-A3-VIS8	191	905	211	18.7	--
WC-B-A3-VIS19	191	901	212	18.0	18.2
WC-B-A3-VIS38	183	899	204	17.0	--

a) determined from solubility data for residues and whole oils diluted with *n*-heptane
b) determined from solubility data for solutions of asphaltenes, distillates, and *n*-heptane

Table 5.4 Properties of saturates from the WC-B-A3 feed and visbroken products.

Sample	Molecular Weight g/mol	Density kg/m³	Molar Volume cm³/mol	Solubility Parameter MPa$^{0.5}$
WC-B-A3 (Feed)	606	900	674	16.5
WC-B-A3-VIS5A	544	899	605	16.1
WC-B-A3-VIS5B	530	901	588	15.4
WC-B-A3-VIS8	538	897	600	16.3
WC-B-A3-VIS19	552	896	616	15.7
WC-B-A3-VIS38	508	891	570	15.2

Table 5.5 Properties of aromatics from the WC-B-A3 feed and visbroken products.

Sample	Molecular Weight g/mol	Density Kg/m^3	Molar Volume cm^3/mol	Solubility Parameter $MPa^{0.5}$
WC-B-A3	637	1008	632	21.0
WC-B-A3-VIS5A	567	1010	561	21.3
WC-B-A3-VIS5B	552	1009	547	20.9
WC-B-A3-VIS8	516	1015	508	21.5
WC-B-A3-VIS19	513	1017	504	21.1
WC-B-A3-VIS38	478	1025	466	19.9

Table 5.6 Properties of resins from the WC-B-A3 feed and visbroken products.

Sample	Molecular Weight g/mol	Density Kg/m^3	Molar Volume cm^3/mol	Solubility Parameter $MPa^{0.5*}$
WC-B-A3	1204	1040	1058	19.95
WC-B-A3-VIS5A	1040	1044	996	20.13
WC-B-A3-VIS5B	1030	1041	989	20.25
WC-B-A3-VIS8	1010	1049	963	20.18
WC-B-A3-VIS19	955	1049	910	20.30
WC-B-A3-VIS38	723	1060	682	20.85

* set equal to minimum asphaltene solubility parameter as reported in Table 5.10.

Table 5.7 Parameters for extracted asphaltene molecular weight distribution for WC-B-A3 feed and visbroken products. Average asphaltene molecular weights measured in toluene at 50°C.

Sample	MW^*_{mono} g/mol	MW_{avg} g/mol	α
WC-B-A3 (Feed)	800	4100	1
WC-B-A3-VIS5A	712	3780	1
WC-B-A3-VIS5B	693	3120	1
WC-B-A3-VIS8	648	3050	1
WC-B-A3-VIS19	644	3160	1
WC-B-A3-VIS38	600	2400	1

* scale to the molecular weight measured for the aromatics.

Table 5.8 Measured average density at 21°C and density correlation parameters for asphaltenes from feed and visbroken products.

Sample	ρ_{avg} kg/m³	ρ_{min} kg/m³	ρ_{max} kg/m³	τ
WC-B-A3	1149	1050	1162	9
WC-B-A3-VIS5A	1162	1050	1181	7
WC-B-A3-VIS5B	1169	1050	1190	7
WC-B-A3-VIS8	1181	1050	1205	7
WC-B-A3-VIS19	1193	1050	1219	7
WC-B-A3-VIS38	1228	1050	1261	7

Table 5.9 Fitted parameters for the solubility parameter distribution of extracted asphaltenes.

Sample	δ_{min} MPa$^{0.5}$	δ_{max} MPa$^{0.5}$	n
WC-B-A3	19.9	21.25	1.4
WC-B-A3-VIS5A	20.0	21.98	1.4
WC-B-A3-VIS5B	20.1	22.00	1.4
WC-B-A3-VIS8	20.2	22.45	1.4
WC-B-A3-VIS19	20.4	22.60	1.4
WC-B-A3-VIS38	20.55	23.45	1.4

Table 5.10 Modified parameters for asphaltenes in bitumen.

Sample	MW_{avg} g/mol	δ_{min} MPa$^{0.5}$	δ_{max} MPa$^{0.5}$	n
WC-B-A3	3000	19.9	20.6	1.2
WC-B-A3-VIS5A	2800	20.15	20.7	1.2
WC-B-A3-VIS5B	2600	20.23	20.83	1.2
WC-B-A3-VIS8	2450	20.15	21.03	1.2
WC-B-A3-VIS19	2300	20.30	21.45	1.2
WC-B-A3-VIS38	1800	20.85	22.10	1.2

5.3.1 Molecular Weight

Figure 5.5a shows that molecular weights of the distillates, saturates, aromatics, and resins decrease with conversion as expected with side chain removal. The side chain fragments become part of the distillate and saturate fractions lowering the average molecular weight of each fraction.

The fragments left in the aromatic and resins fractions have lost side chains and also lower the average molecular weight of each fraction. The molecular weight of the resins decreases more steeply particularly at higher conversions. It is possible that the larger resins undergo condensation reactions and are converted to asphaltenes and coke. Figure 5.5b shows the number average molecular weight of the asphaltene nano-aggregates decreases even more dramatically with conversion. It is likely that both the monomer size of the thermally cracked asphaltenes is smaller on average but also that the cracked asphaltenes self-associate less than the original asphaltenes (Wiehe, 1993). Fainberg *et al*., 1996 reported similar results where the molecular weight of initial feeds and their fractions (saturates, naphtheno-aromatics, aromatics total, and asphaltenes) were reduced after visbreaking.

As discussed in Chapter 4, the broad range of the molecular weights of the asphaltene nano-aggregates is to be represented with a Gamma distribution. The monomer molecular weight was set to 800 g/mol and the shape factor, α, to unity as recommended by Powers *et al.* (2016). The average molecular weights were measured and are shown in Figure 5.5b. Figure 5.6 presents the molecular weight distributions obtained for the feed and for the reacted samples.

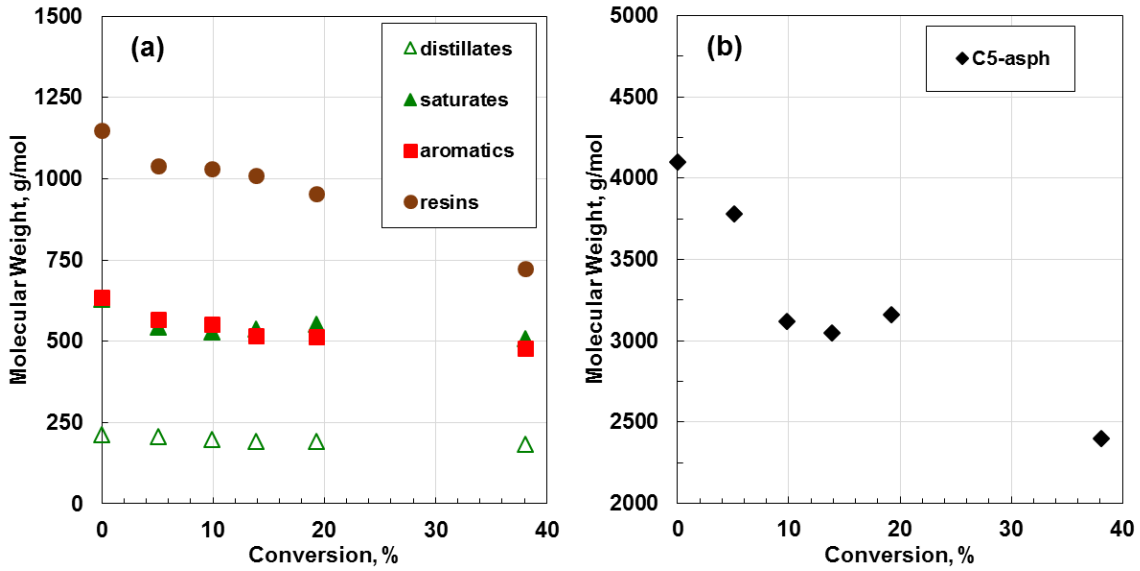

Figure 5. 5 Molecular weight of WC-B-A3 SARA and distillate fractions measured in toluene at 50ºC. The repeatability of the molecular weight measurements was ±15%.

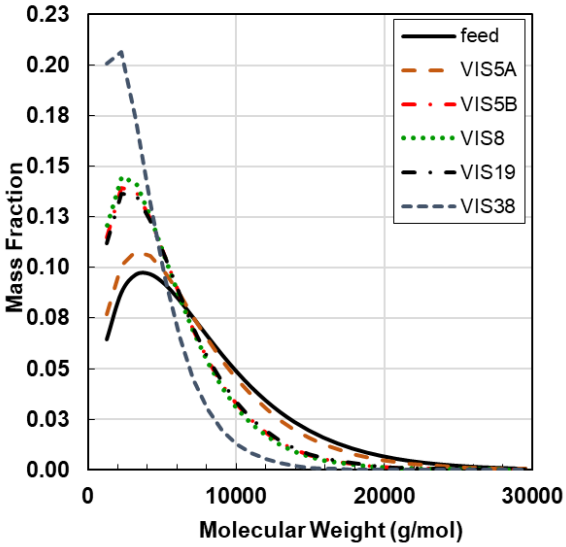

Figure 5.6 Calculated molecular weight distribution at 50ºC for asphaltenes from WC-B-A3 feed and visbroken products.

5.3.2 Density

Figure 5.7 shows the change in density of the distillates and SARA fractions with conversion. The density of saturates and distillates decreased as the conversion increased, consistent with the addition of small, relatively low density fragments from the aromatic, resin, and asphaltene fractions. The density of the aromatics, resins and asphaltenes increased with the conversion. The fragments left in these fractions after side chain removal are more aromatic and therefore denser. The asphaltenes had the greatest increase in density. Condensation products from the aromatics or resins that become asphaltenes would also be more aromatic and denser and could contribute to increase in asphaltene density.

As discussed in Chapter 4, the density distribution of the asphaltene nano-aggregates is to be represented with an empirical correlation proposed by Powers *et al.*, 2016. The minimum density for the correlation was set to 1050 kg/m³ and the shape factor, τ, was set to 9 for the feed and 7 for the products, as recommended by Powers *et al.*, 2016. The maximum density was adjusted to match the measured average density. The density distribution parameters were provided in Table 5.8. Figure 5.8 shows the calculated density distributions.

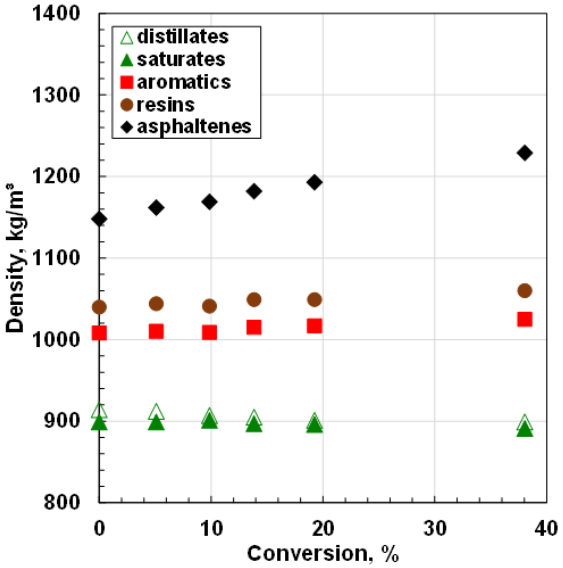

Figure 5.7 Density of WC-B-A3 distillates and SARA fractions at 21°C versus conversion. The repeatability of the density measurements was ±0.03 kg/m³, ±0.9 kg/m³, ±1.05 kg/m³, ±7.7 kg/m³, and 8.5 kg/m³ for distillates, saturates, aromatics, resins, and asphaltenes respectively.

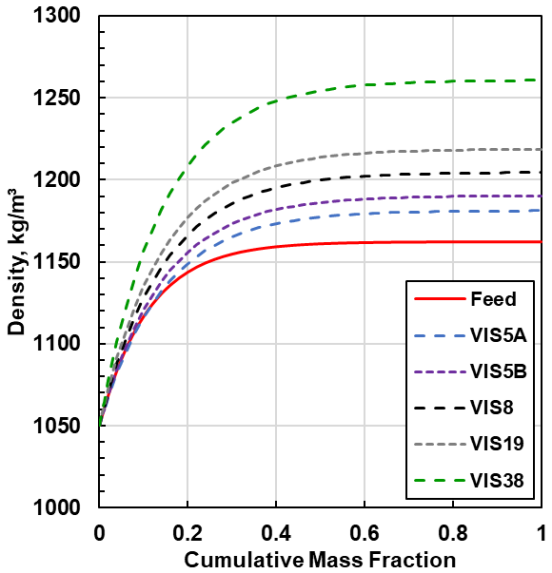

Figure 5.8 Density distribution at 21°C for asphaltenes from WC-B-A3 feed and visbroken products.

5.3.3 Solubility Parameters

As discussed in Chapter 4, the solubility parameters of the distillates and SARA fractions were determined by fitting the Modified Regular Solution (MRS) model to solubility measurements. The parameters obtained for each fraction are discussed below.

Asphaltenes and Resins

The asphaltene solubility parameter distributions were determined from the solubility data of asphaltenes in solutions of toluene and *n*-heptane shown in Figure 5.9. The yield curves shifted to lower *n*-heptane contents with increasing conversion, indicating that the cracked asphaltenes were less soluble in these mixtures. As was discussed in Chapter 4, the solubility parameter distribution of the asphaltene nano-aggregates is represented as follows:

$$\delta_A = \delta_{min} + (\delta_{max} - \delta_{min}) * w_A^n \quad (5.1)$$

The δ_{max} parameter determines the onset of precipitation, δ_{min} determines the amount of precipitation at high dilution, and the exponent, *n*, alters the shape of the yield curve as shown in Figure 5.9. The exponent was set to 1.4 as recommended by Powers *et al.* (2016) for asphaltenes in solvents.

Figure 5.10 shows the model fitted to the solubility data for the feed and visbroken asphaltenes. The fitted parameters were provided in Table 5.9. The solubility parameters of the asphaltenes increased with conversion and the distribution broadened. Aromatics species have higher solubility parameters than paraffinic species. The removal of alkyl side chains increased the aromaticity of asphaltenes and therefore increased their solubility parameters. The solubility curve of the most reacted asphaltenes (VIS38) indicates that asphaltenes may have precipitated even without the addition of *n*-heptane; the fitted model shows a low asphaltene yield at zero heptane content. In other words, the VIS38 sample appears to have reached the stability limit.

Since, the solubility parameters of resins could not be determined experimentally, as discussed in Chapter 4 (Section 4.2.3), the resin solubility parameters were set to the minimum asphaltene solubility parameters (δ_{min}) from Table 5.10.

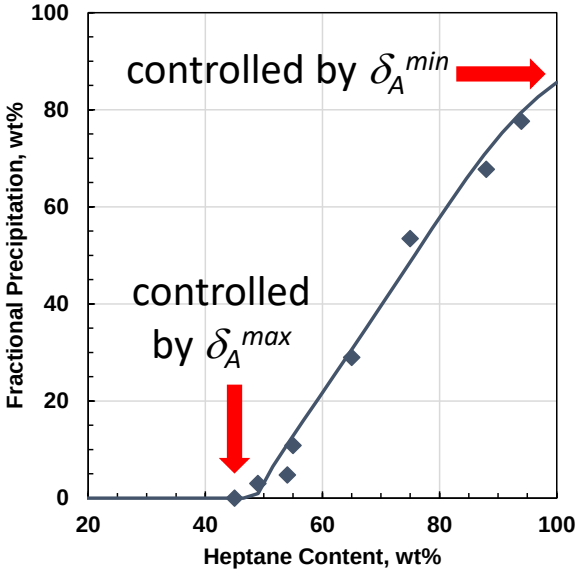

Figure 5.9 Fractional precipitation of asphaltenes in solutions of toluene and *n*-heptane at 20ºC for the WC-B-A3 feed.

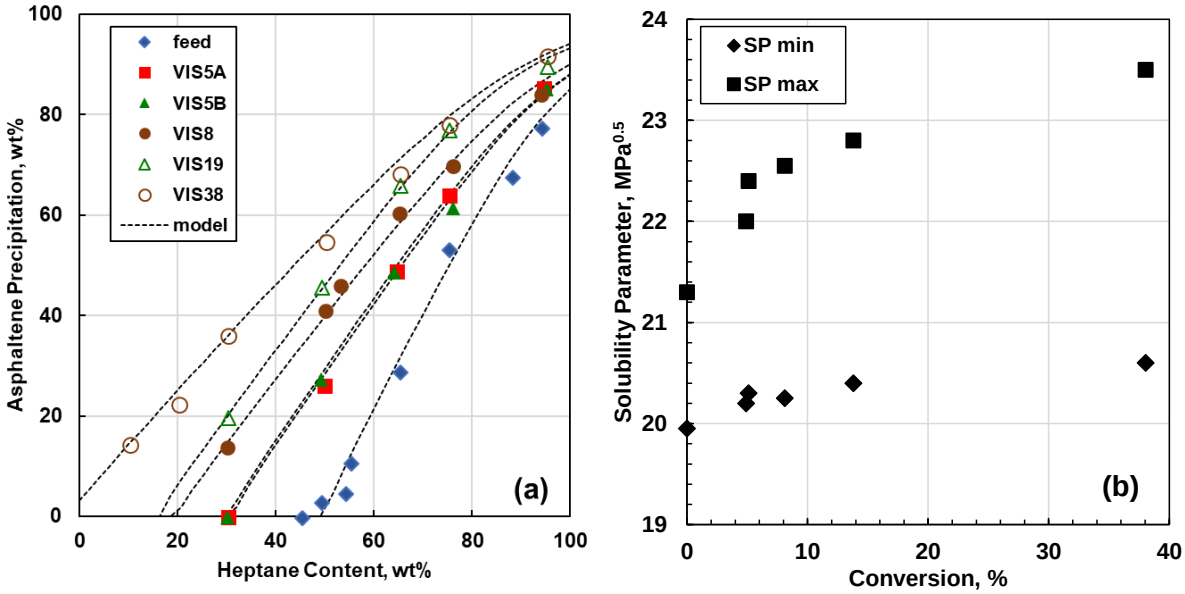

Figure 5.10 Solubility of asphaltenes in heptane/toluene solutions at 21ºC for WC-B-A3 feed and visbroken products: a) fractional precipitation; b) minimum and maximum solubility parameters (SP) in asphaltene solubility parameter distribution. The repeatability of the yield measurements was ±0.5 wt% and the uncertainty of the calculated solubility parameters was ±0.03 MPa$^{0.5}$.

Distillate, Saturates, and Aromatics

The solubility parameters of the distillates, saturates, and aromatics were determined by fitting the MRS model to asphaltene yield data from distillates/heptane, saturates/toluene and aromatics/heptane mixtures, respectively. The solubility parameter of the distillates was also determined by fitting the MRS model to residue and whole oil solubility data. The only difference between the residue and the whole oil is the presence of distillates in the whole oil. In each case, the only unknowns in the model input was the solubility parameter of the distillates, saturates, or aromatics in the mixture and they were adjusted to fit the data. The fitted solubility parameters for all three fractions are shown in Figure 5.11.

The solubility parameter of the distillates decreased from 19.3 to 17 $MPa^{0.5}$ with increasing conversion, consistent with the addition of relatively small, paraffinic or naphthenic side-chain fragments to the distillates. The solubility parameter of the VIS8 sample is higher than expected based on the trend of the other visbroken samples. The deviation could be caused by an experimental error associated with the distillation assay or solubility measurements.

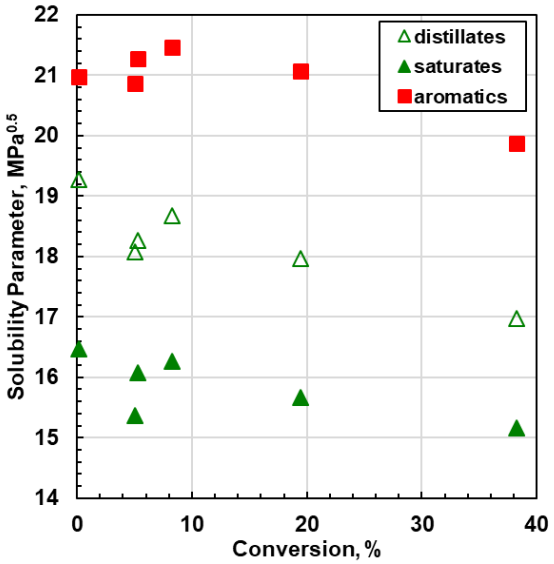

Figure 5.11 Solubility parameters of distillates, saturates, and aromatics from WC-B-A3 feed and visbroken products at 21°C. The repeatability of the calculated solubility parameters was ±0.3 $MPa^{0.5}$.

The solubility parameter of the saturates decreased with conversion from 16.5 to 15.2 $MPa^{0.5}$. The decrease in the solubility parameter is likely caused by the addition of relatively small, paraffinic or naphthenic side-chain fragments. However, the change in solubility parameter is large considering the relatively small change in saturate content within the residue. In fact, the solubility parameters of the visbroken products, particularly VIS5B and VIS38, approach that of *n*-heptane (15.3 $MPa^{0.5}$). Some of the difference can be attributed to experimental error; for example, the VIS5B data point is below the trend of the other samples. It is also possible that the MRS model does not accurately account for the solubility parameter of naphthenic material such as saturates (Yarranton *et al*., 2018 and Mannistu *et al*., 1997).

The solubility parameter of reacted aromatics was approximately 21 $MPa^{0.5}$ except for the most reacted sample (VIS38) with a solubility parameter of 19.8 $MPa^{0.5}$. The consistent solubility parameter at lower conversions suggests that aromatic fractions may lose relatively few side-chains or that the loss of side-chains is compensated by a gain of formerly asphaltene aromatic fragments. At conversions above 20%, the most aromatic components likely undergo secondary reactions such as polymerization and condensation. The conversion of those compounds to resins or asphaltenes decreases the proportion of aromatics structures remaining in the aromatics fraction. Therefore, at higher conversion, the residual aromatics becomes a more paraffinic fraction with a lower solubility parameter. Yarranton *et al*. (2018) also reported an initial increase and subsequent reduction in the solubility parameter of aromatics at conversions of 17 and 51% respectively.

5.4. Solubility Modeling

5.4.1. Distillation Residues

The modified regular solution approach was first used to model asphaltene solubility in the distillation residues. The residues consist of all of the SARA fractions but no distillates. Since the samples were too viscous to take accurate precipitation measurements, they were first mixed with toluene (0.5 g toluene / g bitumen). Figure 5.12 shows the asphaltene yield curves from heavy residue samples mixed with toluene and diluted with *n*-heptane. The asphaltenes in the heavy residue samples became less soluble as the conversion increased for two reasons: 1) the average

solubility parameter of the oil decreased making it a poorer solvent for the asphaltenes; 2) the asphaltene solubility parameters increased making them less soluble in the oil.

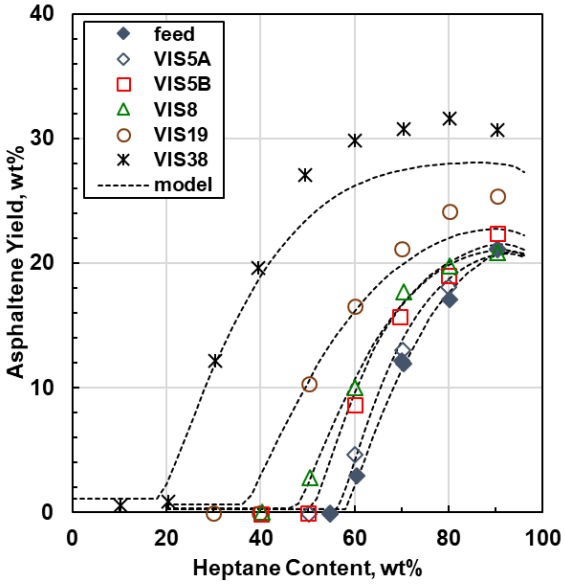

Figure 5.12 Asphaltene yield for feed and visbroken heavy residues mixed with toluene (0.5 g/g) and diluted with heptane at 20°C. The repeatability of the yield measurements was ±0.5 wt%.

Figure 5.12 also shows the fitted MRS model results. Recall that the required input data for the model are SARA characterization data (mass composition and physical properties such as densities, molecular weight and solubility parameters). All of the properties were taken directly from the previously reported measurements (Tables 5.4 to 5.9) except for the asphaltene average molecular weights and solubility parameter distributions. The asphaltenes in the crude oil are surrounded by resins and are expected to self-associate less than the extracted (and extensively washed) asphaltenes used in the previous measurements. Therefore, average molecular weight and the solubility parameter distribution were both tuned to fit the asphaltene yield data in the heavy residues. First, the average molecular weight of the native asphaltenes in the bitumen was constrained as discussed in Appendix C and then the solubility parameter was adjusted to fit the yield data. The molecular weights were also smoothed using a correlation which will be discussed later. The adjusted parameters for the asphaltenes were listed in Table 5.10 and are shown in Figure 5.13. The minimum solubility parameters were almost the same as those of the extracted asphaltenes.

The adjusted molecular weights and maximum solubility parameters were lower than those of the extracted asphaltenes. The overall effect was to make the asphaltenes more soluble at all *n*-heptane contents.

At conversions below 19%, the model fit the data with an AAD of 0.45 wt%; that is, to within the experimental error of 0.5 wt%. At conversions at or above 19%, the model underestimated the asphaltene yields at *n*-heptane contents above 60 wt%. The deviation is attributed to the unreliability of the data at these conditions; for example, the measured asphaltene yields of the VIS38 sample were greater than the asphaltene content obtained from the SARA method (27.6%). The highly converted visbroken asphaltenes appear to have a strong affinity for the other bitumen components and it was not possible to remove the non-asphaltene components consistently. Therefore, the error in the yields and the asphaltene content from SARA may be inaccurate at high conversion. Although it is not clear if the model correctly predicts the yields for highly reacted samples at high heptane ratios, it did fit the onset of asphaltene precipitation for all of the samples. In most industrial applications, predicting the onset of precipitation is usually more important than predicting yields at high dilution.

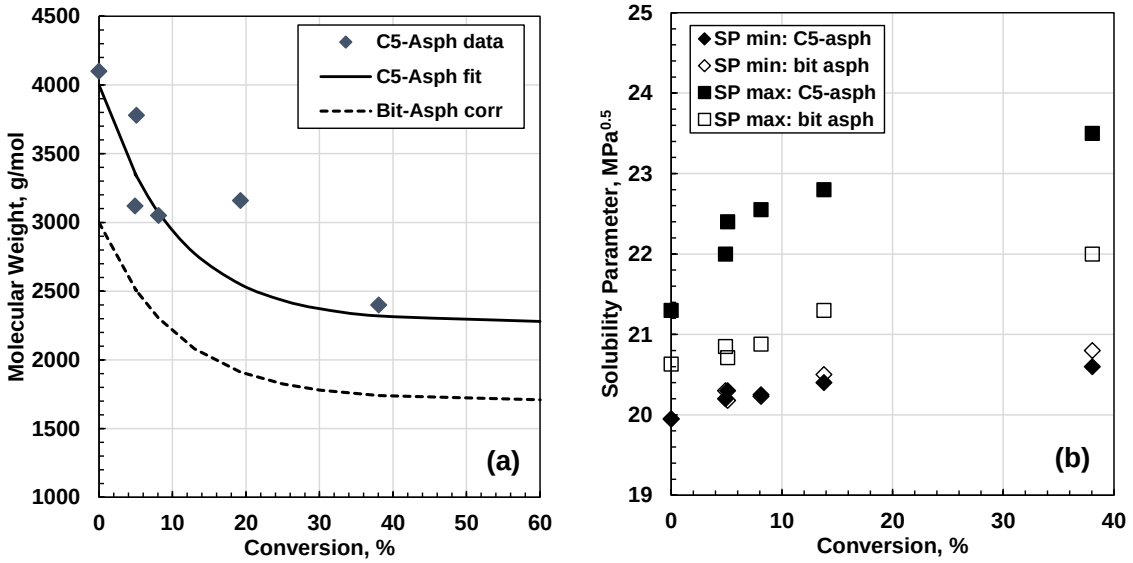

Figure 5.13 Modified properties for asphaltenes in bitumen: a) average molecular weight of extracted asphaltenes measured in toluene (C5-asph) and fitted average molecular weight of asphaltenes in bitumen (bit asph); b) minimum and maximum solubility parameters for extracted asphaltenes and asphaltenes in bitumen.

5.4.2. Whole Oils

The MRS approach was next used to model the asphaltene stability in whole oils. The whole oils are equivalent to the residues plus the distillates. For consistency with the residue data, all of the samples were first diluted with toluene (0.5 g toluene / g bitumen). Figure 5.14 shows the asphaltene yield curves for whole oils mixed with toluene and diluted in with *n*-heptane. The yield data were modeled as described for the residues with the addition of distillates to the fluid characterization. As noted previously, the molecular weight and density of the distillates was determined from the distillation assay. Their solubility parameters were adjusted to fit the whole oil yield data. The fitted solubility parameters were provided in Table 5.3. Figure 5.14 shows that the model fit the data with an AAD of 0.41 wt%; that is, to within the measurement error of ±0.5 wt%.

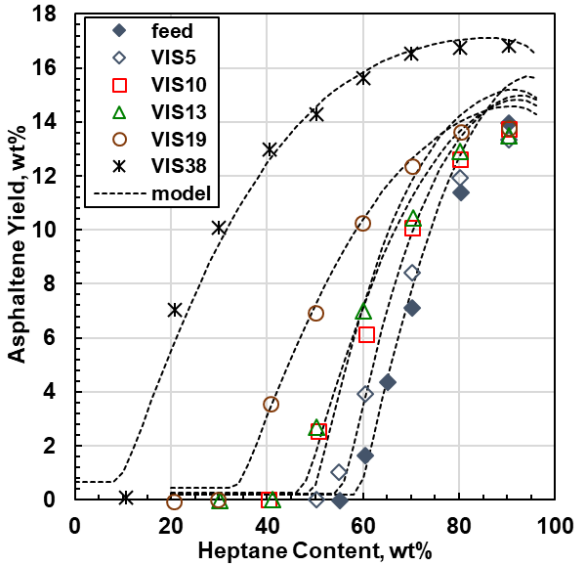

Figure 5.14 Asphaltene yield for feed and visbroken whole oils mixed with toluene (0.5 g/g) and diluted with heptane at 20°C. The repeatability of the yield measurements was ±0.5 wt%.

Recall that the distillate solubility parameters were also determined from asphaltene precipitation yields from solutions of asphaltenes, distillates, and *n*-heptane. The distillate parameters from fitting the whole oil yield data are compared with these values in Table 5.3. The distillate solubility parameters from each method match within the accuracy of the measurement except for the feed distillates (19.3 $MPa^{0.5}$ in the whole oil versus 18.7 $MPa^{0.5}$ in the solvent solution). The reason for this discrepancy is likely experimental error. It was challenging to dissolve the asphaltenes in the

distillates and, if the asphaltenes were not completed dissolved, the reported yields and calculated solubility parameters will be incorrect. In fact, the solubility experiments VIS8 and VIS38 were not performed because it was too difficult to completely solubilize the asphaltenes in these distillates even though the mixtures were sonicated at 60ºC for about 4 hours. Therefore, the solubility parameter determined from the whole oil data is used in all further modeling.

The model was then tested on yield data from the whole oil samples without toluene addition. Figure 5.15a shows that the model matched the yields at low conversions (< 19%) with an AAD of 0.41 wt%; that is, to within the error of the measurements. Figure 5.15b shows that the model did not match the data at high conversions; the predicted onset was lower than the measured onset and the predicted yield was lower than the measured yield at high dilution. In this case, the deviation is attributed to the failure of the experimental method with low solubility samples. There are two issues with the measurements. First, the onset of precipitation occurs at a low *n*-heptane content and the mixture may be viscous enough to prevent precipitated asphaltenes from settling. The precipitated asphaltenes are not detected and the yield is reported as zero even though precipitation has occurred. Second, the precipitated material was resistant to washing particularly at high yields. Therefore, other bitumen components were trapped in the precipitate inflating the measured yield.

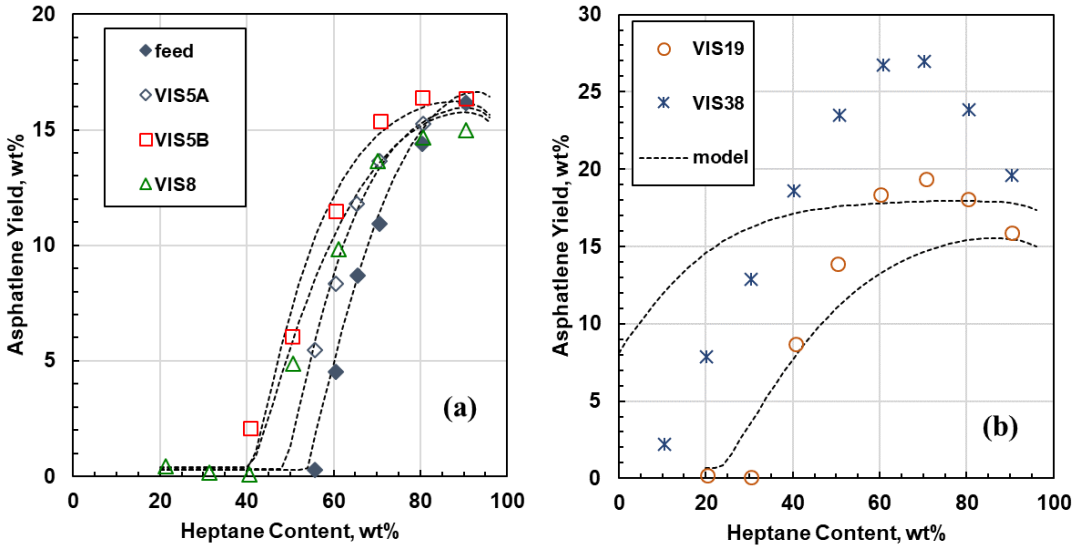

Figure 5.15 Asphaltene Yield for whole oils from a) feed and low converted samples (VIS5A, VIS5B, and VIS8) and b) high reacted samples (VIS19 and VIS38) diluted with *n*-heptane at 20ºC and atmospheric pressure. The repeatability of the yield measurements was ±0.47 wt%.

5.5. Preliminary Property Correlations for Visbroken Oils

The proposed MRS model is intended to start with known distillate and SARA compositions either measured or predicted with an independent reaction model. Therefore, the only step required to generalize the model is to develop correlations for the properties of the distillates and SARA fractions. In a previous study (Powers *et al*., 2016; Yarranton *et al*., 2018), correlations were proposed for the molecular weight, density, and solubility parameters of SARA fractions as a function of conversion based on a limited dataset. The dataset included the properties of a vacuum bottom feed from a Western Canadian bitumen and three thermally cracked products from this feed with conversions of 17, 31, and 51%. Additional information about the source of each sample is provided elsewhere (Powers *et al*., 2016). The data from this thesis is used to update the correlations and new correlations for the distillates properties are proposed. The correlations are still considered to be preliminary because the effect of different feedstocks and different reactors with potentially different reaction pathways has not been considered.

5.5.1 Molecular Weight

The molecular weights of each fraction were fitted with first order differential equations with the solutions provided in Table 5.11. Figure 5.16a shows the fit to the distillate data. No comparisons are made to the previous study because no distillate data were collected in that study.

Table 5.11 Proposed correlations for molecular weight of visbroken products (MW = molecular weight, subscript f denotes feed, X = percent conversion).

Fraction	Correlation
Distillates	$MW = MW_f\left[1 - 0.139\left(1 - exp(-0.116\,X)\right)\right]$
Saturates	$MW = MW_f\left[1 - 0.122\left(1 - exp(-0.512\,X)\right)\right]$
Aromatics and Resins	$MW = MW_f\left[1 - 0.306\left(1 - exp(-0.095\,X)\right)\right]$
Asphaltenes	$MW = MW_f\left[1 - 0.338\left(1 - exp(-0.1\,X)\right)\right]$

Figure 5.16b shows the correlation fitted to the saturate data. The data were normalized by the molecular weight of the feed for comparison with data from the previous study (Yarranton *et al.*, 2018). The saturate molecular weights from previous study did not change with conversion while data from this study decreased by 12%. The repeatability of the molecular weight measurements

is 15% and therefore the difference may be a result of an experimental error. The correlation was modified to match the data from this thesis because the functional form was consistent with that of the other SARA fractions.

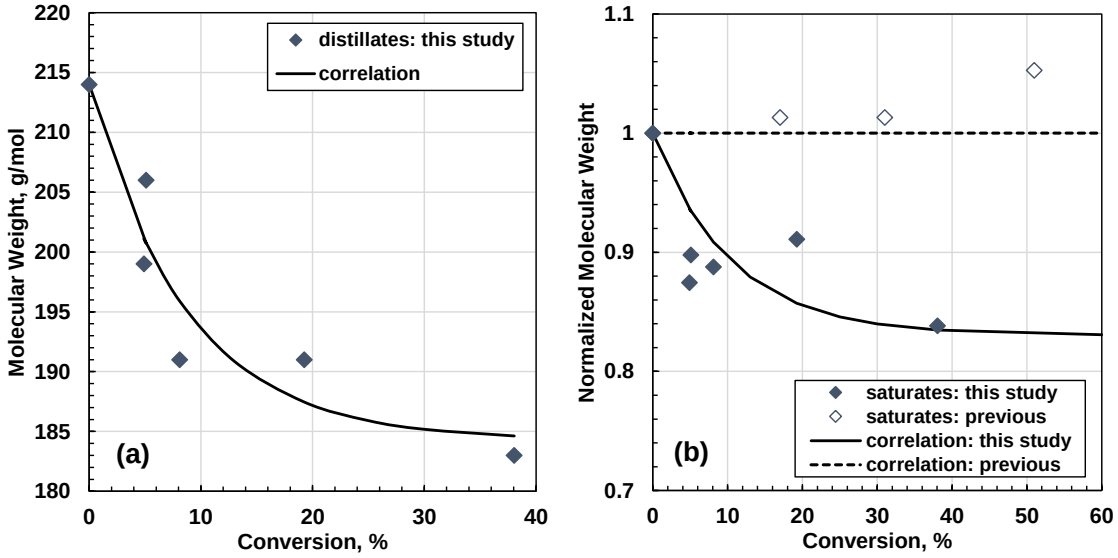

Figure 5.16 Proposed molecular weight correlations for visbroken: a) distillates; b) saturates. "Previous" is from Yarranton *et al*. (2018). The repeatability of the molecular weight measurements was ±15%

Figure 5.17a shows the correlation fitted to the normalized aromatic and resin molecular weights. The aromatic and resin data were fit together because, once normalized to the feed values, they followed the same trend. The data from this study followed an exponential trend while the data from the previous study (Yarranton *et al.*, 2018) followed a linear trend. Some of the difference could be experimental error. It is also possible that the different feeds (whole oil versus vacuum bottom) respond differently to thermal cracking.

Figure 5.17b shows the normalized molecular weights of the extracted asphaltenes versus conversion. In this case, the data from this study and the previous study (Powers *et al.*, 2016) followed the same trend with conversion. Therefore, a correlation was developed using the data from both studies. There was no previous correlation to compare against. Recall that the same

correlation was used for the bitumen asphaltenes. The only difference is that the feed molecular weight was set to 3000 g/mol (See Appendix C).

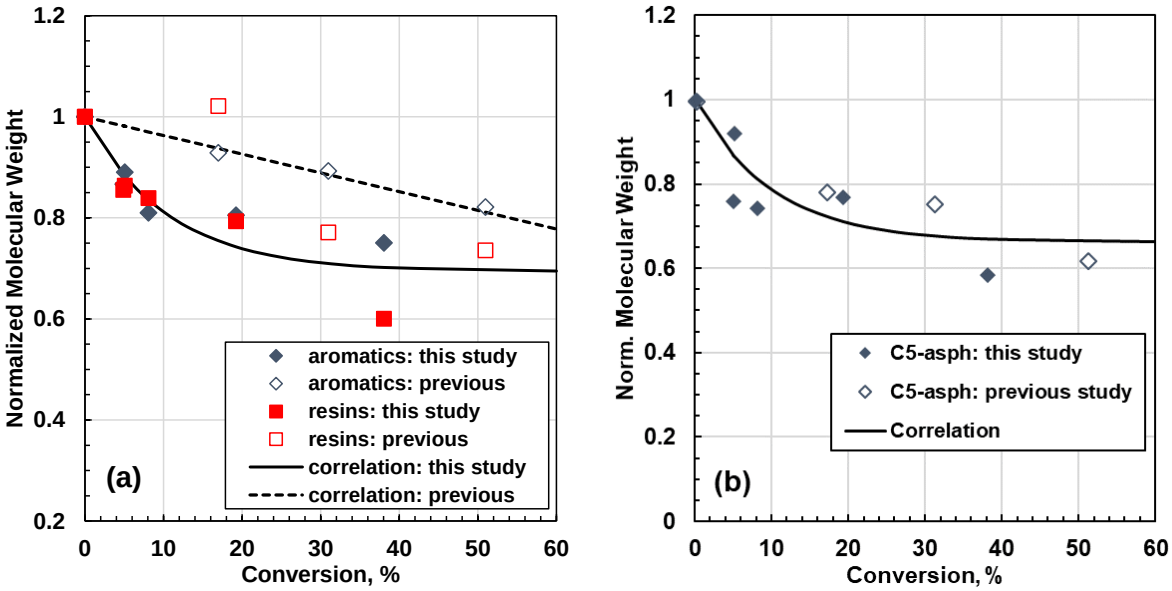

Figure 5.17 Proposed molecular weight correlations for visbroken: a) aromatics and resins; b) extracted asphaltenes (C5-asph) at 50°C. "Previous" is from Yarranton *et al.* (2018) for aromatics and resins and from Powers *et al.* (2016) for extracted asphaltenes. The repeatability of the molecular weight measurements was ±15%.

5.5.2 Density

The densities of each fraction were fitted with the equations provided in Table 5.12. The density of the SARA fractions decreased linearly with conversion while the density of the distillates decreased following a first order differential equation. The different trends likely reflect different mechanisms: side chain removal from the SARA fractions versus the accumulation of side-chain fragments in the distillate.

Figure 5.18a shows the correlation for the distillate densities. No comparisons are made to the previous study because no distillate data were collected in that study. Figure 5.18b shows the correlation fitted to the saturate densities. The density of the feed saturates from the previous study (Yarranton *et al.*, 2018) was anomalously low and therefore only the data from this thesis were used for the correlation.

Table 5.12 Proposed correlations for density at 21°C of visbroken products (ρ = density, subscript f denotes feed, X = percent conversion).

Fraction	Correlation
Distillates	$\rho = \rho_f[1 - 0.174(1 - exp(-0.0823\,X))]$
Saturates	$\rho = \rho_f[1 - 0.00020\,X]$
Aromatics and Resins	$\rho = \rho_f[1 + 0.00050\,X]$
Asphaltenes	$\rho = \rho_f[1 + 0.00196\,X]$

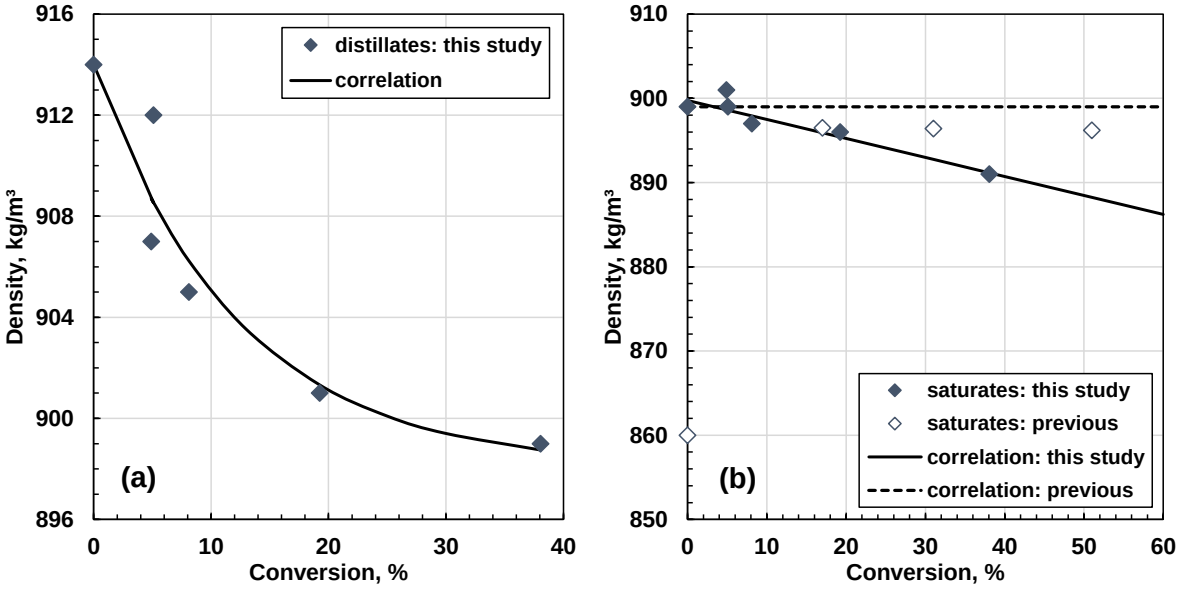

Figure 5.18 Proposed density correlations for visbroken: a) distillates; b) saturates. "Previous" is from Yarranton *et al*. (2018). The repeatability of the density measurements was ±0.03 kg/m³ and ±0.9 kg/m³ for distillates and saturates respectively.

Figure 5.19a shows the correlation fitted to the normalized aromatic and resin densities. The aromatic and resin data were fit together because, once normalized to the feed values, they followed the same trend. The correlation from the previous study (Yarranton *et al.*, 2018) and the correlation modified after considering all of the data are almost identical.

Figure 5.19b shows the normalized densities of the extracted asphaltenes versus conversion. The data from this study and the previous study (Powers *et al.*, 2016) followed the same trend with conversion except possibly for the data point at the highest conversion. Since the aromatic and

resin densities followed a linear trend and this high conversion point deviated from an otherwise linear trend for the extracted asphaltenes, it was excluded from the data fitting. The density of the asphaltenes in bitumen was assumed to be equal to the density of the extracted asphaltenes.

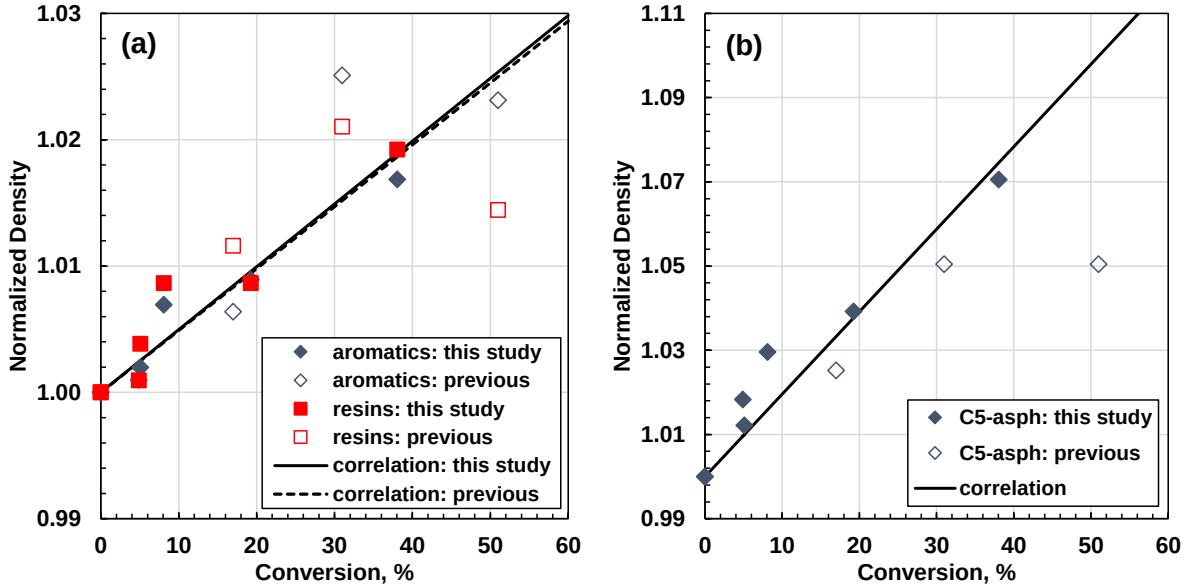

Figure 5.19Proposed density correlations for visbroken: a) aromatics and resins; b) extracted asphaltenes (C5-asph). "Previous" is from Yarranton *et al.* (2018) for aromatics and resins and from Powers *et al.* (2016) for extracted asphaltenes. The repeatability of the density measurements was ±1.1 kg/m³ for aromatics and ±8.1 kg/m³ for resins and asphaltenes.

5.5.3 Solubility Parameter

The solubility parameters of each fraction were fitted with the equations provided in Table 5.13. The solubility parameters of all fractions except the aromatics decreased following a first order differential equation. The aromatics likely followed a similar trend but there were insufficient data to justify any function more complex than a linear trend. Recall that the resin solubility parameters could not be experimentally determined and were instead set equal to the minimum asphaltene solubility parameter.

Figure 5.20a shows the correlation for the distillate solubility parameters. No comparisons are made to the previous study because no distillate data were collected in that study. Figure 5.20b

shows the correlation for the saturate solubility parameters. The solubility parameters from the previous study (Yarranton *et al*., 2018) were anomalously low (lower than *n*-pentane solubility parameters) and therefore were not used in developing the correlation.

Table 5.13 Proposed correlations for solubility parameter at 21°C of visbroken products (δ = solubility parameter, subscript f denotes feed, X = percent conversion); C5-Asph = extracted asphaltenes and Bitumen Asph. = asphaltenes in bitumen.

Fraction	Correlation
Distillates	$\delta = \delta_f\left[1 - 0.118\left(1 - exp(-0.069\,X)\right)\right]$
Saturates	$\delta = \delta_f\left[1 - 0.074\left(1 - exp(-0.084\,X)\right)\right]$
Aromatics	$\delta = \delta_f[1 - 0.000925\,X]$
Resins	$\delta = \delta_{min}\ of\ bitumen\ asphaltenes$
C5-Asph. minimum	$\delta = 20.2\left[1 + 0.455\left(1 - exp(-3.325\text{E} - 0.4\,X)\right)\right]$
C5-Asph. maximum	$\delta = 21.3\left[1 + 0.0902\left(1 - exp(-0.0754\,X)\right)\right]$
Bitumen Asph. minimum	$\delta = 20.02\left[1 + 0.0557\left(1 - exp(-0.0226\,X)\right)\right]$
Bitumen Asph. maximum	$\delta = \delta_f + \Delta\delta\left(1 - exp(-0.00930\,\Delta\delta\,X)\right)$; $where\ \Delta\delta = 23.22 - \delta_f$

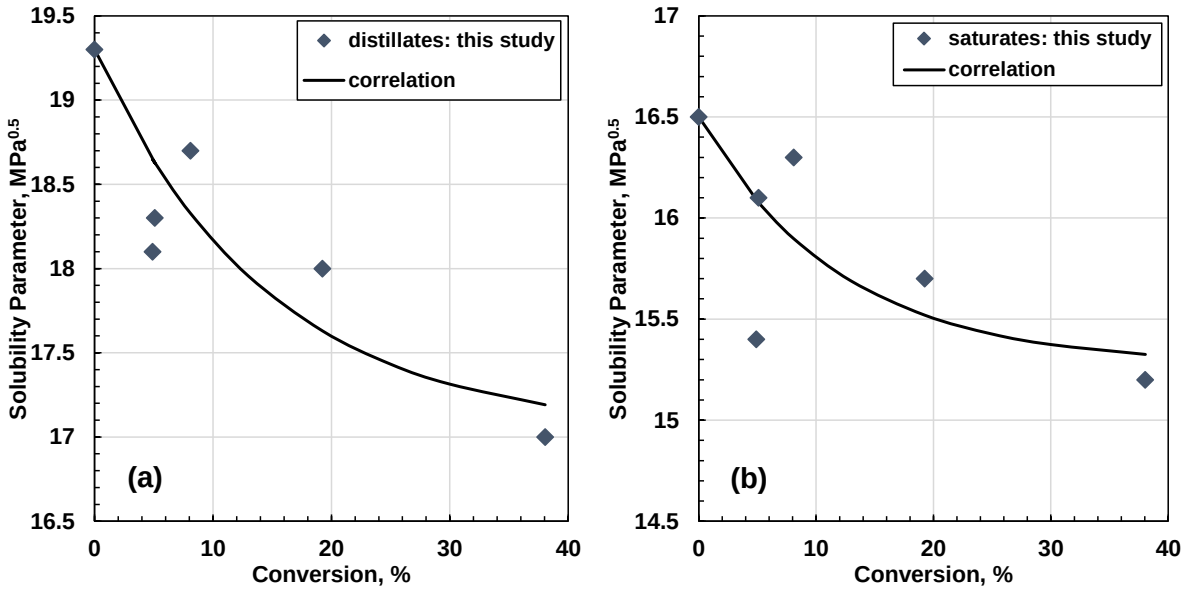

Figure 5.20 Proposed solubility parameter correlations for visbroken: a) distillates; b) saturates. "Previous" is from Yarranton *et al*. (2018). The uncertainty of the solubility parameter measurements was found to be ±0.3 $MPa^{0.5}$.

Figure 5.21 shows the correlation for the aromatic solubility parameters. The solubility parameters from the previous study (Yarranton *et al*., 2018) were scattered and no correlation was reported. To develop a correlation, the solubility parameter of the aromatics was set to a value of 21.3 $MPa^{0.5}$ based on an average of the low conversion data from this thesis. Then, the slope was determined using all of the data.

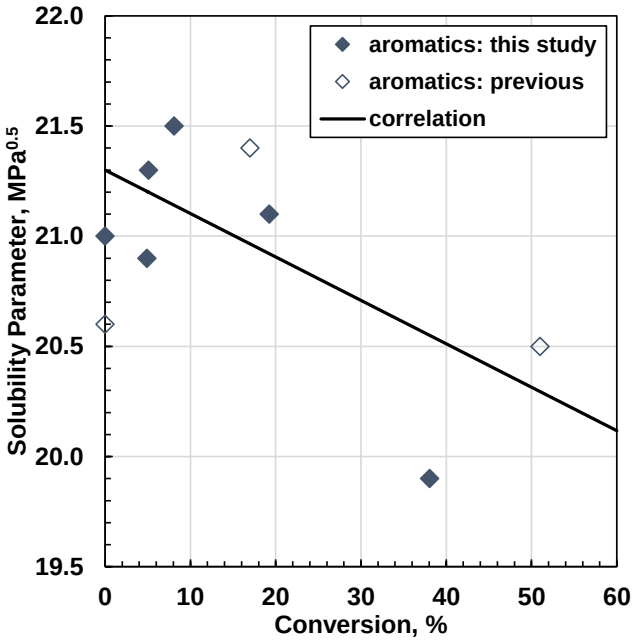

Figure 5.21 Proposed solubility parameter correlation for visbroken aromatics. Previous is from Yarranton *et al.* (2018). The uncertainty of the solubility parameter measurements was ±0.3 $MPa^{0.5}$.

Figure 5.22a shows the solubility parameters of the extracted asphaltenes versus conversion. The data from this study and the previous study (Powers *et al.*, 2016) followed the same trend with conversion. In addition, most extracted asphaltenes from unreacted oils have been found to have similar minimum and maximum solubility parameters (see Appendix D). Therefore, the average minimum and maximum solubility parameter for the feed were set to the average values obtained from a variety of asphaltenes from different sources; that is, $\delta_{f,min}$ = 20.2 $MPa^{0.5}$ and $\delta_{f,max}$ = 21.3 $MPa^{0.5}$. The correlation to conversion was then developed using all of the data from Figure 5.22a.

Figure 5.22b shows the correlation for the bitumen asphaltene solubility parameters. The solubility parameter data are from this thesis and from fitted yield data from Powers (2014). Excluding the maximum solubility parameters of the feeds, the data from this study and the previous study (Powers *et al.*, 2016) followed the same trend with conversion. The minimum solubility parameter for the feed was set to the average value obtained from fitting the model to a variety of *n*-heptane diluted bitumens from different sources (see Appendix E); that is, $\delta_{f,min}$ = 20.02 MPa$^{0.5}$. There was more variation in the maximum solubility parameter of the feed and therefore it was left as an input parameter. If this value is not known, the average value from the same sources cited above can be used; that is, $\delta_{f,max}$ = 20.3 MPa$^{0.5}$. The data for the reacted samples from Powers (2014) were similar to the data from this study and, therefore, both datasets were used to develop the correlations reported in Table 5.13.

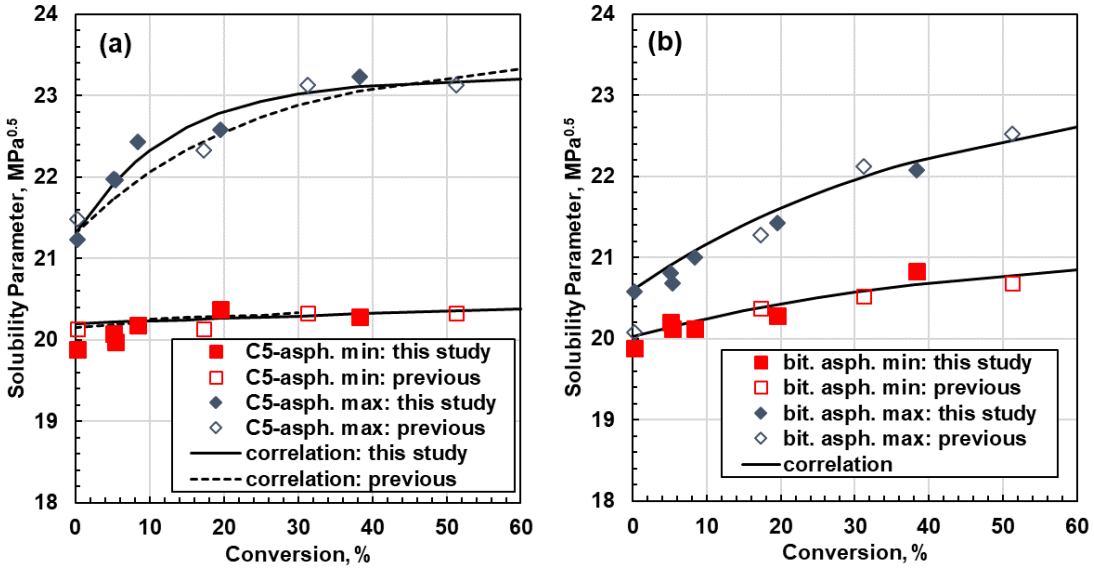

Figure 5.22 Proposed solubility parameter correlations for a) extracted asphaltenes (C5-asph.) in solvents; b) asphaltenes in bitumen. Previous is from Powers *et al.* (2016) for extracted asphaltenes and based on yield data from Powers (2014) for bitumen asphaltenes. WC-B-A3 is the bitumen feed from this study and WC-VB-B2 is a vacuum bottom feed from Powers (2014).

5.5.4 Preliminary Test of the Correlations

The proposed correlations were tested using the data from which they were developed in order to assess the error they introduce into the prediction of asphaltene onsets and yields with the MRS model. The required input parameters are the mass composition of the feed (in terms of distillates,

SARA fractions, and toluene insoluble content), the properties (molecular weight, density, and solubility parameter) of the feed components, the mass composition of the product, and the conversion.

Figures 5.23 and 5.24 show the measured and modeled asphaltene yields for the distillation residues with toluene, the whole oils with toluene, and the low conversion data for whole oils without toluene. In this case, all of the input properties were determined using the proposed correlations. The errors in the fitted and correlated onsets and yields are compared in Table 5.14. The average absolute deviation when using the correlations were 3.1 and 1.3 wt% for the onsets and yields, respectively. The use of the proposed correlations increased the average absolute deviations compared with the fitted data by 2.4 and 0.6 wt% for the onset and yield data, respectively. The main reason for the difference is likely the accuracy of the measured conversions and the high sensitivity of the model to changes in the solubility parameter of asphaltenes. As will be shown later, the conversion and the solubility parameter distribution of asphaltenes are the parameters which have a significant impact on the model predictions.

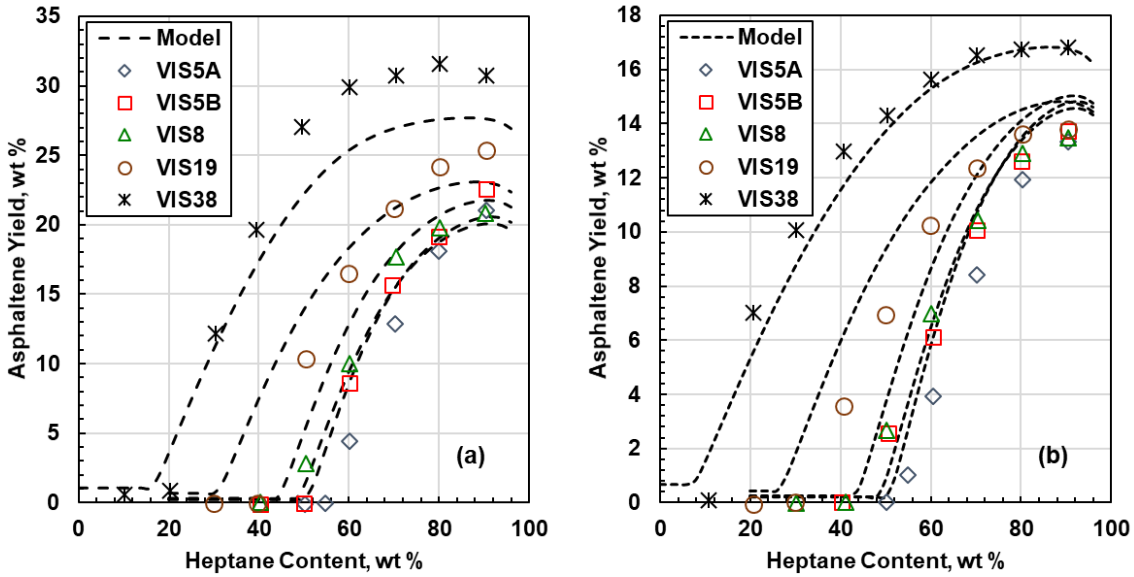

Figure 5.23 Predicted asphaltene yield curves for: a) visbroken heavy residue; b) visbroken whole oils mixed with toluene and diluted with heptane.

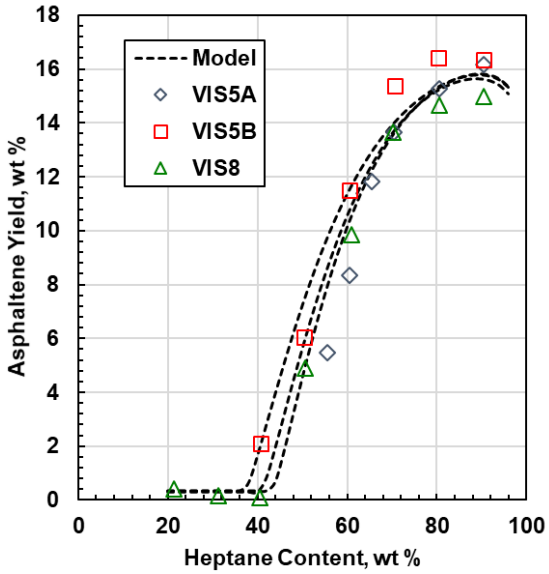

Figure 5.24 Predicted asphaltene yield curves for whole oils from low converted samples (VIS5A, VIS5B, VIS8) diluted with heptane.

Table 5.14 Average absolute deviation (AAD) of the fitted and correlated onsets and yields.

System	AAD (wt%) of Onsets		AAD (wt%) of Yields	
	Fitted	Correlated	Fitted	Correlated
Visbroken Distillation Residue	0.52	2.80	1.1	1.88
Visbroken Whole Oils (diluted with toluene)	0.95	2.84	0.42	1.05
Visbroken Whole Oils (low conversion; no toluene)	0.84	3.72	0.43	0.92

5.6 Sensitivity Analysis of the MRS Model

A sensitivity analysis was performed to identify the most significant parameters in the MRS model and to evaluate how the input parameter uncertainties influence the prediction of the asphaltene stability in visbroken oils. The parameters selected for this analysis were molecular weight, solubility parameter, density, oil composition, and conversion (when using proposed correlations). The properties were varied for the distillate and asphaltene fractions because the distillates make up the largest mass fraction of the oil and the asphaltenes parameters have the most impact on onset and yield predictions. The following asphaltenes properties were analyzed: molecular weight distribution (molecular weight of the monomer and shape factor α), density distribution (shape

factor τ, minimum and maximum densities) and solubility distribution (minimum and maximum solubility parameters). Two cases studies were analyzed: one for a low conversion sample (VIS8) and another for a high conversion sample (VIS38). Both samples showed the same tendencies in the evaluated parameters except for the conversion. Therefore, only the results obtained for the VIS38 sample in the molecular weight, composition, and density are presented. For the conversion, the results of both samples are discussed.

Molecular Weight

The uncertainty in the measured molecular weight is approximately ±15%. Therefore, the model was rerun with distillate and average asphaltene molecular weights increased and decreased by 15%. Figure 5.25a shows that the change in the molecular weight of distillates had little effect on the asphaltene yield predictions for the VIS38 visbroken sample. Figure 5.25b shows that the model was also relatively insensitive to a decrease in the average molecular weight of the asphaltenes but the predicted yields increased by up to 0.47 wt% with an increase of the asphaltene molecular weight, Figure 5.25b. This deviation is within the ±0.5 wt% error of the solubility measurements.

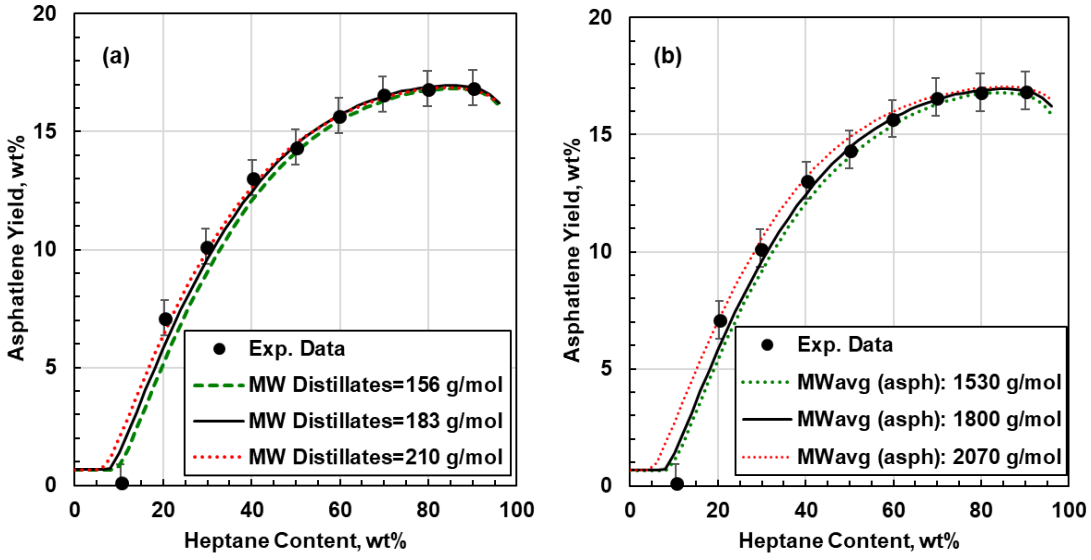

Figure 5.25 Effect on predicted asphaltene yield of a ±15% variation in the input molecular weight of: a) distillates; b) asphaltenes. Results for VIS38 whole visbroken oil mixed with toluene and diluted with n-heptane at 20°C and atmospheric pressure.

Figure 5.26a shows the effect of varying the asphaltene monomer molecular weight by ±200 g/mol on the predicted yield. The maximum deviation was 0.62 wt%. Figure 5.26b shows the effect of adjusting the shape factor of the asphaltene molecular weight distribution from 1 to 3. The yield curves became steeper as the shape factor increased but the predicted yields deviated from the baseline prediction by 0.6 wt% which is slightly above the error of the yield measurements.

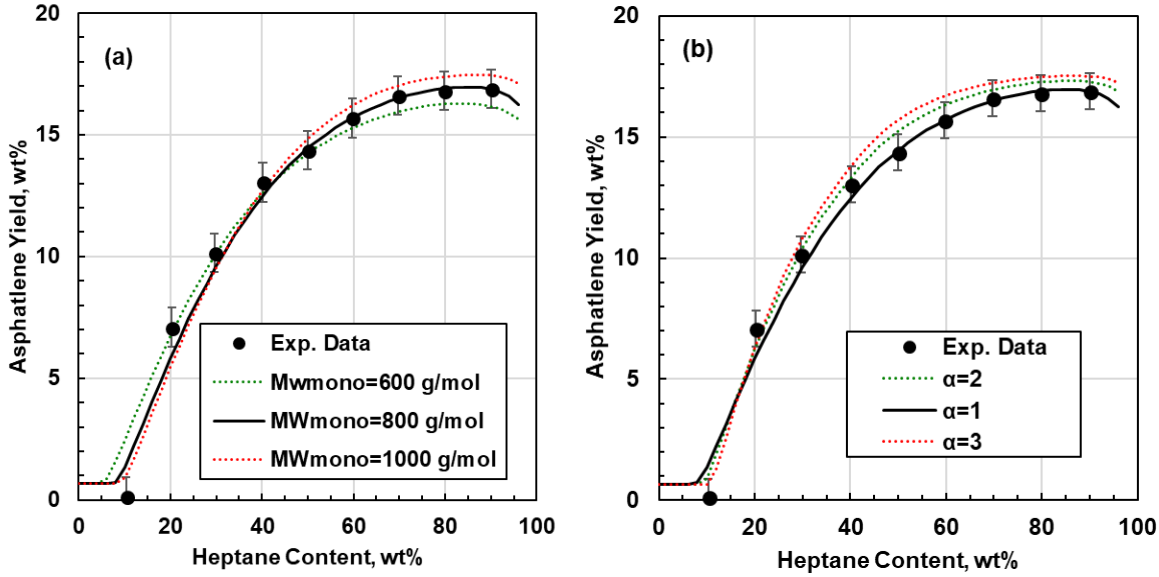

Figure 5.26 Effect of variations in the input asphaltene distribution parameters on the predicted asphaltene yield: a) ± 200 g/mol in monomer molecular weight; b) shape factor from 1 to 3. Results for VIS38 whole visbroken oil mixed with toluene and diluted with n-heptane at 20°C and atmospheric pressure.

Density

The repeatability of the distillate density measurements was ±0.5 kg/m³. The uncertainty of the asphaltene density parameters are provided in Table 5.15. Figures 5.27 and 5.28 shows that the model was insensitive to the variations in the input distillate density and asphaltene density parameters, respectively.

Table 5.15 Uncertainties for the asphaltene density distribution parameters.

Parameter	Range
Minimum Density	± 50 kg/m^3
Maximum Density	± 50 kg/m^3
Shape factor (τ)	± 3

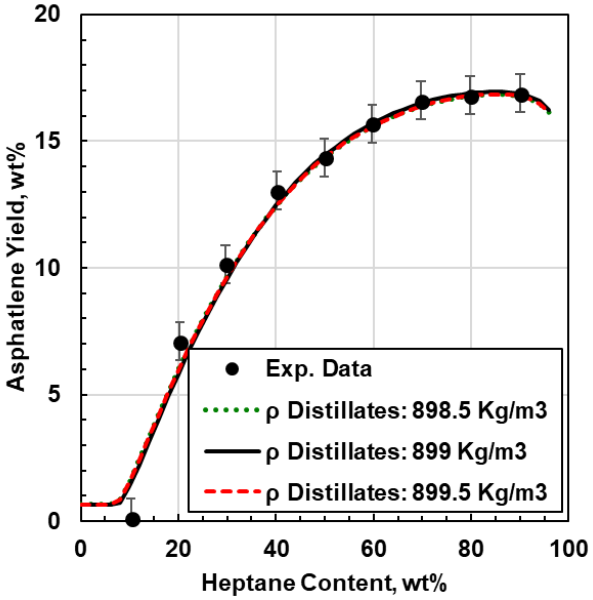

Figure 5.27 Effect of a ±0.5 kg/m³ variation in the input density of the distillates on the predicted asphaltene yield. Results for VIS38 whole visbroken oil mixed with toluene and diluted with n-heptane at 20°C and atmospheric pressure.

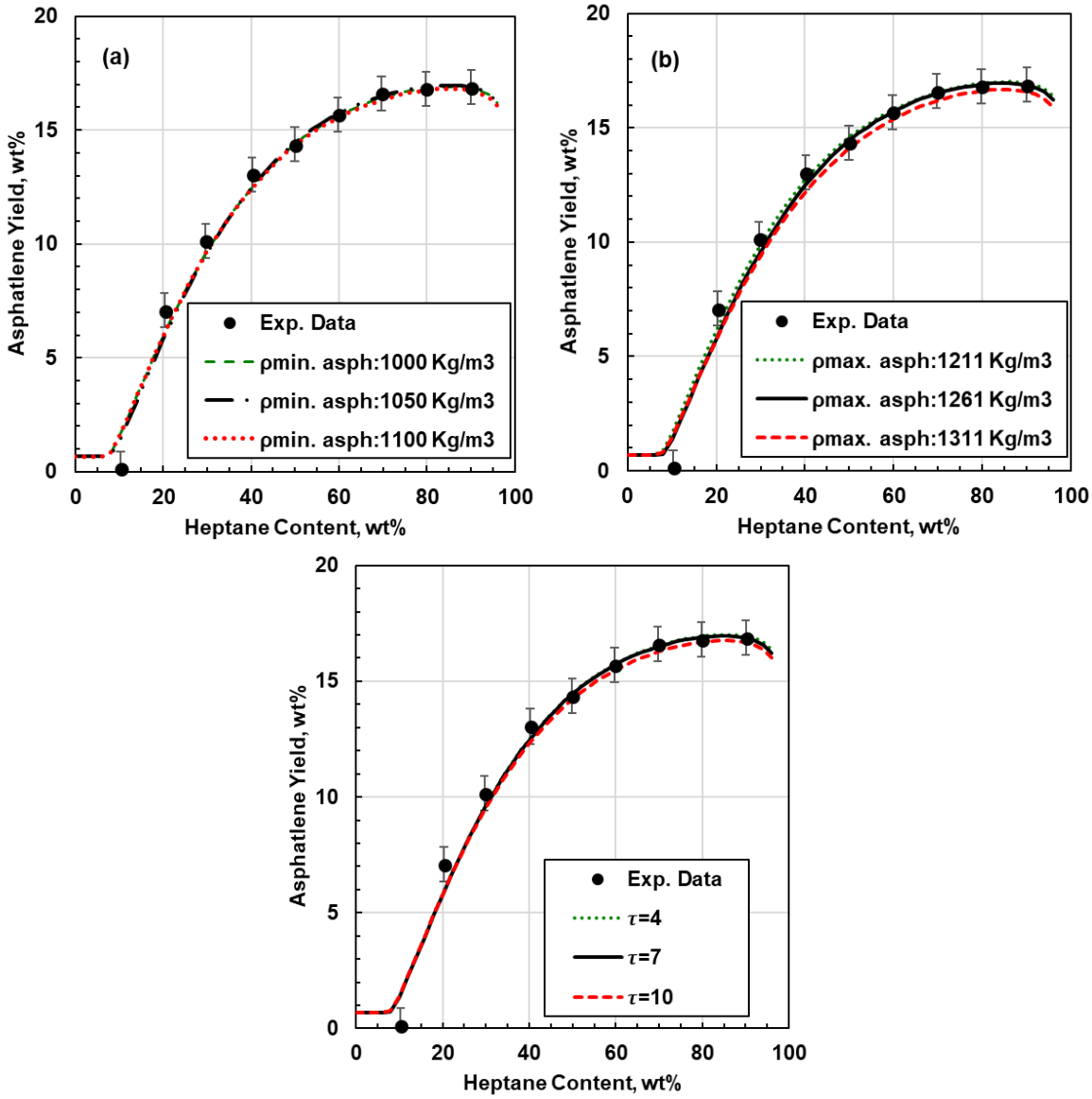

Figure 5.28 Effect of variations in the input asphaltene density distribution parameters on the predicted asphaltene yield: a) ± 50 kg/m³ in minimum density; b) ± 50 kg/m³ in maximum density; c) shape factor in density distribution from 4 to 10. Results for VIS38 whole visbroken oil mixed with toluene and diluted with n-heptane at 20°C and atmospheric pressure.

Solubility Parameter

The repeatability of the distillate solubility parameter measurements was ±0.3 $MPa^{0.5}$. Based on fitting asphaltenes from different sources, the minimum and maximum solubility parameter of the asphaltenes could vary by ±0.16 $MPa^{0.5}$ and by ±0.21$MPa^{0.5}$ respectively. Figure 5.29 shows that

the model is more sensitive to the variation in the distillate solubility parameter near the onset of precipitation than at higher heptane contents, but the deviations were 0.5 wt% within is the error of the yield measurement.

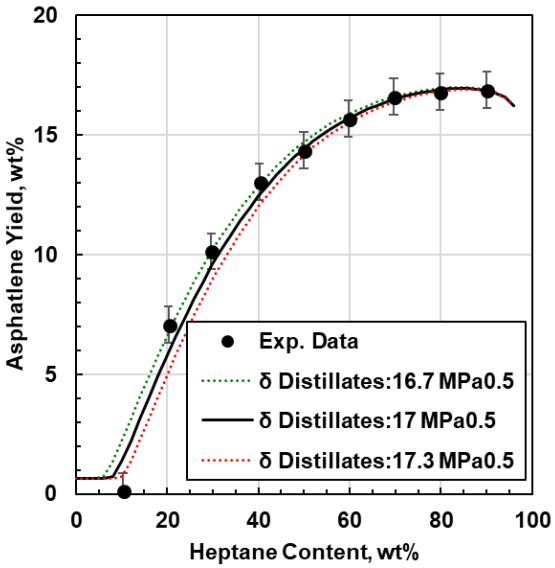

Figure 5.29 Effect of a ±0.3 $MPa^{0.5}$ variation in the input solubility parameter of the distillates on the predicted asphaltene yield. Results for VIS38 whole visbroken oil mixed with toluene and diluted with n-heptane at 20°C and atmospheric pressure.

Figure 5.30 shows that the model is sensitive to changes in the solubility parameter of asphaltenes. A variation in the minimum and maximum solubility parameter shifted the yield but up to 1 wt%, and 2.9 wt%, respectively. These deviations are significant higher than the error of the yield measurements.

Composition

The repeatabilities of the distillate and asphaltene contents were ±0.3 and ±1.2 wt%, respectively. Figure 5.31a shows that the change in the composition of distillates has no any effect on the asphaltene yield predictions. Figure 5.31b shows that the model is more sensitive to errors in the composition of asphaltenes and the deviation in the predicted yields is 0.96 wt% which is above the error of the measurements.

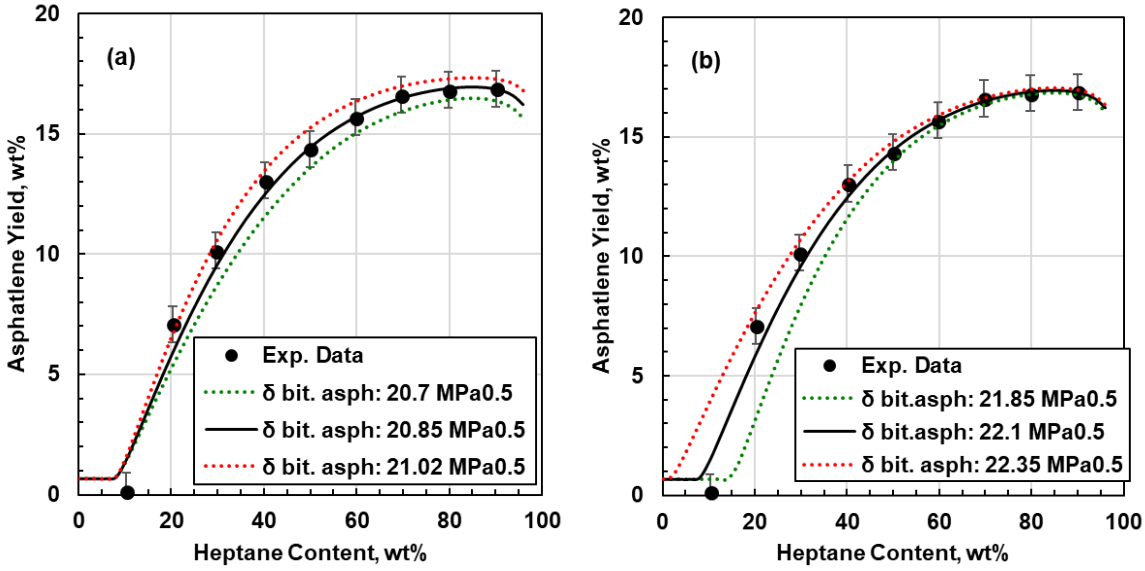

Figure 5.30 Effect of a ±0.1 $MPa^{0.5}$ variation in the asphaltene input on the predicted asphaltene yield: a) minimum solubility parameter; b) maximum solubility parameter. Results for VIS38 whole visbroken oil mixed with toluene and diluted with *n*-heptane at 20°C and atmospheric pressure.

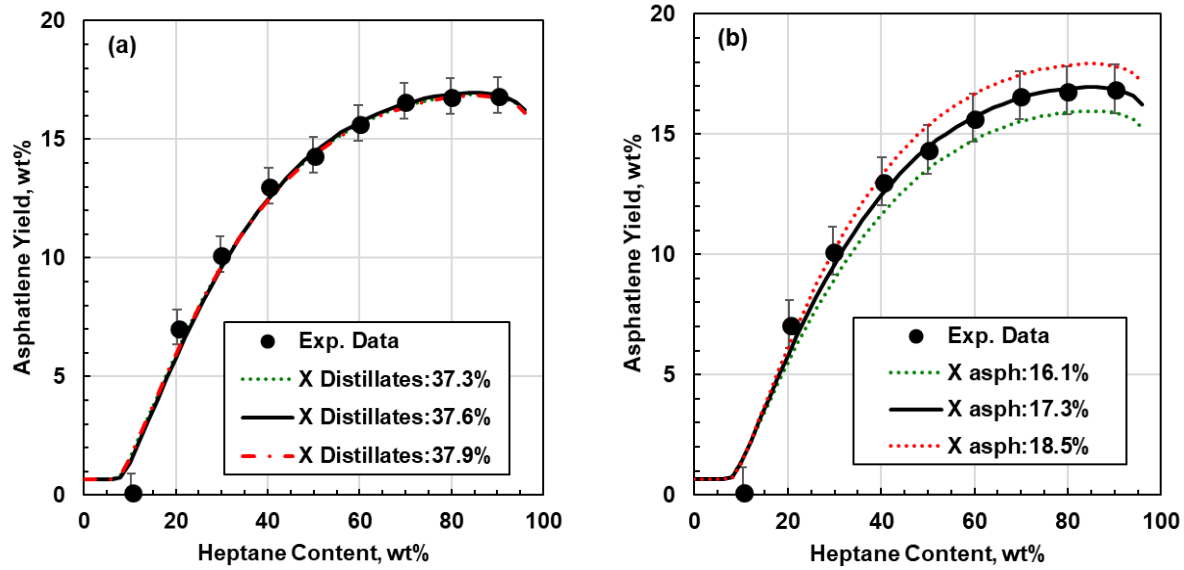

Figure 5.31 Effect of a variation of: a) ±0.3 wt% in input distillate content on the predicted asphaltene yield; b) ±1.2 wt% in input asphaltene content. Results for VIS38 whole visbroken oil mixed with toluene and diluted with *n*-heptane at 20°C and atmospheric pressure.

Conversion

The repeatability of the conversion was calculated from SimDist data based on a repeatability of ±7°C in the boiling temperature. The corresponding deviation in the conversion was ±2.7%. The empirical correlations listed in Tables 5.11 to 5.13 were used to recalculate the physical properties (ρ, MW, δ) at the upper and lower limits of the measured conversion. Figure 5.32 shows the model predictions for the VIS8 sample are sensitive to a deviation within the repeatability of conversion. The average deviation was 1.7 wt% which is above the error measurements of the asphaltene yields. The main source of the deviation was the change in the minimum and maximum solubility parameters which varied by ± 0.06 and ±0.24 MPa0.5, respectively. Figure 5.33 shows that the model is less sensitive for the VIS38 sample with an average absolute deviation was 0.98 wt%, mainly near the onset. Overall, the MRS model is sensitive to conversion changes and the sensitivity is more pronounced at low conversion values.

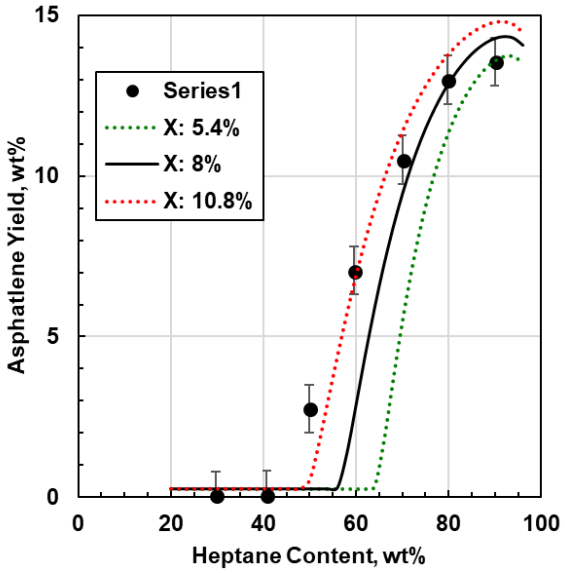

Figure 5.32 Effect of a ±2.7% variation in the thermal conversion on the predicted asphaltene yield. Results for VIS8 whole visbroken oil mixed with toluene and diluted with n-heptane at 20°C and atmospheric pressure. The base case model (solid line) is below the data because the correlations were used to determine the fraction properties.

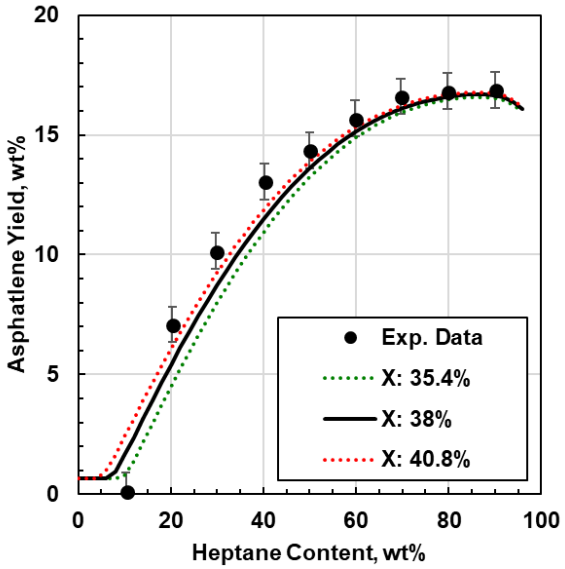

Figure 5.33 Effect of a ±2.7% variation in the thermal conversion on the predicted asphaltene yield. Results for VIS38 whole visbroken oil mixed with toluene and diluted with n-heptane at 20°C and atmospheric pressure.

5.7 Limitations of the Model

The correlations proposed in this thesis only requires the pseudo-component properties of the feed (density, molecular weight, and solubility parameter) and thermal conversion as input variables to predict the asphaltene stability of reacted Western Canadian bitumen. However, these variables are not enough to fully represent the chemical differences in crude oils from different sources or possibly even from different cuts such as the residue fraction. The distribution of chemical species in a crude oil will define the preferential kinetic pathway and the susceptibility of the hydrocarbon molecules to react under certain thermal cracking conditions. Therefore, the applicability of the correlations is limited to crude oils which have a similar chemical composition as the Western Canadian bitumen used in this study, most likely to crude oils from the same source rock.

There is potential to generalize the correlation if properties directly related to chemical composition and reactivity of the petroleum fractions are added to the set of input variables. The results from this study demonstrate that visbreaking has far more effect on the asphaltene properties than any other fraction. Therefore, the most promising target to improve the model is a

generalized correlation for effect of visbreaking on the asphaltene properties. Recently, VMG process simulator incorporated a PIONA slate in its software with the purpose of making a better characterization of a crude oil based on a molecular basis (Hay *et al.*, 2018). In this application, the asphaltenes are treated as a mixture of hydrated and dehydrogenated aromatics at differing molecular weights, the latter are responsible for the formation of coke. A methodology is required to assign mass fractions for each of these two categories and to correlate the changes in the physical properties of each fraction to conversion and other inputs, if necessary. Potential inputs are the Conradson carbon residue (CCR) and the hydrogen-to-carbon ratio of the asphaltenes. Properties such as carbon residue (CCR) can capture the reactivity of the asphaltenes during the visbreaking process (Joshi *et al.*, 2008). The hydrogen-to-carbon ratio strongly correlates to the solubility parameter and density (Gray, 2015).

Chapter 6 Conclusions and Recommendations

The main contribution of this thesis is to extend the Modified Regular Solution model to predict the stability of visbroken bitumen. Existing correlations were adapted, and new correlations proposed for predicting the required input properties for the model; that is, the molecular weight, density, and solubility parameter of reacted distillates and SARA fractions. The properties were correlated to the properties of the feed and the thermal conversion. The model can be used to optimize processes involving visbreaking; for example, to determine how much diluent can be added to a visbroken product without causing the precipitation of asphaltenes. The major conclusions and recommendations for future work are provided below.

One component of extending the model to visbroken products was to add distillates to the oil characterization which formerly only included SARA fractions. A methodology was established to determine the properties of the distillates from spinning band distillation data and a measured density. The Modified Soreide and Sanchez-Lemus correlations were successfully applied to calculate the molecular weight and specific gravity distributions (Sanchez-Lemus *et al*., 2016).

6.1 Conclusions

Visbreaking was found to have the following effects on the properties of the whole bitumen as conversion increased:

- The distillate content increased significantly but there was relatively little change in the relative proportion of saturates, aromatics, resins, and asphaltenes in the residue. The proportion of saturates increased slightly while the proportion of resins decreased. The proportion of asphaltenes decreased at lower conversions but increased at higher conversions.
- The molecular weight, density, and solubility parameter of the distillates and saturates decreased.
- The molecular weight of the aromatics, and resins, and asphaltene decreased while their density and solubility parameters increased.

- The asphaltene molecular weight distribution became narrower and their solubility distribution became wider.
- The toluene insoluble content increased at higher conversions.

The changes in properties are consistent with side-chain removal mainly from the resins and asphaltenes and an accumulation of fragments in the distillates. The increase in the proportion of asphaltenes and toluene insolubles at higher conversion suggests that condensation reactions in the asphaltenes also take place. The most significant changes in the chemistry of the visbroken products were the increase in the distillates content and the asphaltene solubility parameters. The distillates are a poor solvent for the asphaltenes and the increase in asphaltene solubility parameter reduces the asphaltene solubility in the oil. Both effects decrease the stability of the asphaltenes in the oil.

The molecular weight, density, and solubility parameter of visbroken distillates and SARA fractions generally followed monotonic trends with conversion and were correlated to conversion and the corresponding feedstock property. Since asphaltenes behave differently when they are surrounded by the other crude oil fractions, the properties found for the extracted asphaltenes were tuned for asphaltenes in bitumen. The correlations proposed in this study are applicable to Western Canadian bitumens and may not be accurate for oils from other sources.

The Modified Regular Solution (MRS) model is suitable for modeling asphaltene precipitation from visbroken bitumens from Western Canada. The model matched asphaltene precipitation yields from visbroken heavy residues and whole oils with average absolute deviations of 1.2 wt% and 0.4 wt%, respectively.

The sensitivity of the MRS model to expected experimental errors in the composition of the oil, the properties of the distillates and SARA fractions was generally close the experimental error of the measured yields. The model was most sensitive to the expected errors in the asphaltene content, solubility parameter distribution of asphaltenes, and conversion. The maximum deviation in the predicted yield (± 1 wt%) was found for the expected error in conversion at low conversion.

6.2 Recommendations

The Modified Regular Solution model did not match the asphaltene yield data from the highly reacted visbroken products at high heptane ratios. While the deviation was attributed to a failure in the experimental methodology, another possibility is an error in the model. It is recommended to collect and model asphaltene yield data at higher toluene dilutions where the experimental method is expected to be accurate to test if the error is in the experiment or the model.

Since most of the refineries use the p-value method to measure the asphaltene stability of the crude oils, it would be useful to measure this parameter in the visbroken products with the purpose of evaluating how close is this approach to the results given by the thermodynamic model that employed for this study.

It is recommended to test the new correlations on other Western Canadian oils to validate their applicability. It is further recommended to test the correlations on oils from other sources and attempt to generalize them.

Previous experimental data collected at atmospheric conditions (Yarranton *et al*., 2007) supports that heavy phase consists only of resins and asphaltenes. This assumption may not be true for reacted oils; some aromatics appeared to form strong interactions with asphaltenes and resins causing an increase in the content of the precipitate. Therefore, it is recommended to extend to model to allow all components to partition to both phases.

Asphaltene yields are known to increase over time until reaching an apparent equilibrium after approximately 100 hours (Duran *et al*., 2017). The asphaltene yields determined from solubility measurements taken at 24 hours of contact time with the solvent may not represent the values at equilibrium conditions. Consequently, the solubility parameters determined by fitting the MRS model to the asphaltene yield data might be underestimated. Therefore, it is recommended to perform solubility tests at different times to determine the equilibrium condition.

References

Akbarzadeh, K.; Dhillon, A.; Svrcek, W.Y.; Yarranton, H.W. Methodology for the Characterization and Modeling of Asphaltene Precipitation from Heavy Oils Diluted with n-Alkanes. *Energy & Fuels*, **2004**, 18, 1434-1441.

Akbarzadeh, K.; Alboudwarej, H.; Svrcek, W.Y.; Yarranton, H.W. A generalized regular solution model for asphaltene precipitation from n-alkane diluted heavy oils and bitumens. *Fluid Phase Equilibria*, **2005**, 232, 159-170.

Alboudwarej, H.; Akbarzadeh, K.; Beck, J.; Svrcek, W.Y.; Yarranton, H.W. Sensitivity of asphaltene properties to extraction techniques. *Energy & Fuels*, 16, **2002**, 462-469.

Alboudwarej, H.; Akbarzadeh, K.; Beck, J.; Svrcek, W.Y.; Yarranton, H.W. Regular Solution Model for Asphaltene Precipitation from Bitumens and Solvents. *AICHE*, **2003**, 49 (11), 2948-2956.

Aliakbari, E., Stedman, A. "The Cost of Pipeline Constraints in Canada", Fraser Institute Report, May 8, **2018**.

AlHammadi, A.A.; Vargas, F.M.; Chapman, W.G. Comparison of Cubic-Plus-Association and Perturbed-Chain Statistical Associating Fluid Theory Methods for Modeling Asphaltene Phase Behavior and Pressure–Volume–Temperature Properties. *Energy Fuels*, **2015**, 29 (5), 2864-2875.

Altgelt, K.H.; Boduszynski, M.M. Composition and Analysis of Heavy Petroleum Fractions. Taylor & Francis Group, **1994**.

Andersen, S. I.; Birdi, K. Aggregation of Asphaltenes as Determined by Calorimetry. *Journal of Colloids and Interface Science*, **1991**, 142 (2), 497–502.

Andersen, S.I.; Lindeloff, N.; Stenby, E.H. Investigation of Asphaltene Precipitation at Elevated Temperature. *J. Petr. Sci. Technol*, **1998**, 16 (3-4), 323-334.
Andersen, S.I. Flocculation Onset Titration of Petroleum Asphaltenes. *Energy & Fuels*, **1999**, 13, 315-322.

Asomaning, S. Test Methods for Determining Asphaltene Stability in Crude Oils. *Petroleum Science and Technology*, **2003**, 21, 581-590.

Arya, A.; Liang, X.; Von Solms, N; Kontogeorgis, G.M. Modeling of Asphaltene Precipitation from Crude Oil with the Cubic Plus Association Equation of State. *Energy Fuels*, **2017**, 31 (2), 2063-2075.

Arya, A.; Liang, X.; von Solms, N.; Kontogeorgis, G.M. Modeling of Asphaltene Onset Precipitation Conditions with Cubic Plus Association (CPA) and Perturbed Chain Statistical Associating Fluid Theory (PC-SAFT) Equations of State. *Energy Fuels*, **2016**, 30 (8), 6835–6852.

Barrera, D.M. Determination and Application of Asphaltene Property Distributions for Native and Refined Crude Oils. Master Thesis, **2012**, University of Calgary, Calgary, Canada.

Barrera, D.M.; Ortiz, D.P.; Yarranton, H.W. Molecular Weight and Density Distributions of Asphaltenes from Crude Oils. *Energy Fuels*, **2013**, 27, 2474-2487.

Barré, L.; Jestin, J.; Morisset, A.; Palermo, T.; Simon, S. Relation between Nanoscale Structure of Asphaltene Aggregates and Their Macroscopic Solution Properties. *Oil & Gas Science and Technology*, **2009**, 64 (5), 617–628.

Bohne, C.; Yang, Z.; Oake, J. On the Size Distribution of Self-Associated Asphaltenes. *Energy Fuels*, **2013**, 27 (9), 5083-5106.

Casalini, A.; Mascherpa, A.; Vecchi, C. Modifications induced by visbreaking on composition and structure of atmospheric residues. *Fuel Science and Technology International*, **1990**, 8, 427-445.

Castellanos-Diaz, O.; Modaresghazani, J.; Satyro, M.A.; Yarranton, H.W. Modeling the phase behavior of heavy oil and solvent mixtures. *Fluid Phase Equilibria*, **2011**, 304, 74-85.

Carbognani, Lante.; Lubkowitz, J.; Gonzalez, M.F.; Pereira-Almao, P. High Temperature Simulated Distillation of Athabasca Vacuum Residue Fractions. Bimodal Distributions and Evidence for Secondary "On-Column" Cracking of Heavy Hydrocarbons. *Energy & Fuels*, **2007**, 21, 2831-2839.

Chapman, W. G.; Gubbins, K. E.; Jackson, G.; Rodosz, M. SAFT: Equation-of-State Solution Model for Associating Fluids. *Fluid Phase Equilibria*, **1989**, 52, 31-38.

Chung, T.H. Thermodynamic Modeling for Organic Solid Precipitation. *In SPE Annual Technical Conference and Exhibition*. Society of Petroleum Engineers, **1992**.

Dawson, W.H.; Chornet, E.; Tiwari, P.; Heitz, M. Hydrocracking of individual components isolated from Athabasca bitumen vacuum resid. *Prep. Div. of Pet. Chem., American Chemical Society,* National Meeting, Dallas, TX, **1989**, 34 (2), 384-394.

Duran, J.A.; Schoeggl, F.; Yarranton, H.W. The Effect of Air on the Kinetics of Asphaltene Precipitation. *67th Canadian Chemical Engineering Conference*, **2017**, Edmonton, Oct. 22-25.

Edmister, W.C.; Okamoto, K.K. Applied Hydrocarbon Thermodynamics, Part 12: Equilibrium Flash Vaporization Correlations for Petroleum Fractions. *Petroleum Refiner*, **1959**, 38 (8), 117-132.

Elsharkawy, A.M.; Al-Sahhaf, T.A.; Fahim, M.A. Characterization of Asphaltenes and Resins Separated from Water-in-Oil Emulsions. *Petroleum Science and Technology*, **2008**, 26, 153-169.

Eyssautier, J.; Levitz, P.; Espinat, D.; Jestin, J.; Gummel, J.; Grillo, I.; Barré, L. Insight into asphaltene nanoaggregate structure inferred by small angle neutron and X-ray scattering. *The Journal of Physical Chemistry*, **2011**, 115 (21), 6827-6837.

Fahim, M.A.; Al-Sahhaf, T.A.; Elkilani, A. Fundamentals of Petroleum Refining. *Elsevier*, **2010**, Chapter 7.

Fainberg, V.; Podorozhansky, M.; Hetsroni, G.; Brauch, R.; Kalchouck, H. Changes in the Composition and Properties of the Vacuum Residues as a Result of Visbreaking. *Fuel Science & Technology International*, **1996**, 14 (6), 839-866.

Fan, T.; Buckley, J.S. Rapid and accurate SARA analysis of medium gravity crude oils. *Energy Fuel*, **2002**, 16, 1571-1575.

Fellow, K.G. "Energy and Environmental Policy Trends: The Invisible Cost of Pipeline Constraints", Report, The School of Public Policy, University of Calgary, March 6, 2018.

Flory, P.J. Thermodynamics of high polymer solutions. *The Journal of Chemical Physics*, **1941**, 9, 660-661.

Gonzalez, D.L. Modeling of asphaltene precipitation and deposition tendency using the PC-SAFT equation of state. Ph.D Thesis, **2008**, Rice University, Houston, Texas.

Gray, M.R. Upgrading Petroleum Residues and Heavy Oils. Marcel Dekker, Inc. **1994**.

Gray, M.R.; Tykwinski, R.; Stryker, J.; Tan, A. Supramolecular Assembly Model for Aggregation of Petroleum Asphaltenes. *Energy & Fuels*, **2011**, 25 (7), 3125–3134.

Gray, M. R. Upgrading Oilsands Bitumen and Heavy Oil. The University of Alberta Press: Edmonton, Alberta, Canada, **2015**.

Gupta, A. K. A model for asphaltene flocculation using an equation of state: Chemical and Petroleum Engineering, **1986**, University of Calgary.

Gupta. R.K.; Gera, P. Process for the Upgradation of Petroleum Residue: Review. *International Journal of Advanced Technology in Engineering and Science*, **2015,** 3.

Guzmán, R.; Ancheyta, J.; Trejo, F.; Rodríguez, Silvano. Methods for determining asphaltene stability in crude oils. *Fuel*, **2017**, 188, 530-543.

Hammami, A.; Phelps, C.H.; Monger-McClure, T.; Little, T.M. Asphaltene precipitation from live oils: an experimental investigation of inset conditions and reversibility. *Energy Fuels,* **2000**, 14 (1), 14–18.

Hay, G.; Carbognani, L.; Nagata, H. Heavy feed characterization: a molecular approach. *Petroleum Technology Quarterly*, Q2, **2018**.

Hildebrand, J.H. A critique of the theory of solubility of non-electrolytes. Chemical Reviews, **1949**, 44 (1), 37-45.

Hirschberg, A.; DeJong, L.N. J.; Schipper, B.A.; Meijer, J.G. Influence of temperature and pressure on asphaltene flocculation. *SPEJ, Soc. Pet. Eng. J,* **1984**, 24 (3), 283−293.

Hoepfner, M.P.; Fávero, C.V.B.; Haji-Akbari, N.; Fogler, H.S. The fractal aggregation of asphaltenes. *Langmuir*, **2013**, 29 (28), 8799–8808.

Hu, Y.; Guo, T. Effect of Temperature and Molecular Weight of n-Alkane Precipitants on Asphaltene Precipitation. *Fluid Phase Equilibria*, **2001**, 192 (1-2), 13-25.

Huggins, M.L. Solutions of long chain compounds. *The Journal of Chemical Physics*, **1941**, 9, 440.

Johnston, K. A. Measurement and Modeling of Pentane-Diluted Bitumen Phase Behavior. Ph.D. Thesis, **2017**, University of Calgary, Calgary, Canada.

Johnston, K.A.; Schoeggl, F.F.; Satyro, M.A.; Taylor, S.D.; Yarranton, H.W. Phase Behavior of Bitumen and *n*-Pentane. *Fluid Phase Equilibria,* **2017**, 442, 1-19.

Joshi, N.B.; Mullins, O.C.; Jamaluddin, A.; Creek, J.; McFadden, J. Asphaltene Precipitation from Live Crude Oil. *Energy & Fuels*, **2001**, 15 (4), 979-986.

Joshi, J.B.; Pandit, A.B.; Kataria, K.L.; Kulkarni, R.P.; Sawarkar, A.N.; Tandon, D.; Ram, Y.; Kumar, M.M. Petroleum Residue Upgradation Via Visbreaking: A Review. *Ind. Eng. Chem Res*. **2008**, 47, 8960-8988.

Khayan, M. Proposed classification and definitions of heavy crude oils and tar sands. In the Future of Heavy Crude and Tar Sands. R.F. Meyer, J.C. Wynn, and J.C. Olson (eds). UNITAR, New York, **1982**.

Kuznicki, T.; Masliyah, J.; Bhattacharjee, S. Aggregation and Partitioning of Model Asphaltenes at Toluene−Water Interfaces: Molecular Dynamics Simulations. *Energy & Fuels*, **2009**, 23 (10), 5027–5035.

Laux, H.; Rahimian, I.; Butz, T. Thermodynamics and mechanism of stabilization and precipitation of petroleum colloids. *Fuel Processing Technology*, **1997**, 53, 69-79.

Leon, A.Y.; Parra, M.J. Determination of Molecular Weight of Vacuum Residue and Their SARA Fractions. *Ciencia, Tecnologia y Futuro*, **2010**, 4 (2), 101-112.

Leontaritis, K. J. Asphaltene Deposition: A Comprehensive Description of Problem Manifestations and Modeling Approaches. *SPE Production Operations Symposium*, SPE 18892, **1989**, Oklahoma City, Oklahoma.

Leprince, P. Petroleum Refining, Volume 3-Conversion Processes. *Editions Technip*, **2001**, 365−379.

Levinter, M.E. Mechanism of coke formation in the cracking of components groups in petroleum residues. *Khim Tekhnol Topl Masel*, **1966**, 9, 31-35.

Li, Z.; Firoozabadi, A. Modeling Asphaltene Precipitation by N-Alkanes from Heavy Oils and Bitumens Using Cubic-Plus-Association Equation of State. *Energy & Fuels*, **2010**, 24 (2), 1106–1113.

Lokhandwala, T.M. Post-Production Heavy Oil Operatios: A Case for Partial Upgrading. Master Thesis, **2012**, Texas A&M University, United States.

Magaril, RZ.; Aksenora, E.L. Study of the mechanism of coke formation in the cracking of petroleum resins. *International Journal of Chemical Engineering*, **1968**, 8, 727-729.

Mancilla-Polanco, A.; Schoeggl, F.F.; Johnston, K.; Richardson, W.D.L.; Yarranton, H.W.; Taylor, S. The Phase Behavior of Heavy Oil and Propane Mixtures. *Society of Petroleum Engineers*, **2017**, 1-26.

Maruska, H.P.; Rao, B.M.L. The Role of Polar Species in Aggregation of Asphaltenes. *Fuel Science and Technology International*, **1987**, 5 (2), 119–168.

Maxwell, J.B.; Bonnell, L.S. Derivation and Precision of a New Vapor Pressure Correlation for Petroleum Hydrocarbons. *Ind. Eng. Chem. Res*, **1957**, 49 (7), 1187-1196.

McKenna, B.M.; Donald, L; Fitzsimmons, J.; Juyal, P.; Spicer, V.; Standing, G; Marshall, B.; Rodgers, R. Heavy Petroleum Composition. 3. Asphaltene Aggregation. *Energy and Fuels*, **2013**, 27, 1246-1256.

Mitra-Kirtley, S.; Mullins, O.C.; Van Elp, J.; George, S.J.; Chen, J.; Cramer, S.P. Determination of the nitrogen chemical structures in petroleum asphaltene constituents using XANES spectroscopy. *Journal of the American Chemical Society*, **1993**, 115 (1), 252-258.

Moschopedis, S.E.; Fryer, J.F.; Speight, J.G. Investigation of Asphaltene Molecular Weights. Energy & Fuel, **1976**, 55 (3), 227–232.

Mullins, O.C. Review of the Molecular Structure and Aggregation of Asphaltenes and Petroleomics. *SPE Journal*, **2008**, 13 (1), 48–57.

Mullins, O.C. The Asphaltenes. Annual Review of Analytical Chemistry, **2011**, 4 (1), 393-418.

Mullins, O.; Sabbah, H.; Pomerantz, A.E; Andrews, A.B.; Ruiz-morales, Y.; Mostow, F.; Mcfarlane, R.; Goual, L.; Lepkowicz, R.; Cooper, T.; Orbulescu, J.; Leblanc, R.M.; Edwards, J.; Zare, R.N. Advances in Asphaltene Science and the Yen − Mullins Model. *Energy & Fuels*, **2012**, 26, 3986–4003.

Murgich, J. Molecular Simulation and the Aggregation of the Heavy Fractions in Crude Oils. *Molecular Simulation*, **2003**, 29 (6-7), 451–61.

Myers, H.S.; Fenske, M.R. Measurement and Correlation of Vapor Pressure Data for High Boiling Hydrocarbons. *Ind. Eng. Chem*, **1955**, 47(8), 1652-1658.

Nazar, A.R.; Bayandory, L. Investigation of Asphaltene Stability in the Iranian Crude Oils. *Iranian Journal of Chemical Engineering*, **2008**, 5 (1), 3-12.

Okafor, J. Characterization of Non-Distillable Crude and Refined Oil Fractions for Asphaltene Precipitation Modeling. Master Thesis, University of Calgary, **2013**.

Östlund, J.A.; Russell, T.; Walker, S.; Hakansson, A.; Greek, L.; Richard, G. Evaluation of a novel method to study oil stability. *4th International Colloquim Fuels*, **2003**, Esslingen.

Overfield, R.E.; Sheu, E.Y.; Sinha, S.K.; Liang, K.S. Sans Study of Asphaltene Aggregation. *Fuel Science and Technology International*, **1989**, 7 (5-6), 611-624.

Pan, H.; Firoozabadi, A. Thermodynamic Micellization Model for Asphaltene Aggregation and Precipitation in Petroleum Fluids. *SPE Production & Facilities*, **1998**.

Panuganti, S.R.; Vargas, F.M.; Gonzalez, D.L.; Kurup, A.S.; Chapman, W.G. PC-SAFT Characterization of Crude Oils and Modeling of Asphaltene Phase Behavior. *Fuel*, **2012**, 93, 658-669.

Panuganti, S. R.; Tavakkoli, M.; Vargas, F. M.; Gonzalez, D.L.; Chapman, W.G. SAFT model for upstream asphaltene applications. *Fluid Phase Equilibria*, **2013**, 359, 2-16.

Pereira-Almao, P. COURSE NOTES, ENCH 503, "Bottom of the Barrel Processing, Refining and Upgrading", University of Calgary, **2017**.

Petersen, J.C.; Barbour, F.A.; Dorrence, S.M. Oxygen identification in asphaltenes. *Association of Asphalt Paving Technologists*, **1974**, 43, 162-169.

Pierre, L. Petroleum Refining. Vol. 3 Conversion Processes, Chapter 6, 11. *Editions Technip*, **2001**.

Piroozan, Z.; Kaharrat, R.; Emamzadeh, A. Study of Asphaltene Precipitation-Deposition Due to Pressure Depletion. *Brazilian Journal of Petroleum and Gas*, **2010**, 4 (2), 71-81.

Powers, D.P.; Sadaghi, H.; Yarranton, H.W.; Van den Berg, F.G.A. Regular solution based approach to modeling asphaltene precipitation from native and reacted oils: Part 1, molecular weight, density, and solubility paramters distributions of asphaltenes. *Fuel*, **2016**, 178, 218-233.

Powers, D.P. Characterization and Asphaltene Precipitation Modeling of Native and Reacted Crude Oils. Ph.D Thesis, **2014**, University of Calgary, Calgary, Canada.

Quignard, A.; Kressmann, S. Visbreaking. In Heavy Crude Oils. From Geology to Upgrading: An Overview. *Editions Technip*, **2011**, Chapter 16.

Rahimi, P.M.; Teclemariam, A.; Taylor, E.; Wiehe, I.A. Thermal Processing Limits of Athabasca Bitumen during Visbreaking Using Solubility Parameters. ACS Symposium Series, **2005**, 895, 183-196.

Rana, M.S.; Samano, V.; Ancheyta, J.; Diaz, J.A.I. A review of recent advances on process technologies for upgrading of heavy oils and residua. *Fuel*, **2007**, 86 (9), 1216-1231.

Ravey, J.C.; Decouret, G.; Espinat, D. Asphaltene macrostructure by small angle neutron scattering. *Fuel*, **1988**, 67 (11), 1560–1567.

Riazi, M.R. Characterization and Properties of Petroleum Fractions, 1st Edition, ASTM international, U.S.B., **2005**.

Rodgers, R.P.; McKenna, B.M. Petroleum Analysis. *Analytical Chemistry*, **2011**, 83 (12), 4665-4687.

Rogel, E. Theoretical Estimation of the Solubility Parameter Distributions of Asphaltenes, Resins, and Oils from Crude Oils and Related Materials. *Energy & Fuels*, **1997**, 11, 920-925.

Rogel, E.; Leon, O.; Contreras, E.; Carbognani, L.; Torres, G.; Espidel, J.; Zambrano, A. Assessment of Asphaltene Stability in Crude Oils Using Conventional Techniques. *Energy and Fuels*, **2003**, 17, 1583-1590.

Ronningsen, H.P.; Skjevrak, I.; Osjord, E. Characterization of North Sea Petroleum Fractions: Hydrocarbon Group Types, Density, and Molecular Weight. *Energy and Fuels*, **1989**, 3, 744-755.

Sadeghbeigi, R. Fluid Catalytic Cracking Handbook. Elsevier, **2012**.

Sánchez-Lemus, M.C.; Schoeggl, F.; Taylor, S.D.; Yarranton, H.W. Physical properties of heavy oil distillation cuts. *Fuel*, **2016**, 180, 457-472.

Scatchard, G. Equilibrium in non-electrolyte mixtures. *Chemical Reviews*, **1949**, 44 (1), 7-35.

Sheremata, J.M.; Gray, M.; Dettman, H.D.; Mccaffrey, W. Quantitative Molecular Representation and Sequential Optimization of Athabasca Asphaltenes. *Energy & Fuels*, **2004**, 18 (5), 1377–1384.

Speight, J.G.; Moschopedis, S.E. On the molecular nature of petroleum asphaltenes. Chemistry of Asphaltene American Chemical Society, Advances in Chemistry, **1981**,195, 1-15.

Speight, J.G.; Pancirov, R.J. Structural types in asphaltenes as deduced from pyrolysis-gas chromatography-mass spectrometry. *Liquid Fuels Technology*, **1984**, 2, 287.

Speight, J.G. Initial reactions in the coking of residua. Preprints, Div. Petrol. Chem. Am. Chem. Soc, **1987**, 32 (2), 413.

Speight, J.G. The Chemistry and Technology of Petroleum, 2nd Edition. Marcel Dekker Inc, **1991**.

Speight, J.G. Chemical and Physical Studies of Petroleum Asphaltenes. *Asphaltenes and Asphalts, Development in Petroleum Science*, **1994,** 40.

Speight, J.G. Petroleum Chemistry and Refining, Chapter 3, 4, 5, 6. Taylor & Francis, **1998**.

Speight, J.G. The Chemistry and Physics of Coking. *Journal of Chemical Engineering*, **1998**, 15, 1-8.

Speight, J.G. The Chemistry and Technology of Petroleum, 3rd Edition. Marcel Dekker Inc, **1999**, New York.

Speight, J.G.; Özün, B. Petroleum Refining Processes, **2002**, New York: Marcel Dekker.

Speight, J.G. Petroleum Asphaltenes - Part 1: Asphaltenes, Resins and the Structure of Petroleum. *Oil & Gas Science and Technology – Rev. IFP*, **2004**, 59, (5), 467-477.

Speight, J.G. The Chemistry and Technology of Petroleum, 4th Edition, Chapter 14, 17, 20. Taylor and Francis Group, LLC, **2007**.

Speight, J.G. Visbreaking: A technology of the past and the future. *Scientia*, **2012**, 19 (3), 569-573.

Sztukowski, D.M.; Jafari, M.; Alboudwarej, H.; Yarranton, H. Asphaltene Self-Association and Water-in-Hydrocarbon Emulsions. *Journal of Colloid and Interface Science*, **2003**, 265 (1), 179–186.

Tharanivasan, A.; Yarranton, H. W.; Taylor, S. D. Application of a Regular Solution-Based Model to Asphaltene Precipitation from Live Oils. *Energy & Fuels*, **2011**, 25 (2), 528-538.

Tharanivasan, A.K. Asphaltene Precipitation from Crude Oil Blends, Conventional Oils, and Oils with Emulsified Water. University of Calgary, **2012**.

Ting, P.D.; Hirasaki, G.J.; Chapman, W.G. Modeling of Asphaltene Phase Behavior with the SAFT Equation of State. *J. Petr. Sci. Technol*, **2003**, 21 (3-4), 647-661.

Vargas, F.M.; Gonzalez, D.L.; Hirasaki, G.J.; Chapman, W.G. Modeling Asphaltene Phase Behavior in Crude Oil Systems Using the Perturbed Chain Form of the Statistical Associating Fluid Theory (PC-SAFT) Equation of State. Energy & Fuels, **2009**, 23 (3), 1140–1146.

Ventech Engineers International Corp. Omimex Resources, Inc. Initial Visbreaker Unit Process Evaluation: Colombian Heavy Oil Production Field, **2005**.

Virtual Materials Group, Inc. VMG 2017, VMGSim Version 10.0, VMG Sim User's Manual, Calgary, Canada.

Wang, Li. Low Temperature Visbreaking. Master Thesis, **2012**, University of Alberta, Edmonton, Canada.

Wei, W.; Bennett, C.A.; Tanaka, R.; Hou, G.; Klein, M.T. Detailed kinetic models for catalytic reforming, *Fuel Proc. Technol*, **2008**, 89 (4), 344-349.

Whitson, C.; Brule, M. Phase Behavior. *Society of Petroleum Engineers (SPE)*, **2000**.

Wiehe, I.A. A Solvent-Resid Phase Diagram for Tracking Resid Conversion. *Industrial & Engineering Chemistry Research*, **1992**, 31, 530-536.

Wiehe, I.A. A Phase-Separation Kinetic Model for Coke Formation. *Industrial & Engineering Chemistry Research*, **1993**, 32, 2447-2454.

Wiehe I.A.; Kennedy R.J. The oil compatibility model and crude oil incompatilibity. *Energy Fuel* **2000,** 14, 56–59.

Wiehe, I.A. Process Chemistry of Petroleum Macromolecules. *Taylor & Francis Group*, **2008**.

Xu, Y.; Koga, Y.; Strausz, O.P. Characterization of Athabasca Asphaltenes by Small-Angle X-Ray Scattering. *Energy & Fuel*, **1995**, 74 (7), 960–964.

Yarranton, H. W.; Alboudwarej, H.; Jakher, R. Investigation of Asphaltene Association with Vapor Pressure Osmometry and Interfacial Tension Measurements. Industrial & Engineering Chemistry Research, **2000**, 39 (8), 2916–2924.

Yarranton, H.W. Asphaltene Self-Association. *Journal of Dispersion Science and Technology*, **2005**, 26, 5-8.

Yarranton, H.W.; Fox, W.A.; Svrcek, W.Y. Effect of Resins on Asphaltene Self-Association and Solubility. Canadian Journal Chemical Engineering, **2007**, 85(5), 635-642.

Yarranton, H.W.; Okafor, J.C.; Ortiz, D.P.; van den Berg, F.G.A. Density and refractive index of petroleum, cuts, and mixtures. *Energy & Fuels*, **2015**, 29, 5723-5736.

Yarranton, H.W.; Powers, D.P.; Okafor, J.C.; van den Berg, F.G.A. Regular solution based approach to modeling asphaltene precipitation from native and reacted oils: Part 2, molecular weight, density, and solubility parameter of saturates, aromatics, and resins. *Fuel*, **2018**, 215, 766–777.

Zhang, L.Y.; Breen, P.; Xu, Z.; Masliyah, J. Asphaltene Films at a Toluene/Water Interface. *Energy & Fuels*, **2007**, 21 (1), 274–285.

Appendix A. Error Analysis

This appendix summarizes the main statistical parameters that were calculated using the data collected in this study. The parameters include, average $\bar{X}$, data number (**N**), standard deviation (**s**), and confidence interval (CI).

The average or sample mean $\bar{X}$ of a set of measurements is defined as,

$$\bar{x} = \frac{\sum_{i=1}^{N} x_i}{N}$$

where x_i is each measured data in the sample and N is the number of measurements. The variability of scatter in the data is described by the sample standard deviation, s, defined by:

$$s = \sqrt{\frac{\sum_{i=1}^{N}(x_i - \bar{x})}{N}}$$

For each set of measurements, the average and the sample standard deviation can be calculated, thus they are assumed to be known, hence, t-distribution can be used to determine the confidence interval as follows:

$$CI = \bar{x} \pm t_{(\alpha,r)} \frac{s}{\sqrt{N}}$$

The *t* value is found from the t-distribution table where r is the degrees of freedom, $\alpha = (1\text{-}C/100)/2$ and C refers to the confidence level which was taken equal to 90%.

A.1 Confidence Intervals (CI) for SARA Composition

Table A.1. Repeatability analysis for SARA fractionation of feed sample (WC-B-A3).

Fraction	**N**	$\bar{X}$ (wt%)	***s***	**±CI** (Mass Fraction)
Saturates	4	9.05	0.7	0.8
Aromatics	4	40.43	0.5	0.5
Resins	4	22.2	0.2	0.2
Asphaltenes	4	28.3	0.7	0.8

Table A.2. Repeatability analysis for SARA fractionation of WC-B-A3-VIS5A sample.

Fraction	**N**	$\bar{X}$ (wt%)	***s***	**±CI** (Mass Fraction)
Saturates	4	11.14	0.7	0.8
Aromatics	4	41.56	0.3	0.3
Resins	4	21.63	0.4	0.5
Asphaltenes	3	25.66	0.8	0.1

Table A.3. Repeatability analysis for SARA fractionation of WC-B-A3-VIS5B sample.

Fraction	**N**	$\bar{X}$ (wt%)	***s***	**±CI** (Mass Fraction)
Saturates	4	12.56	0.5	0.6
Aromatics	4	41.06	0.3	0.4
Resins	4	21.6	0.4	0.5
Asphaltenes	3	24.78	0.5	0.6

Table A.4. Repeatability analysis for SARA fractionation of WC-B-A3-VIS8 sample.

Fraction	**N**	$\bar{X}$ (wt%)	***s***	**±CI** (Mass Fraction)
Saturates	3	12.05	0.6	0.8
Aromatics	3	40.30	0.5	0.8
Resins	3	21.15	0.6	0.8
Asphaltenes	3	26.50	0.8	0.1

Table A.5. Repeatability analysis for SARA fractionation of WC-B-A3-VIS19 sample.

Fraction	**N**	$\bar{X}$ (wt%)	***s***	**±CI** (Mass Fraction)
Saturates	3	11.85	0.4	0.5
Aromatics	3	40.83	0.3	0.4
Resins	3	20.54	0.1	0.1
Asphaltenes	3	26.77	0.1	0.1

A.2 Confidence Intervals (CI) for Molecular Weight

Table A.6 Repeatability analysis for molecular weight from WC-B-A3 sample.

Fraction	**N**	$\bar{X}$ (g/mol)	***s***	**±CI** (g/mol)
Saturates	2	606	9.2	41.1
Aromatics	3	637	12.8	21.6
Resins	2	1204	12.4	55.6
Asphaltenes	2	4100	95.3	425.8

Table A.7 Repeatability analysis for molecular weight from WC-B-A3-VIS5A sample.

Fraction	**N**	$\bar{X}$ (g/mol)	***s***	**±CI** (g/mol)
Saturates	2	544	3.9	17.6
Aromatics	2	567	9.8	43.7
Resins	2	1040	16.7	75.9
Asphaltenes	3	3780	110.5	493.8

Table A.8 Repeatability analysis for molecular weight from WC-B-A3-VIS5B sample.

Fraction	**N**	$\bar{X}$ (g/mol)	***s***	**±CI** (g/mol)
Saturates	2	530	16.1	71.9
Aromatics	2	552	14.8	66.4
Resins	1	--	--	--
Asphaltenes	2	3120	62.4	278.8

Table A.9 Repeatability analysis for molecular weight from WC-B-A3-VIS19 sample.

Fraction	**N**	$\bar{X}$ (g/mol)	***s***	**±CI** (g/mol)
Saturates	2	552	18.6	83.4
Aromatics	2	513	8.5	38.0
Resins	2	953	7.1	31.8
Asphaltenes	2	3160	54.7	244.4

A.3 Confidence Intervals (CI) for Densities

Table A.10 Repeatability analysis for density from WC-B-A3 sample.

Fraction	**N**	$\bar{X}$ (kg/m^3)	***s***	**±CI** (kg/m^3)
Distillates	2	872	0.003	0.03
Saturates	2	900	0.108	0.97
Aromatics	2	1008	0.651	1.46
Resins	2	1040	0.880	7.90
Asphaltenes	2	1148	0.980	8.80

Table A.11 Repeatability analysis for density from WC-B-A3-VIS5A sample.

Fraction	**N**	$\bar{X}$ (kg/m^3)	***s***	**±CI** (kg/m^3)
Distillates	2	911	0.004	0.04
Saturates	2	899	0.082	0.74
Aromatics	2	1010	0.212	0.64
Resins	2	1044	1.042	7.64
Asphaltenes	2	1162	0.920	8.26

A.4 Confidence Intervals (CI) for Crude Oil Solubility Measurements Diluted in Toluene

Table A.12 Repeatability analysis for solubility measurements in the whole crude oil WC-B-A3 diluted in toluene.

Heptane Mass Fraction	**N**	$\bar{X}$ (wt%)	***s***
0.55	2	0.02	0.03
0.60	2	2.61	1.25
0.65	2	5.19	0.99
0.70	2	7.45	0.39
0.80	2	10.89	0.80
0.90	2	12.93	1.33
		Average	0.8
		CI	0.5

Table A.13 Repeatability analysis for solubility measurements in the visbroken sample WC-B-A3-VIS5A diluted in toluene.

Heptane Mass Fraction	**N**	$\bar{X}$ (wt%)	***s***
0.50	2	0.03	0.05
0.55	2	1.99	1.27
0.60	2	4.77	1.08
0.70	2	8.57	0.13
0.80	2	11.30	1.00
0.90	2	12.58	1.17
		Average	0.78
		CI	0.49

Table A.14 Repeatability analysis for solubility measurements in the visbroken sample WC-B-A3-VIS5B diluted in toluene.

Heptane Mass Fraction	**N**	$\bar{X}$ (wt%)	***s***
0.40	2	0.04	0.05
0.50	2	3.69	1.12
0.60	2	6.97	1.10
0.70	2	9.92	0.30
0.80	2	11.87	1.14
0.90	2	12.90	0.98
		Average	0.78
		CI	0.49

Table A.15 Repeatability analysis for solubility measurements in the visbroken sample WC-B-A3-VIS8 diluted in toluene.

Heptane Mass Fraction	**N**	$\bar{X}$ (wt%)	***s***
0.30	2	0.03	0.04
0.40	2	1.86	0.98
0.50	2	4.34	0.88
0.60	2	7.42	0.51
0.70	2	9.89	0.87
0.80	2	11.66	1.27
0.90	2	12.35	1.11
		Average	0.81
		CI	0.46

Table A.16 Repeatability analysis for solubility measurements in the visbroken sample WC-B-A3-VIS19 diluted in toluene.

Heptane Mass Fraction	**N**	$\bar{X}$ (wt%)	***s***
0.20	2	0.005	0.007
0.30	2	0.042	0.060
0.40	2	4.433	1.136
0.50	2	7.565	0.775
0.60	2	10.218	0.144
0.70	2	11.951	0.663
0.80	2	13.025	0.958
0.90	2	13.376	0.682
		Average	0.553
		CI	0.3

Table A.17 Repeatability analysis for solubility measurements in the visbroken sample WC-B-A3-VIS38 diluted in toluene.

Heptane Mass Fraction	**N**	$\bar{X}$ (wt%)	***s***
0.10	2	0.27	0.18
0.20	2	6.98	0.16
0.30	2	10.37	0.31
0.40	2	13.11	0.08
0.50	2	14.48	0.16
0.60	2	15.59	0.14
0.70	2	16.32	0.40
0.80	2	16.60	0.31
0.90	2	16.73	0.21
		Average	0.22
		CI	0.11

Appendix B
Determination of Distillates Properties from Spinning Band Distillation Data

The methodology applied to estimate the properties of the distillates was discussed in Chapter 4 (Section 4.2.2). This appendix is intended to illustrate the procedure on an example (the visbroken sample VIS8). A schematic of the procedure is provided in Figure B.1. Initial values for the molecular weight of each boiling cut are set to calculate the corresponding specific gravity using the Sanchez-Lemus correlation (Sanchez-Lemus *et al*., 2016). Then, the normal boiling point for each cut is calculated from the molecular weight and density using the modified Soreide correlation (Sanchez-Lemus *et al*., 2016). The molecular weights are iterated until calculated boiling points match the experimental values. Then, the calculated average specific gravity is compared with the measured value. If it does not match, the procedure is repeated with a common multiplier applied to the calculated specific gravities. The multiplier is adjusted until both the boiling points and densities match the measured values. Tables B.1 provides the common multiplier and average density of the distillates of the VIS8 visbroken sample. Table B.2 lists the boiling points, molecular weights, and densities for the VIS8 boiling cuts.

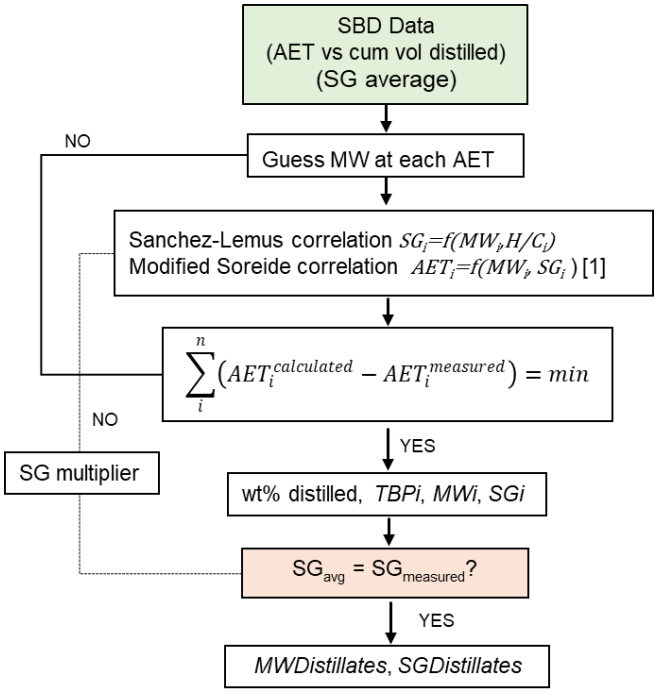

Figure B.1 Schematic procedure to estimate the distillates properties from SBD distillation data.

Table B.1 Measured and calculated specific gravity and multiplier for VIS8 visbroken sample.

Sample	SG multiplier	SG calculated	SG measured
Whole distillates	1.013	0.9074	0.9074

Table B.2 Calculated boiling cut properties for VIS8 visbroken sample.

Boiling Cut	Volume Distilled (ml)	Measured AET (K)	Calculated MW (g/mol)	Calculated SG	Calculated AET (K)
1	0	438	122	0.8058	435
2	2	456	131	0.8239	454
3	2	477	141	0.8426	474
4	2	498	153	0.8607	496
5	2	514	163	0.8733	511
6	2	525	170	0.8821	523
7	2	531	174	0.8868	529
8	2	546	185	0.8978	544
9	2	560	195	0.9072	558
10	2	571	204	0.9145	569
11	2	579	211	0.9198	577
12	2	589	219	0.9257	587
13	2	595	225	0.9297	594
14	2	605	234	0.9352	603
15	2	611	240	0.9390	610
16	2	617	246	0.9424	616
17	2	621	250	0.9446	620
18	2	632	262	0.9503	631
19	2	641	272	0.9552	640
20	1	644	275	0.9563	643

Appendix C
Setting the Average Molecular Weight of Asphaltenes in Native Bitumen

In this thesis, the asphaltene stability in whole oils was modeled by fitting the MRS model to the asphaltene yield data. This procedure requires the adjustment of the average molecular weight (MW_{avg}) and the minimum and maximum solubility parameters (δ_{min}, δ_{max}) of the asphaltenes. However, multiple combinations of MW_{avg} and δ_{min} match the yield data. A solution with physical meaning was obtained by recognizing the two following constraints: 1) too high a value for MW_{avg} gives unreasonably low values for δ_{min}, and; 2) too low a value for MW_{avg} for the feed gives unreasonably low molecular weights for reacted asphaltenes at high conversions. A case study was carried out to study the effect of setting different average molecular weights on the fitted values for the solubility parameter distribution. The average molecular weight of asphaltenes was varied from 2000 to 6500 g/mol and δ_{min} and δ_{max} were adjusted at each molecular weight to fit the measured yield data for two native oils (WC-B-B2 and WC-B-A3) with the results shown in Figures C.1 to C.3.

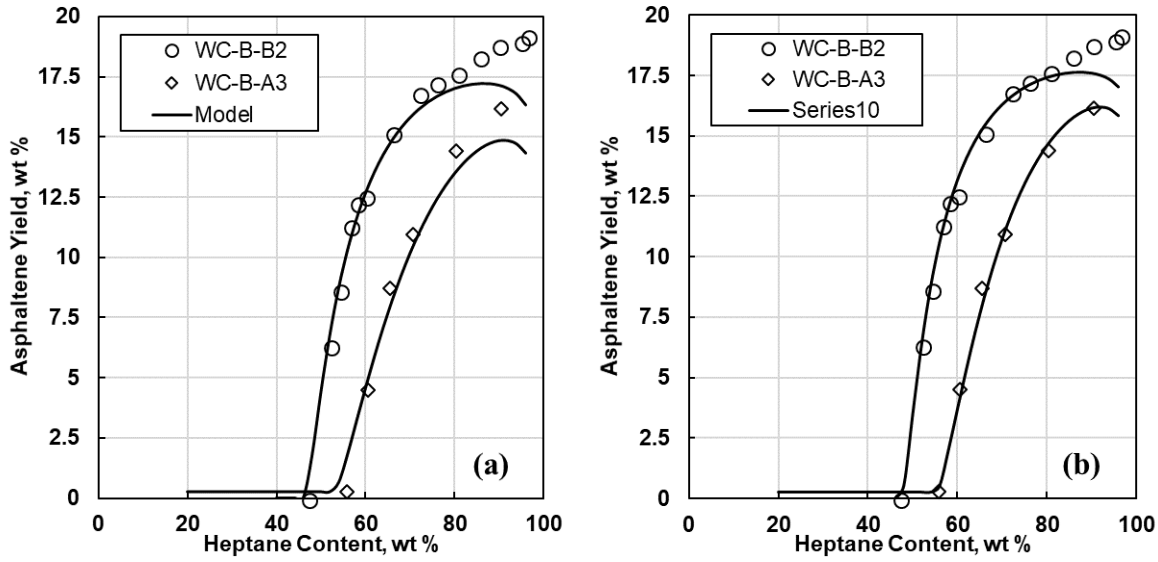

Figure C.1 Asphaltene yield for two native oils (WC-B-B2 and WC-B-A3) diluted with heptane at 20ºC. The average molecular weight of asphaltenes in bitumen was set to (a) 2000 g/mol and (b) 2500g/mol.

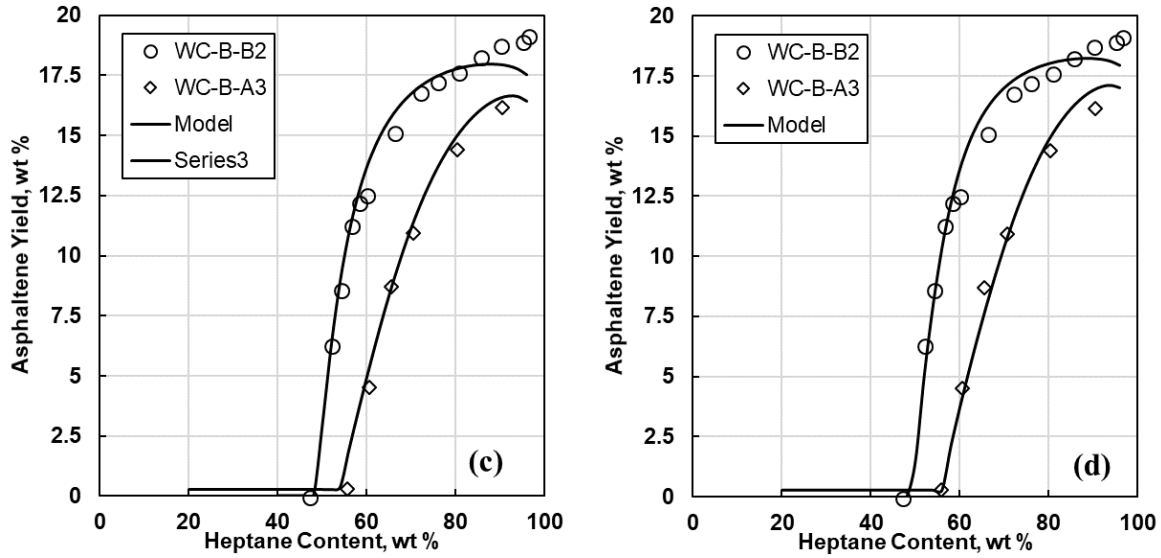

Figure C.2 Asphaltene yield for two native oils (WC-B-B2 and WC-B-A3) diluted with heptane at 20ºC. The average molecular weight of asphaltenes was set to (c) 3000 g/mol and (d) 4000g/mol.

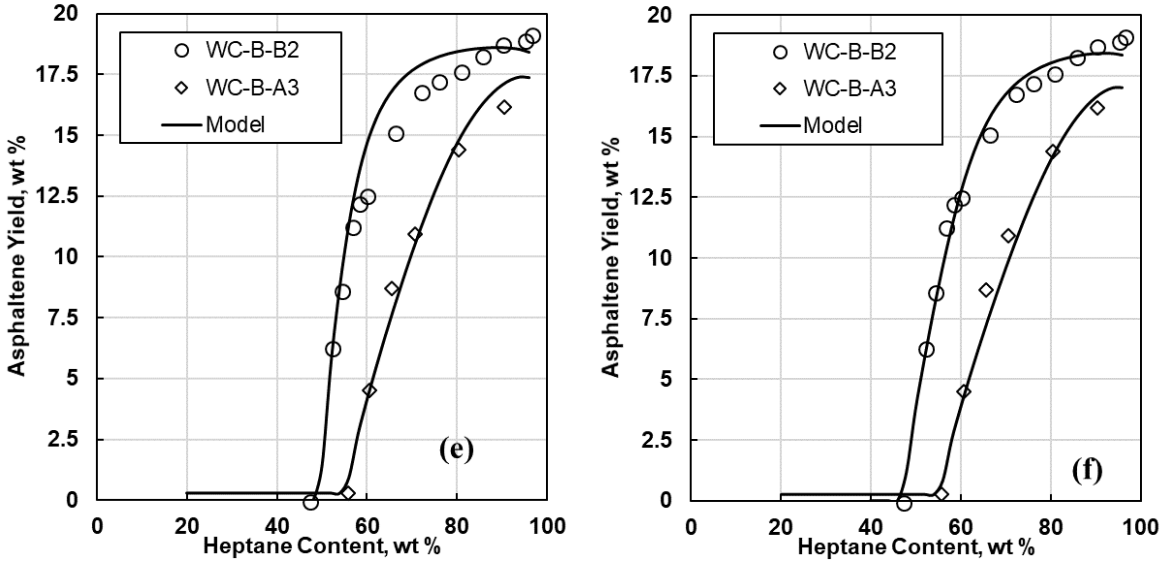

Figure C.3 Asphaltene yield for two native oils (WC-B-B2 and WC-B-A3) diluted with heptane at 20ºC. The average molecular weight of asphaltenes was set to (e) 5500 g/mol and (f) 6500g/mol.

Table C.1 reports the fitted solubility parameters for the asphaltenes in bitumen from the WC-B-A3 native oil. When the average molecular weight is higher than 4000 g/mol, the minimum solubility parameter is less than 19.8 $MPa^{0.5}$ which is lower than typically reported values for

asphaltenes (Andersen, 1999; Powers *et al*., 2016). Therefore, the first constraint requires that the average molecular weight be less than 4000 g/mol.

Table C.1 Fitted solubility parameter of asphaltenes from WC-B-A3 oil using different average molecular weight of asphaltenes for the feed.

MW_{avg} g/mol	δ_{min} $MPa^{0.5}$	δ_{max} $MPa^{0.5}$
2000	20.18	20.61
2500	20.02	20.56
3000	19.94	20.52
4000	19.8	20.52
5500	19.7	20.53
6500	19.65	20.53

To evaluate the second constraint, the correlation reported in Section 5.5.1 was applied to predict the molecular weight of the reacted asphaltenes at high conversions. Figure C.4 shows the molecular weight versus conversion when the average molar value for the feed is set between 2000 to 4000 g/mol. A molar mass for the feed above 2000 g/mol gives values for the molecular weight of the reacted asphaltenes at high conversions that are above the monomer molecular weight (800 g/mol) with some margin for error. Therefore, the second constraint requires that the average molecular weight be above 2000 g/mol.

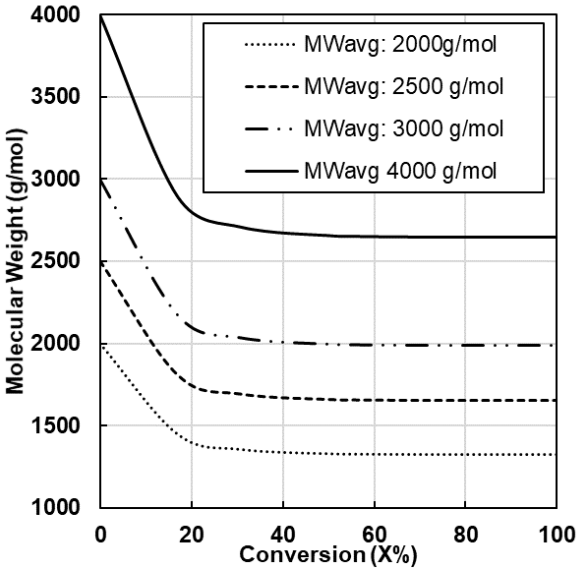

Figure C.4 Molecular weight versus conversion. The average molar mass for the feed was set between 2000 to 4000 g/mol.

For WC-B-A3 sample, 3000 g/mol was set as the average molar mass of asphaltenes in the feed. This value can predict molecular weights for reacted asphaltenes no lower than 2000 g/mol. In fact, Powers *et al*. (2016) reported a molecular weight of 2300 g/mol for a thermocracked asphaltene at a conversion of 51%.

The same exercise was performed on another native crude oil named WC-B-B2 (Johnston, 2017). Table C.2 reports the fitted solubility parameters for the bitumen asphaltenes when different average molar masses are set for the feed. The minimum average molecular weight is 2000 g/mol for the same reasons given previously. An average molar mass higher than 5500 g/mol gives minimum solubility parameters that are too low. Furthermore, if the average molecular weight is above 4000 g/mol, the predicted molecular weights for asphaltenes reacted at high conversions are high compared with experimental data. Molecular weights for thermocracked and hydrocracked asphaltenes have been reported to range between 2100 to 2900 g/mol up to a conversion level of 56% (Powers *et al*., 2016). Therefore, for the asphaltene sample WC-B-B2, the molecular weight of the feed was also set at 3000 g/mol.

Table C.2 Fitted solubility parameter of asphaltenes from WC-B-B2 oil using different average molar masses for the asphaltenes in the feed.

MW_{avg} g/mol	δ_{min} $MPa^{0.5}$	δ_{max} $MPa^{0.5}$
2000	20.4	20.48
2500	20.35	20.38
3000	20.1	20.4
4000	20	20.4
5500	19.88	20.42
6500	19.85	20.43

Appendix D
Solubility Data and Model Results for Native Asphaltenes in Heptane-Toluene Mixtures

Extracted asphaltene yield data from Akbarzadeh *et al*. (2005) and Powers *et al*. (2016) were fitted with the Modified Regular Solution model. The average molecular weights of the asphaltenes were set to the measured values (VPO measurement in toluene corrected to 23°C). The fitted asphaltene parameters are provided in Table D.1. The fitted model is compared with data in Figures D.1 to D.4.

Table D.1. Fitted parameters for the solubility parameter distribution of extracted asphaltenes based on data from Akbarzadeh et al. (2005) and Powers et al. (2016).

Sample	δ_{min} **MPa$^{0.5}$**	δ_{max} **MPa$^{0.5}$**	***n***	***MW* (g/mol)**
Athabasca	20.1	21.2	1.4	7900
Cold Lake	20.24	21.44	1.4	7400
Lloydminster	20.26	21.51	1.4	6660
Venezuela No.1	20.3	21.55	1.4	10005
Venezuela No.2	20.25	21.31	1.4	7662
Russia	20.18	21.26	1.4	7065
Indonesia	20.18	20.68	1.4	4635
WC-B-B2	20.15	21.3	1.4	4500
WC-DB-A2	19.95	21.1	1.4	4200
WC-B-C1	20.15	21.3	1.4	7000
WC-VB-B2	20.15	21.5	1.4	3700
ME-CO-A1	20.15	21.15	1.4	3800
Average	20.2	21.3	1.4	

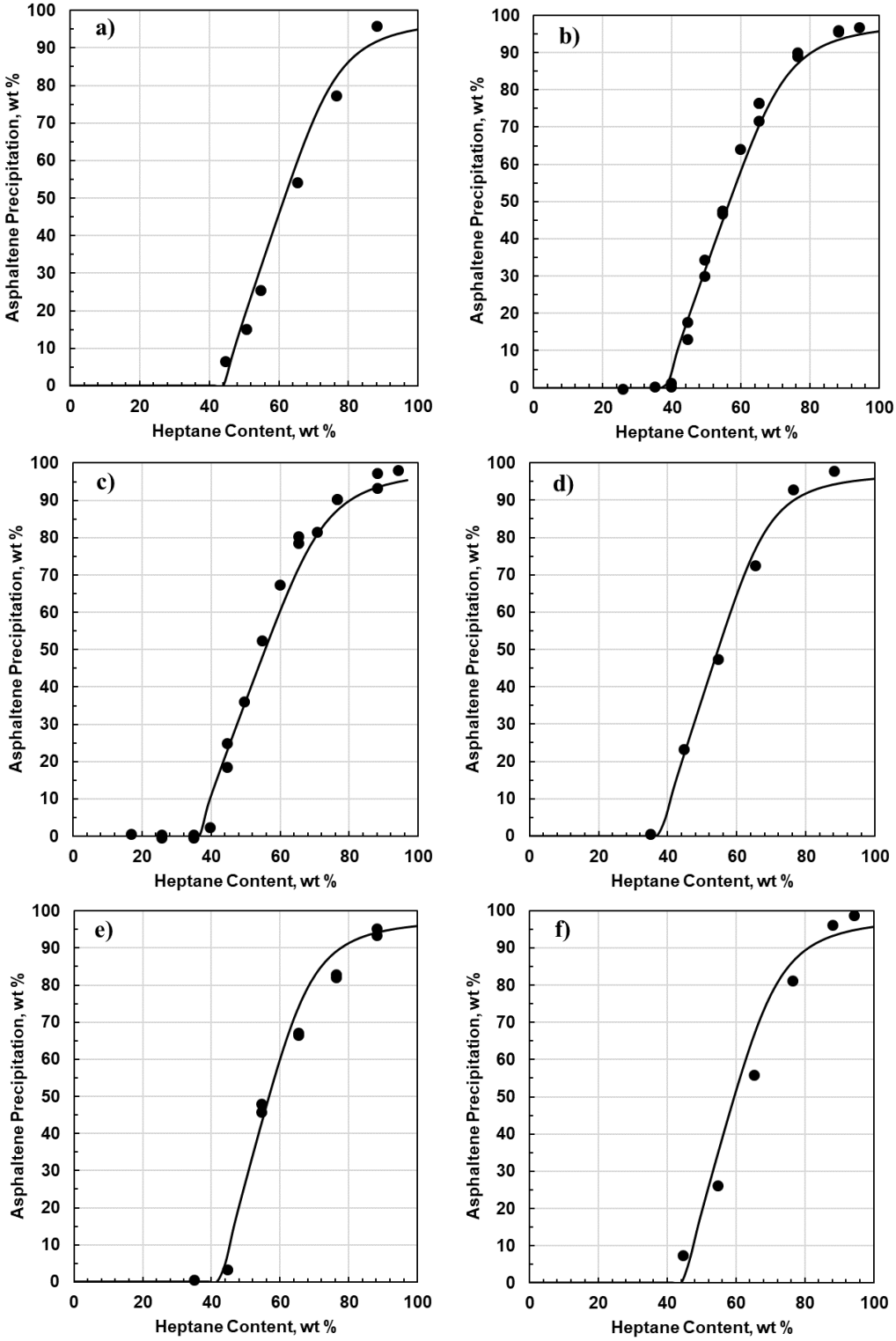

Figure D.1 Measured and modeled yield of asphaltenes in heptane and toluene solutions at 20ºC and 1 atm: a) Athabasca, b) Cold Lake, c) Lloydminster, d) Venezuela 1, e) Venezuela 2, f) Russia. Experimental data from Akbarzadeh et al. (2005).

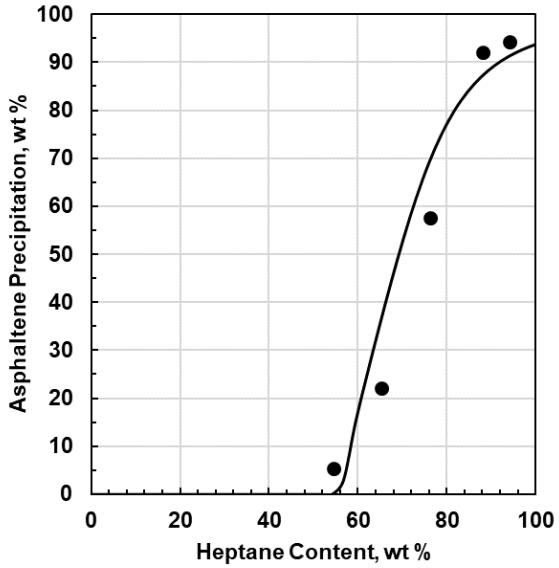

Figure D.2 Measured and modeled yield of asphaltenes from Indonesian oil in heptane and toluene solutions at 20ºC and 1 atm. Experimental data from Akbarzadeh et al. (2005).

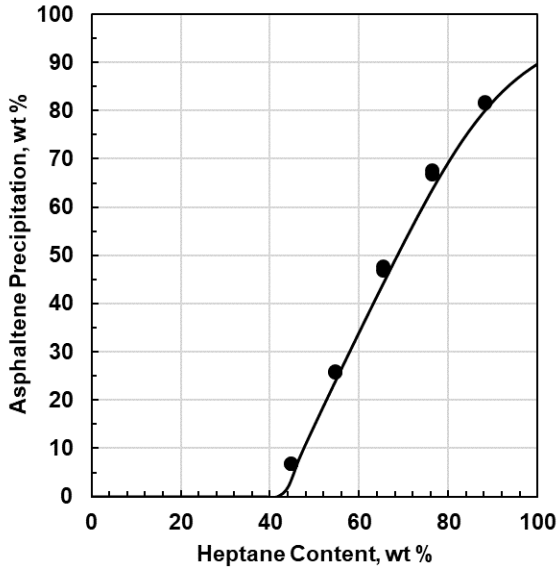

Figure D.3 Measured and modeled yield of WC-VB-B2 (vacuum bottoms) asphaltenes in heptane and toluene solutions at 20ºC and 1 atm. Experimental data from Powers et al. (2016).

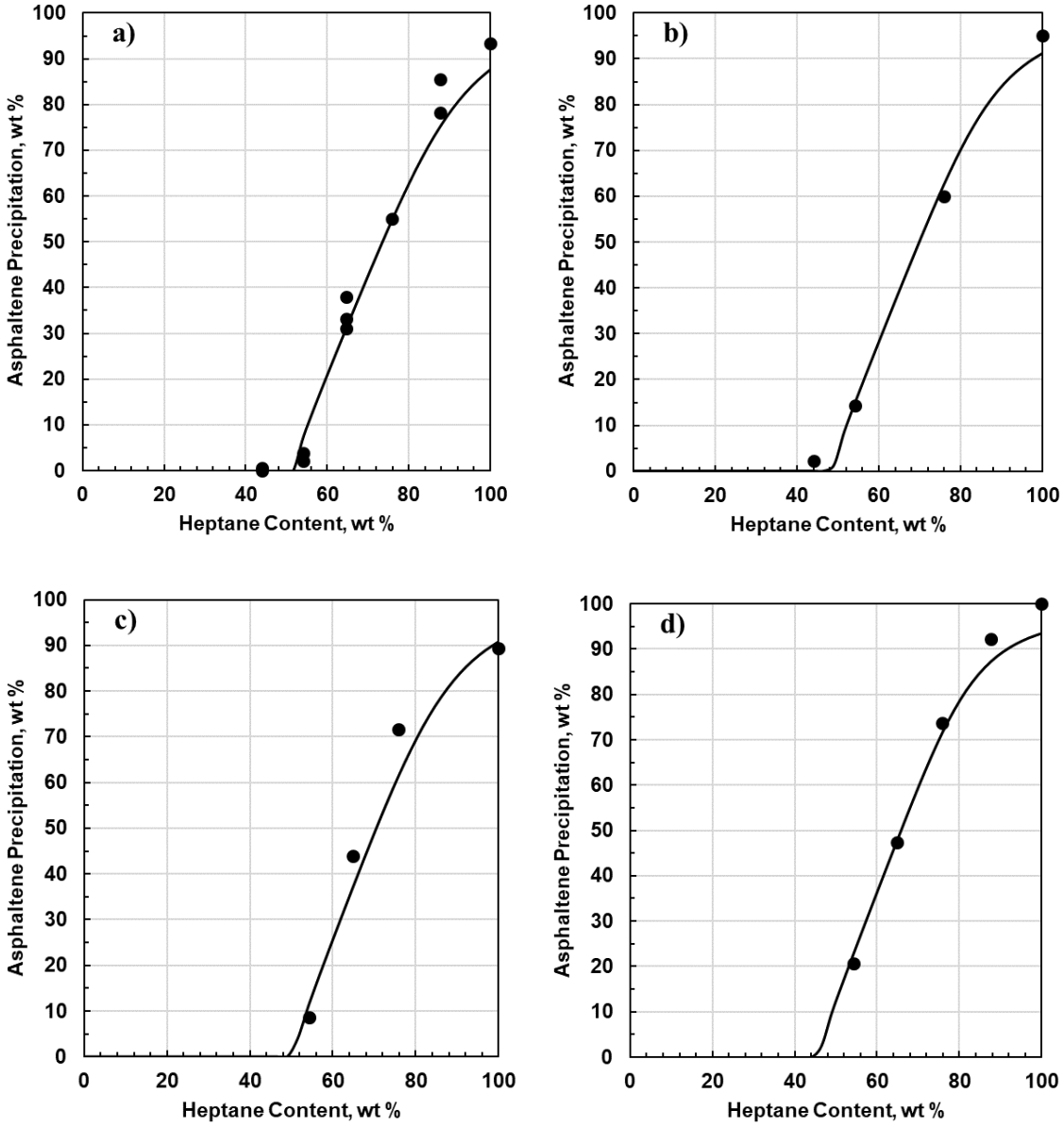

Figure D.4 Measured and modeled yield of asphaltenes in heptane and toluene solutions at 20ºC and 1 atm: a) WC-DB-A2, b) WC-B-B2, c) ME-CO-A1, d) WC-B-C1. Experimental data from Powers *et al.* (2016).

Appendix E
Solubility Data and Model Results for Asphaltenes in Native Bitumen

Yield data for *n*-heptane diluted bitumens from Akbarzadeh *et al*. (2004), Johnston *et al.*, (2017), Yarranton *et al*., 2018 and Powers (2014) were fitted with the Modified Regular Solution model. The average molecular weights of the asphaltenes were set to 3000 g/mol in all cases. The fitted asphaltene parameters are provided in Table E.1 and the average values and standard deviations are reported in Table E.2. The fitted model is compared with data in Figures E.1 to E.3.

Table E.1 Fitted parameters for the solubility parameter distribution of asphaltenes in bitumen.

Sample	**δ_{min} MPa$^{0.5}$**	**δ_{max} MPa$^{0.5}$**	**n**
Athabasca	20	20.28	1.2
Cold Lake	20	20.37	1.2
Lloydminster	20	20.37	1.2
Venezuela 1	20	20.22	1.2
Venezuela 2	20.18	20.31	1.2
Russia	20	20.28	1.2
WC-B-B2	20.05	20.51	1.2
ME-CO-A1	19.95	20.29	1.2
WC-B-C1	19.98	20.03	1.2

Table E.2 Statistics for the fitted solubility parameters of asphaltenes in bitumen.

Statistical Parameter	**δ_{min} MPa$^{0.5}$**	**δ_{max} MPa$^{0.5}$**
Average	20.02	20.30
Standard Deviation	0.07	0.13
Range	0.23	0.48

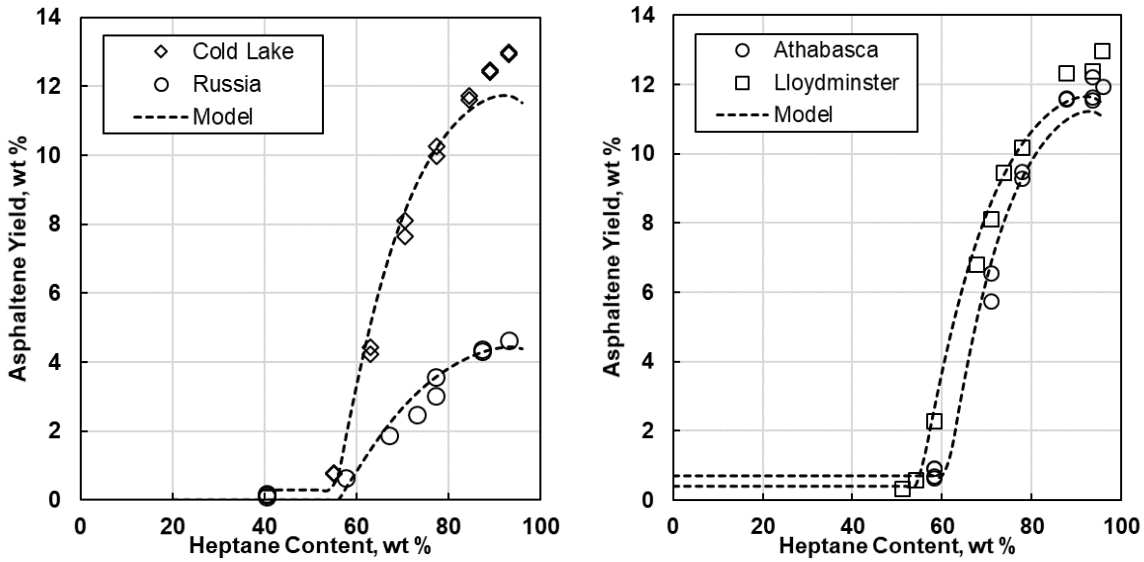

Figure E.1. Measured and modeled asphaltene yields from n-heptane diluted bitumen: a) Cold Lake and Russia oils; b) Athabasca, and Lloydminster oils. Data from Akbarzadeh et al. (2004).

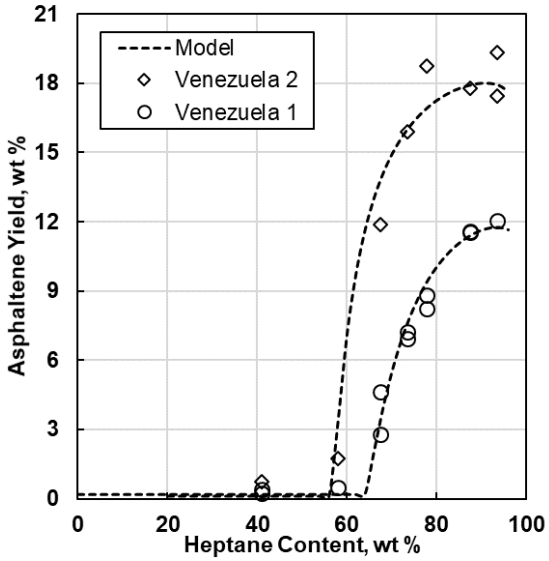

Figure E.2. Measured and modeled asphaltene yields from n-heptane diluted Venezuela 1 and Venezuela 2 oils diluted with n-heptane at 23ºC. Data from Akbarzadeh et al. (2004).

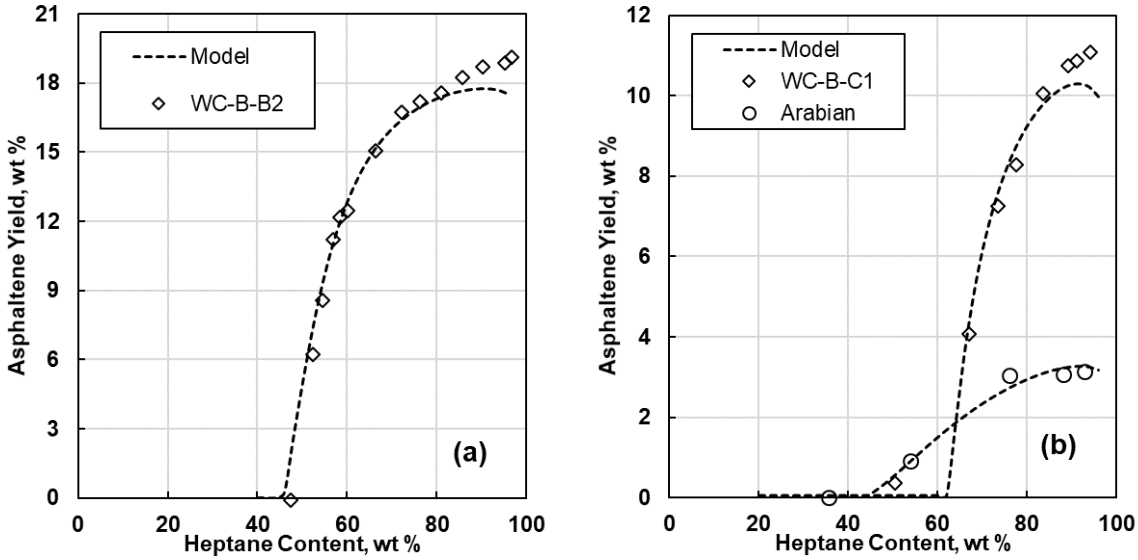

Figure E.3. Measured and modeled asphaltene yields from: a) WC-B-B2 bitumen diluted with n-pentane at 21°C (Johnston, 2017); b) WC-B-C1 and Arabian oils diluted with n-heptane at 23°C (Yarranton et al., 2018; Powers, 2014).